

# 1 Introduction

## 1.1

### Preliminary Remarks

The word comet originates from the Latin *comēta* or *comētēs* and from the Greek κομήτης or *komētēs*. It is derived from κόμη *kómē*, which means “the hair of the head” or “long hair.” The astronomical symbol for comets is ( $\comet$ ), which shows a circle with three hair-like lines.

Comets are fascinating and important objects that merit profound and serious scientific investigation for various, often multidisciplinary reasons [1]: comets are assumed to reveal information about

- the early history of the Solar System, including the formation of cometesimals and comets because of condensation processes on dust grains and their subsequent agglomeration;
- the cometary coma–solar wind interaction, which provides a large and unique plasma physics laboratory to be further investigated;
- the evolution of planets (including Earth and Mars) through comet impacts, which may have delivered volatile water and organic molecules; and
- the chemical evolution that resulted in the molecular origins of life on Earth and its biosphere, including the origin of chirality-related phenomena.

## 1.2

### Motivation to Land a Probe on a Cometary Nucleus

We have now reached a particularly interesting time in cometary research: after the remarkable success of the Giotto cometary mission in 1986, the European Space Agency (ESA) has devoted significant attention to cometary research and has aimed – for the very first time – to create a space probe capable of landing on a cometary nucleus. Such a landing would open possibilities for imaging a cometary surface in previously unachievable detail and enable chemical and physical analyses of cometary matter with hitherto unknown precision. Consequently, the Rosetta cometary mission was designed and constructed, becoming ESA’s cornerstone mission, with a significant budget of approximately 1 billion €.

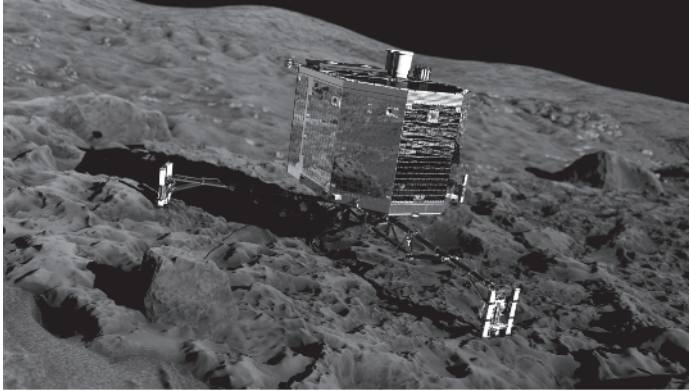


**Figure 1.1** Simulation of the Philae lander after touchdown on the dark surface crust of the 67P/Churyumov-Gerasimenko comet. After landing under nearly zero-gravity conditions in November 2014, Philae will be fixed with two harpoons onto the cometary

surface. The Philae lander contains three legs, each of which will also use a drill to fix the instrument to the cometary surface and prevent it from drifting off. (Image credit: ESA/ATG Medialab.)

The Rosetta probe was successfully launched in March 2004 from Kourou, French Guiana. It will reach a comet called *67P/Churyumov-Gerasimenko* in August 2014. Rosetta carries a small subsatellite, the Rosetta lander, which is called *Philae* and will detach from the orbiter to land on the surface of the comet's nucleus in November 2014 (Figure 1.1). The landing of Philae on the cometary ice will likely be highly spectacular, viewed via live streams all over the world and covered by nearly all news channels and media sources. Today, only a few specialists know about the Rosetta mission, but in 2014, this mission is expected to become well known worldwide.

The Rosetta orbiter contains 10 scientific instruments, as does the Philae lander. These 20 instruments are designed to answer questions that are of general and interdisciplinary scientific importance. One of these questions concerns the origin of water on Earth. Earth has a considerably higher water content than any other body of the inner Solar System. What is the origin of terrestrial water? After the landing of Rosetta's probe Philae, the cometary ice will be analyzed; in particular, its isotopic composition will be determined. Liquid water on Earth has a strict and precisely known composition of three hydrogen isotopes and two oxygen isotopes. After the landing of Philae on 67P/Churyumov-Gerasimenko, the isotopic composition of the cometary water ice will be recorded. This composition will be compared with the isotopic composition of liquid water on Earth, and we think that this comparison will elucidate the origin of terrestrial water.

Another fascinating question that is of tremendous relevance for the scientific community concerns the chemical evolution that resulted in the origin of life on Earth. We assume that comets conserve information about the beginnings of the Solar System in a manner that is analogous to a refrigerator. Consequently,

the scientific instruments of the Rosetta mission will systematically try to detect molecules in the cometary ice. We will focus, in particular, on the detection of molecules that are considered important for the origin of life on Earth. In 2002, during the preparation for the Rosetta mission, our research team was able to identify 16 different amino acid structures in an artificial comet [2]. This finding was accompanied by an increase in the interest of the general public in cometary research. Measurements of the molecular composition of the 67P/Churyumov-Gerasimenko comet will help us to understand crucial steps in the chemical evolution that was responsible for the origin and early evolution of living organisms on Earth.

### 1.3

#### Introduction to the Physical Characteristics of Comets

The physical structure and chemical composition of cometary nuclei, comae, dust, and plasma tail structures, along with orbital theories and comet nomenclature, will be introduced in this section. A more profound analysis and the most recent knowledge will be provided in upcoming chapters.

#### 1.3.1

##### Physical Characteristics of Comets

A comet is a small icy body that belongs to the Solar System. It contains a solid nucleus that is composed of dust and ice. The sublimation of cometary ices from the cometary nucleus yields gases and dust that form the coma, hydrogen cloud, as well as dust and ion (plasma) tails. A comet's nucleus is fragile and – because of its low density, mass, and gravity – has an irregular shape. Comets exhibit highly eccentric trajectories that guide them close to the Sun and back into the outer regions of the Solar System, mostly beyond Pluto. Today, ~5000 comets are known.<sup>1)</sup> Our understanding of comets and cometary processes, however, remains in a primitive state [3].

##### 1.3.1.1 The Cometary Nucleus

The central piece of a comet is a frozen icy nucleus, which is usually a few kilometers in size. The shape and surface structure of the nucleus itself cannot be directly observed by ground-based or Earth-orbiting telescopes [4]. A small cometary nucleus measures several hundred meters in diameter; for example, the nucleus of the 71P/Clark comet has an estimated radius of 340 m [5]. The largest cometary nucleus reported is that of the Hale-Bopp (C/1995 O1) comet, which is ~30 km in diameter [6]. The 95P/Chiron comet, which has an estimated diameter of 200 km, seems to be exceptional in terms of its age and orbit, as

1) Out of a total of 4894 known comets, 289 are numbered, 3362 have been given provisional designations, and 1243 lack designations.

we will see later. As a result of the relatively small size of cometary nuclei, the gravitational force is minute; consequently, gravitational compaction of the fluffy material does not occur [4]. The escape velocity varies between 1 and 5 m s<sup>-1</sup> [7]. In the outer Solar System far from the sun, comets are inactive and consist solely of their nuclei. There the temperature is extremely low (<50 K), which provokes the condensation of volatile molecules such as water out of the gas phase. In astrophysics, a material is considered “volatile” if it has a vapor pressure that is equal to or greater than that of H<sub>2</sub>O. All other materials are refractories; examples of such materials include silicates, polymers, polycyclic aromatic hydrocarbons (PAHs), and mixtures of many other complex organic molecules [8]. The nucleus itself contains a loose collection of condensed volatiles, such as water, carbon dioxide, carbon monoxide, methane, ammonia, and other condensed molecules, in a matrix of small dust and mineral particles. Cometary nuclei can be visualized as conglomerates of ices [9]. To a first approximation and according to comet pioneer Fred Whipple, cometary nuclei can be considered “dirty snowballs” or “dirty icebergs.” New investigations of the outer regions of the Tempel 1 comet revealed that solid particles can even dominate over condensed molecules. Comets might therefore also be considered “snowy dirtballs.”

The precise molecular composition of cometary nuclei is – in contrast with the composition of cometary comae – not yet well understood because cometary nuclei contain particles and molecules in the condensed phase that are inaccessible to spectral analysis using Earth- and space-based telescopes. There is reason to believe that cometary nuclei contain organic molecules in even greater quantities and of higher complexity than those organic molecules that have been identified during the last 45 years in meteorites. In cometary nuclei ices that have been simulated in the laboratory, several amino acids have been identified. Exobiologists and cosmochemists, therefore, hope for the further exploration of cometary nuclei. Some theories for the origin of the biosphere on Earth assume that organic molecules that had been included in comets and meteorites favored chemical evolution and triggered the appearance of life on Earth.

Observations of the nucleus of the Halley comet by the Giotto space probe revealed that cometary nuclei are surrounded by a dark, nearly black crust. This surface crust is dry, dusty, or rocky and hides the cometary ices, which are composed of volatiles and located below the crust. As observed for 1P/Halley [10], this cometary surface crust reflects only 4% of the light that impinges on it (see also [11]), which corresponds to a very small albedo value. For comparison, asphalt reflects approximately 7% of incident light. Cometary nuclei are darker than asphalt and are the least reflective objects found in the entire Solar System. This fact is astonishing because comets are known to be bright objects that are visible in the sky. A sooty surface layer as dark as tar or crude oil that is composed of carbon, hydrogen, oxygen, and nitrogen and contains organic molecules that surround cometary dust particles and absorb photons has been proposed to explain the low albedo. The thickness of this layer is not yet known [12]. Data about the small albedo of dark cometary surfaces were confirmed in 2001 by the Deep Space 1 (DS1) spacecraft, which took high-resolution images of the surface

of the 19P/Borrelly comet. Cometary nuclei that are very distant from the Sun are invisible because of their small size, and comets can become visible only because of reflected sunlight.

The crust formation process was well described by Rickman and Huebner [8], who considered the cometary nucleus crust to be composed of a layer of dust particles; this model does not require refractory organics. Rickman and Huebner assumed that there is a maximum size of cometary dust particles that can be lifted from a cometary nucleus with an active surface area and be entrained by the escaping gas. All dust grains that are larger than the maximum size stay in the surface. If the comet is far from the Sun, outside the orbit of Jupiter, the flux of sublimating molecules, such as water, is so low that all dust grains, even down to submicrometer sizes, remain on the surface. Once the comet approaches the Sun, small- and medium-sized grains start to be removed by the gas flow, but very large dust grains continue to be left on the surface. The critical radius of entrained dust particles reaches its maximum value near perihelion; at each perihelion passage, the surface of the nucleus is purged of most particles that are smaller than this limiting size. Secular enrichment of the largest particles can occur on the cometary surface because smaller grains may adhere to the large particles and be sintered. In such situations, an increasing number of grains reside on the cometary surface and form a coherent dust layer [8] that is characteristic of cometary nuclei and important for their further understanding.

#### 1.3.1.2 The Cometary Coma

As a comet approaches the Sun and its solar radiation, the outer surface of the cometary nucleus becomes warmer and develops a spherically shaped coma. The coma forms because of sublimation of volatile molecules from the cometary nucleus and carryover of dust particles that are embedded in the ice on the Sun-directed side of the comet. It is important to note that there are two distinct components of the cometary coma: neutral gas and dust particles [13]. Gas sublimates from the nucleus, expands outwards, and drags the liberated dust particles along with it. The sublimating gas entrains the dust from the icy surface into the coma [4]. The coma is known to begin forming at a distance of  $\sim 3\text{--}4$  AU from the Sun and can obtain a size of up to  $2\text{--}3$  million km, which is even larger than the Sun. A cometary nucleus has an insufficient mass to gravitationally bind its atmosphere [14]; thus, the coma is interpreted as a steady state. The typical outflow velocity of volatiles near the nucleus is estimated to be  $v = 100 \text{ m s}^{-1}$ , and the mean free path length is  $\lambda = 0.1 \text{ m}$  [4], which is much smaller than the size of the cometary coma, suggesting that there are frequent molecular interactions (see Section 2.5.7, which discusses chemical reactions in cometary comae). It is interesting to note that sunlight is assumed to irradiate all molecules in the coma [13]. The sublimation of volatile molecules and carryover processes of dust particles occurs on  $\sim 10\text{--}15\%$  of the visible cometary surface ( $20\text{--}30\%$  of the sunlit surface) [3] on crumbly fractured parts of the black crust. The key contribution to cometary mass loss is believed to be sublimation processes that are driven by solar illumination. More exotic processes have been considered to

explain commonly observed cometary outbursts; one example is the formation of surface craters through internal explosions that are similar to steam-explosion craters on Earth called *maars* [15]. Crystallization of amorphous ice at depths of a few tens of meters [16] might also release heat that triggers cometary outbursts. The inner cometary coma is made up of sublimated molecules and particles. Because of spectral analyses, the chemical composition of cometary comae is now rather well understood. A description of the chemical species, such as water, ammonia, carbon dioxide, methane, methanol, and many others, observed by remote spectroscopy of cometary comae will be presented in Section 2.4. Further heating, ionization, and dissociation processes form the visible coma, which is composed of ions and radicals. As we will see later in this book, cometary comae provide a natural laboratory for many intriguing phenomena in astrophysical environments [17]. The nucleus and coma together are called the *head of the comet*. The head of the comet is surrounded by a hydrogen cloud. This cloud will be described in Section 1.4 in the context of the Suisei cometary space probe.

### 1.3.1.3 The Cometary Plasma Tail

The neutral and ionic constituents of the cometary coma are blown away by solar radiation pressure and the solar wind, thereby causing cometary tail formation, once comets approach the Sun [18]. Typical cometary tails have sizes of 10 million km (but can be hundreds of millions of kilometers long) and are known to point away from the Sun (see Figure 1.2). Interestingly, closer examination reveals that the cometary tail is composed of two morphologically different tails

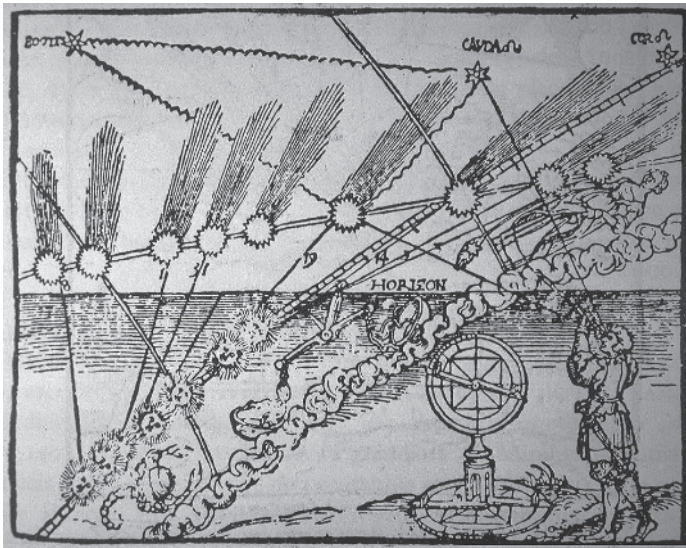


**Figure 1.2** Comet 1P/Halley as observed by Peter Apian in 1531; this figure shows its tails pointing away from the Sun. Together with the Italian Astronomer Fracastoro (1480–1553), Peter Apian was the first scientist to observe this phenomenon [18].



**Figure 1.3** Comet Hale-Bopp was discovered independently on 23 July 1995 by Alan Hale in New Mexico and Thomas Bopp in Arizona. Comet Hale-Bopp exhibits two tails. The plasma tail (type I) on the left of the

image appears blue in reality because of its  $\text{CO}^+$  ions. The diffuse dust tail (type II) is on the right. (The image was taken by Geoff Chester from Blackwater Falls State Park, Davis.)

(see Figure 1.3), a thin long tail (type I tail), which is the plasma tail, and a diffuse curved tail (type II tail), which is the dust tail. The two tails point in two different directions, and it is now known that both tails do not point exactly in the antisolar direction. The coma and, subsequently, plasma and dust tails develop during the comet's approach to the Sun and subside and disappear in reverse order after perihelion passage [14].

The long plasma tail, which often appears blue in color, is composed of molecular ions such as  $\text{H}_2\text{O}^+$ ,  $\text{OH}^+$ ,  $\text{CO}^+$ ,  $\text{CO}_2^+$ ,  $\text{CH}^+$ , and  $\text{N}_2^+$ , and electrons [18]. It is also known as the *ion tail*. The solar wind is believed to interact with the cometary ions and result in the formation of the plasma tail. The typical velocities of ions in the plasma tail range from  $10 \text{ km s}^{-1}$  near the cometary head to  $250 \text{ km s}^{-1}$  far from the cometary head [18]. Detailed information about the ionosphere, interaction with the solar wind (which causes the plasma tail), bow shock, cometopause, and contact surface of comet 1P/Halley was obtained by the Vega and Giotto cometary missions and will therefore be described in more detail in Section 1.4.

#### 1.3.1.4 The Cometary Dust Tail

A cometary dust tail is composed of microscopic dust particles. It is believed that volatile molecules carry dust particles with them when they sublimate out of the cometary nucleus. The carried dust particles are then accelerated by the drag of the outflowing coma gases from essentially zero velocity to a few tenths of a kilometer per second; this velocity is reached within 20–100 km of

the nucleus [18]. Submicrometer-sized particles almost reach the speed of the escaping gases ( $\sim 1 \text{ km s}^{-1}$ ), whereas centimeter- and decimeter-sized particles barely reach the gravitational escape velocity from the nucleus ( $\sim 1 \text{ m s}^{-1}$ ) [19]. The further motion of the fine dust particles is influenced by neither the gravitational field of the nucleus nor the gravitational field of the Sun. Forces other than gravity determine the behavior of these particles; in particular, solar radiation pressure is known to generate a significant interaction with the dust particles. The solar radiation pressure force originates from the interaction of electromagnetic radiation (the sunlight) with matter and describes the momentum transfer from the radiation field, or photon stream, to the scattering and absorbing dust [19]. Radiation pressure is very effective for particles that have sizes comparable to the wavelength of the radiation. For large particles, radiation pressure is ineffective.<sup>2)</sup> This interaction between radiation pressure and dust particles that are present in the cometary coma causes the formation of a curved dust tail, as illustrated in Figure 1.4. Particles of different sizes move with different speeds and are therefore separated in the dust tail [19]. Other dust tail features, such as sunward spikes and fans, neckline structures, dust trails, dust tail fine structures such as striae and striations, and sodium gas tails are described by Brandt and Chapman [18]. After passing through the dust tail, particles are dispersed into interplanetary space [19]. A more detailed description of dust tail features, including the radiation pressure parameter  $\beta$ , the size of the dust cross section, and the optical properties of the scattered light are well presented in the reference by Grün and Jessberger [19].

### 1.3.1.5 Cometary Material Loss and Brightness

A comet that approaches the Sun for the first time loses a nontrivial fraction [15] of its mass in the form of ions, molecules, and dust particles. For typical comets, the mass loss is estimated to be 10–50 t of material per second. A smaller perihelion distance – the perihelion is the shortest distance of the elliptical trajectory of the comet to the Sun – results in greater mass loss. After several approaches to the Sun, the mass loss of comets is estimated to less than  $0.1 \text{ t s}^{-1}$ . The mass loss of 0.03–0.2% of the cometary mass reveals that the cometary tails are not very dense. The enormous brightness of cometary ion and dust tails can be explained by the large surface of the microscopically small dust particles for the dust tail and by the contribution of each ionized species to the brightness of the plasma tail. The large active surface increases the brightness of the cometary ion and dust tails, compared with the cometary nucleus, by many orders of magnitude.

A cometary nucleus reflects sunlight, and this reflected light can be observed from Earth. The brightness of the reflected sunlight flux from a bare comet nucleus varies, to first approximation, proportionally to  $r^{-2}$  and  $\Delta^{-2}$ , where

2) Large dust particles are not significantly influenced by radiation pressure. Their trajectories continue in the same orbit as the comet, where they contribute to meteor streams. Studies of meteor streams have indicated the release from cometary nuclei

of large, centimeter- to decimeter-sized, particles of low density [19]. The emitted intermediate-sized dust particles contribute to the zodiacal dust cloud and can be detected and captured by airplanes that fly through Earth's stratosphere.

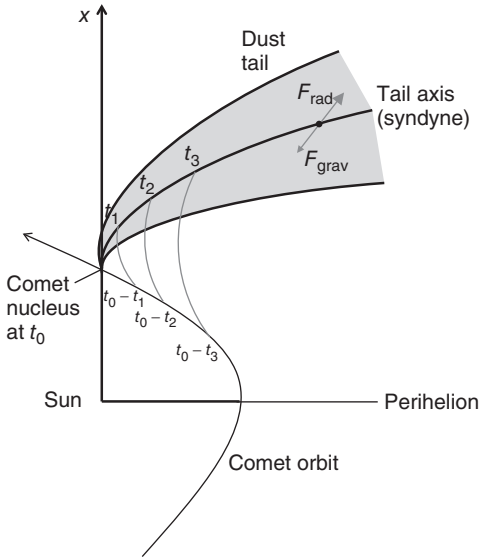


**Figure 1.4** Dust particles entrained by emitted gases from the sunlit hemisphere of the cometary nucleus are subjected to solar radiation pressure and form the cometary dust tail. The dust particles at  $t_1$ ,  $t_2$ , and  $t_3$  on the tail axis (syndyne) are released at different times and at different orbital positions from the cometary nucleus. The sum of the

dust particle trajectories results in the observation of a curved dust tail that is oriented in an anti-sunward direction.  $F_{\text{rad}}$ , which is the force of the solar radiation pressure on a dust particle, is a function of the size of the dust particle and – for small dust particles – significantly exceeds the gravitational force  $F_{\text{grav}}$ . (Adapted from [19].)

$r$  is the heliocentric distance and  $\Delta$  is the geocentric distance [4]. The  $r^{-2} \Delta^{-2}$  relationship is influenced by the rotation of the cometary nucleus, which produces considerable brightness variations. According to Eq. (1.1), the flux  $F_c$  of the reflected sunlight is proportional to the cross section of the nucleus,  $S$ , and the geometric albedo  $p$  and depends on the phase function  $\phi(\alpha)$  normalized to the phase angle  $\alpha = 0^\circ$  [4].

$$F_c = r^{-2} \Delta^{-2} \phi(\alpha) p S F_\odot \pi^{-1} \quad (1.1)$$

$F_\odot$  denotes the solar flux at  $r = 1$  AU. As shown, the photometric estimation of the size of the nucleus at large heliocentric distances requires knowledge of the albedo,  $p$ . Note that maintaining the flux of reflected sunlight constant when decreasing the cometary albedo requires an increased cometary nucleus cross section (see Section 1.5 and the underestimates of the size of comet 1P).

### 1.3.1.6 Comet Fragmentation and Meteor Showers

Condensed volatile molecules are assumed to form the sticky cometary ice. When a comet approaches the Sun, volatile molecules begin to sublime, thereby causing the cometary nucleus to lose some of its cohesion and – because of thermal stress and internal gas pressure variations [20] – become fragile. This fragility can



**Figure 1.5** Comet Shoemaker-Levy 9 as imaged on 17 May 1994 by the Wide Field Planetary Camera 2 onboard NASA's Hubble Space Telescope. The image shows the train of 21 fragments on a collision course with Jupiter. The collisions, which were of velocity  $60 \text{ km s}^{-1}$  and represent a once-

in-a-millennium event that galvanized the worldwide astronomical community into action [18], occurred from 16 to 22 July 1994 behind Jupiter's visible disk and rotated into view from Earth within some minutes. (Image credit: NASA, ESA, and H. Weaver and E. Smith (STScI).)

cause the cometary nucleus to break into parts (fragments) and eventually disappear. Fragmentation of cometary nuclei was exhibited from 1833 to 1852 by comet 3D/Biela [18] and by comet Shoemaker-Levy 9 (official name D/1993 F2), which was discovered in 1993.<sup>3)</sup> The 21 fragments of comet Shoemaker-Levy 9 are depicted in Figure 1.5. They landed on Jupiter from 16 to 22 July 1994, and their traces remained visible for several weeks. Prior to landing on Jupiter, the nucleus of comet Shoemaker-Levy 9 broke into parts because of tidal forces in 1992, when it passed – according to orbital calculations – at a distance of 0.0006 AU from Jupiter; this value is less than the Roche limit.<sup>4)</sup>

Comet 73P/Schwassmann-Wachmann, which is also known as *Schwassmann-Wachmann 3* (or, among astronomers, simply *Schwachmann*), was discovered in 1930 by Friedrich Karl Arnold Schwassmann and Arthur Arno Wachmann at Hamburg Observatory. 73P has an orbital period of 5.36 years. It began its spectacular splitting into fragments during its perihelion passage in 1995. Five large fragments, called 73P-A, B, C, D, and E, were observed initially. In 2001, three of these fragments, B, C, and E, were found again. During the perihelion passage of the fragmented 73P in 2006, further spectacular fragmentation processes occurred, as illustrated in Figure 1.6a–c, and these processes were planned to be observed in 2006 by the closely approaching Cometary Nucleus Tour CONTOUR space mission (see Section 1.6). Today, at least 66 73P-fragments have been described, with 73P-C being the biggest of them. It is very possible

3) Comet Shoemaker-Levy 9 is one of numerous comets that was discovered by Eugene Shoemaker (1928–1997) along with his wife Carolyn Shoemaker and was also discovered by David Levy.

4) The *Roche limit* is defined as the distance from a large body (e.g., a planet) at which a smaller body (e.g., a comet) will be torn apart by tidal forces. Consider a small body of mass  $m$  and radius  $r$  with a smaller body of mass  $\delta m$  positioned at its surface. This assembly approaches a larger body of mass  $M$  and radius  $R$  at a distance  $\rho$ . The Roche limit is the distance  $\rho$  inside which the tidal

force that disrupts  $m$  and  $\delta m$  becomes greater than the gravitational force that holds the two bodies together [18]. The Roche limit calculated for comet Shoemaker-Levy 9, with an estimated nucleus size of  $r=2 \text{ km}$  and mass of  $m=4 \times 10^{16} \text{ g}$ , provides a Roche limit of  $\rho=0.001 \text{ AU}$ , which agrees well with observations made during its approach near Jupiter in 1992 [18].

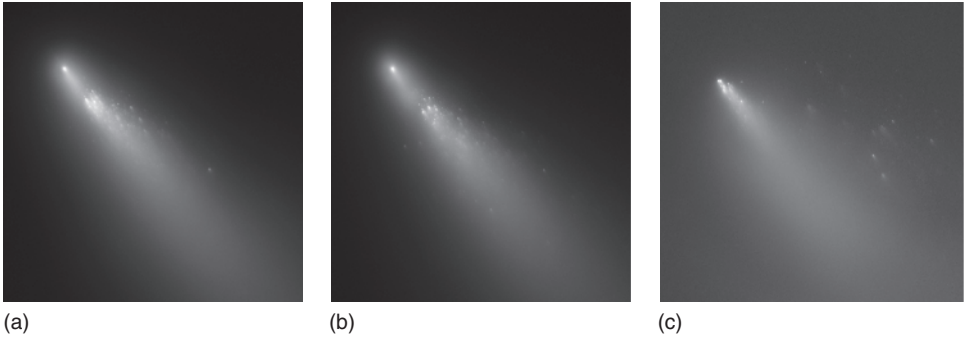


**Figure 1.6** (a) The breakup of fragment “B” of comet 73P/Schwassmann-Wachmann as observed on 18 April 2006. (b) A follow-up view of fragment “B” of comet 73P/Schwassmann-Wachmann as observed on 19 April 2006. (c) Fragment “G” of comet 73P/Schwassmann-Wachmann 3 observed on 18 April 2006. All images were taken by the Hubble Space Telescope. (Image Credit: NASA, ESA, H. Weaver (APL/JHU), M. Mutchler and Z. Levay (STScI).)

that 73P will entirely disintegrate such that no fragments remain observable. In this case, its name will change from 73P to 73D (see Section 1.3.3). The next perihelion passage of 73P is expected to occur in March 2017, and the next should be in the year 2022.

In July 2000, comet Lincoln Near-Earth Asteroid Research (LINEAR) (C/1999 S4) was observed to disintegrate into several small fragments during its perihelion passage (Figure 1.7). Prior to disintegration, the nuclear diameter of comet LINEAR was estimated to be 900 m [21], and after the cometary splitting event, 16 fragments or cometsimals were identified. The largest fragments had spherical diameters of  $\sim 100$  m [22]. A total of more than 40 split comets have been observed over the last 150 years. A review of split comets is given by Sekanina in [23], and a list of them can be found in the reference of Boehnhardt [20]. Keller, from the same Max Planck Institute, reported that the splitting of a cometary nucleus can occur anywhere in an orbit, before or after perihelion, close to the Sun, or at  $r > 3$  AU, and at any comet age [4]. The causes of cometary splitting events remain unknown.

The splitting of comets can provoke the gradual distribution of cometary fragments along their elliptical orbital trajectories. These fragments are called *meteoroids*. If the path of Earth crosses the elliptical trajectory of meteoroids, cometary fragments enter the Earth’s atmosphere and cause the formation of meteor showers<sup>5)</sup>, which can often be observed with the naked eye. The best known meteor showers are the Leonids, which are associated with comet 55P/Tempel-Tuttle, and the Perseid meteor showers, which originate from the parent body of comet 109P/Swift-Tuttle. The Perseid meteor showers can be observed each year between August 9 and August 13. Comet 1P/Halley causes the Orionid

5) The word “meteor” describes the light phenomenon in the Earth’s atmosphere. It does not refer to any object.

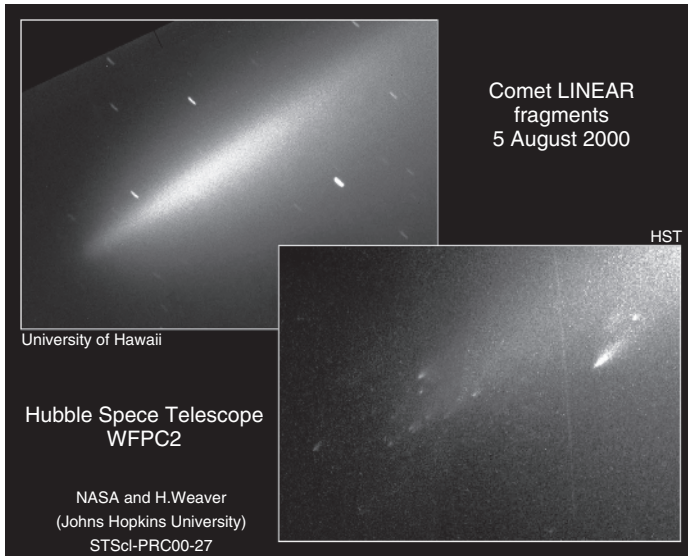


**Figure 1.7** The fragmentation of comet LINEAR (C/1999 S4) as captured by the Hubble Space Telescope on 5 August 2000. The bright dust tail extends to the lower

left. Cometary fragments are clearly visible. (Image credit: NASA, University of Hawaii, H. Weaver (John Hopkins University).)

meteor showers, which are visible each year from approximately 19 October until 23 October, and the Eta Aquariids, which are visible from 21 April until 20 May. Approximately 15 comets have been identified as sources of meteor showers [4].

Usually, the fragile, low-density cometary fragments disintegrate during their passage through Earth's atmosphere at distances of tens of kilometers [18]. Studies of meteor showers can reveal important information about comets because (i) the nature of the dust particles provides information about the composition of comets, (ii) the orbital evolution of the meteor streams provides information about the age of the parent comet on its present orbit, and (iii) the meteors' total mass gives a lower limit for the comet mass [4].

Smaller particles that decelerate in the atmosphere without producing meteors are called *micrometeorites* if they reach the Earth's surface [18]. High-density meteoroids of asteroidal origin may also produce meteors but do not burn up completely and reach Earth's surface. They are called *meteorites*. An unpredicted impact event of an asteroid of estimated 17–20 m diameter was observed in Chelyabinsk, Russia, on 15 February 2013 [24, 25]. The asteroid broke into small pieces between the altitudes of 45 and 30 km, preventing more serious damage on the ground [26]. A meteorite that certainly originated from a comet has not yet been discovered.<sup>6</sup> However, the direct exploration of cometary material is of

6) For rare meteorites, such as C1 chondrites, a cometary origin has been proposed but never confirmed and supported by evidence. In addition, micrometeorites primarily originate from the asteroid belt, although in some cases, a cometary parent body has been proposed.

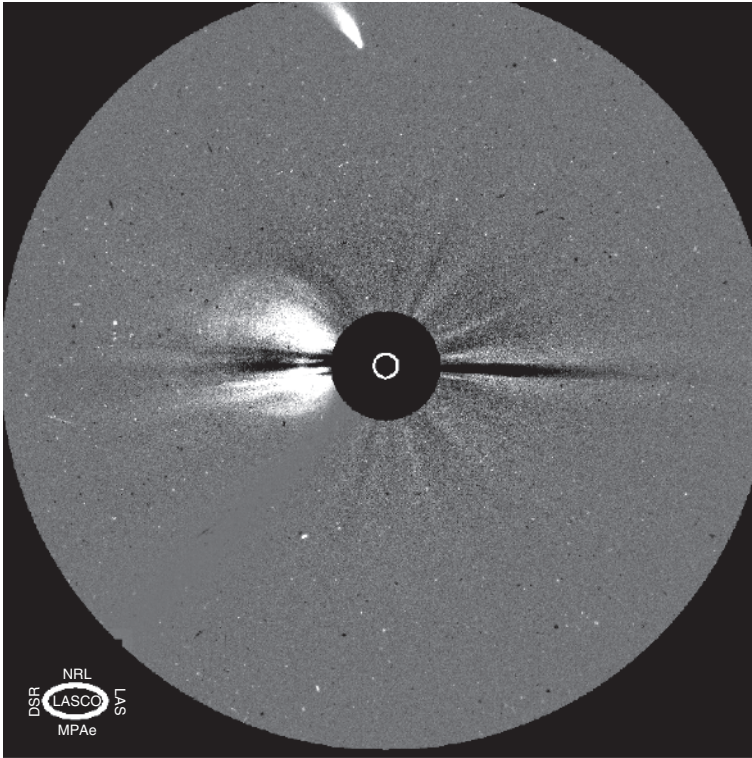


**Figure 1.8** Comet Hyakutake was imaged by SOHO as it passed perihelion. The comet is at the top of the image. The coronal mass ejections on the left of the Sun is unrelated to the comet. (Image credit: ESA and NASA.)

great importance for understanding both the origin of the Solar System and the chemical evolution that was responsible for the molecular origin of the biosphere on Earth. Therefore, complex space missions and space probes, such as Deep Impact, Stardust, and Rosetta, are of crucial scientific importance.

#### 1.3.1.7 Sungrazers

Sungrazers are comets that approach the Sun very closely, usually within a distance of a few million kilometers [27]. More than 1000 sungrazers were imaged by the Solar and Heliospheric Observatory (SOHO). SOHO, the Sun observation spacecraft that was realized by an international cooperation between ESA and NASA, was launched into an orbit around the Earth–Sun L1 Lagrangian point, which allowed it to observe the Sun without interruption [18]. As of 2013, SOHO has discovered more than 2400 comets, which corresponds to one-half of all known comets and to one comet discovery every 2.59 days. Comet Hyakutake, as imaged by SOHO, is depicted in Figure 1.8. The total number of sungrazers is estimated to be 200 000 objects. When approaching the Sun at close distances, sungrazers often fragment into parts. Most of the fragments are small, with diameters less



**Figure 1.9** Comet ISON as captured by the Hubble Space Telescope on 21 October 2013. The image does not provide information about whether the cometary nucleus had already disintegrated into several fragments. (Image credit: NASA, ESA, and the Hubble Heritage Team (STScI/AURA).)

than 10 m. Comet Ikeya-Seki, which is formally designated *C/1965 S1*, is the most prominent sungrazer and became visible at daylight. Its diameter was estimated to be a few kilometers. Ikeya-Seki belongs to the cluster of Kreutz Sungrazers [28], which is assumed to originate from a large “super” comet that broke apart several centuries ago.<sup>7)</sup>

The most recently discovered comet International Scientific Optical Network (ISON) (Figure 1.9), which is also called *C/2012 S1* or comet Nevski-Novichonok, belongs to the family of sungrazers. It originates from the Oort cloud and is not a fragment of the Kreutz Sungrazers. The diameter of its nucleus is estimated to be 5 km. On 28 November 2013, comet ISON approached the Sun at a close distance of 0.012 AU (its perihelion), which corresponds to the diameter of the Sun. Comet ISON was freshly discovered in 2012 by the telescope of the ISON and obtained its name because of this organization. When it approached the Sun,

7) Because comets hit all bodies in the Solar System, even the Sun, the potential hazard posed by comets that may collide with Earth has been thoroughly studied. The LINEAR project performs systematic quantification and classification of near-Earth asteroids and comets to identify impact risks. It has identified hundreds of thousands of asteroids

and several periodic comets, including comet LINEAR (*C/1999 S4*). In 2005, LINEAR was superseded by the Catalina Sky Survey, which searches for potentially hazardous asteroids (PHAs). LINEAR had been preceded and supported by the Near-Earth Asteroid Tracking (NEAT) program from 1995 until 2007.

comet ISON disintegrated into fragments because it approached the Sun at such a small distance. Soon thereafter, the tail, which remained visible for some days because bigger tail particles continued traveling along the comet's orbital trajectory, was lost.

#### 1.3.1.8 Comets and Asteroids

In contrast with asteroids, comets contain a significant fraction of volatiles in the form of ices that allow them to develop an atmosphere composed of a coma and tail when they approach the Sun [3]. The coma and tail are not gravitationally bound to the cometary nucleus. Asteroids do not contain such an atmosphere. They are incapable of exhibiting cometary activity [3]. Comets are defined as icy/snowy bodies that are formed in the outer Solar System, whereas asteroids are rocky bodies that are formed between Mars and Jupiter [18]. However, it is sometimes difficult to clearly distinguish between comets and asteroids. For example, it is believed that some objects with elliptic trajectories that are officially classified as asteroids are in reality burnt-out comets that are surrounded by a thick layer of nonvolatile substances. The centaurs are such an example, and 14 827 Hypnos [29] and 3552 Don Quixote are also possibly nuclei of extinct comets. It is estimated that approximately  $6 \pm 4\%$  of the near-Earth asteroids are burnt-out or dormant nuclei of comets [3, 29]. In the evolution of comets, many of the dormant and extinct comets might end by exhibiting typical asteroid characteristics. On the other hand, after the discovery of Meech and Belton [30] of a coma that surrounds the asteroid 2060 Chiron and a modeling study of its activity [31], the asteroid was renamed comet 95P/Chiron. 95P/Chiron has an estimated diameter of 200 km [18]. The demarcation line between comets and asteroids is not always clear.

#### 1.3.1.9 Exocomets

An exoplanet or extrasolar planet is a planet that surrounds a star other than the Sun. Approximately 1000 exoplanets have been discovered so far, and their number is steadily increasing. Exoplanets attract considerable scientific interest because they are related to the question of the existence of life outside Earth. What about exocomets? Exocomets are comets that do not belong to our Solar System. They can either occur in interstellar space, where they are not gravitationally bound to a star (an interstellar comet has not yet been discovered) or in other Solar Systems. Approximately 10 exocomets in other Solar Systems have been detected since the first identification in the  $\beta$  Pictoris circumstellar disk in 1990 [32]. The authors interpreted the visible and ultraviolet (UV) absorption lines of metal ions, such as  $\text{Al}^{3+}$ ,  $\text{Ca}^{2+}$ , and  $\text{Mg}^{2+}$ , that are believed to exist in cometary coma. More recently, a model of colliding exocomets that are rich in CO and most likely also  $\text{CO}_2$  was proposed to explain the formation of a gaseous cloud that surrounds Ceti 49 [33].

## 1.3.2

**Oort Cloud and Kuiper Belt Comets****1.3.2.1 The Discovery of Comets' Periodicity**

At Oxford University in 1704, Edmond Halley (1656–1742) discovered that the comets that apparently appeared in years 1531 (as described by Peter Apian; see Figure 1.2), 1607 (as described by Johannes Kepler), and 1682 were in fact a single comet that Halley predicted to periodically appear again in 1759 [34]. Following the confirmation of Edmond Halley's prediction by other astronomers, this comet was called *Halley's Comet* or *comet Halley* (officially 1P/Halley). It has an elliptical orbit with a period of  $\sim 76$  years. Comets were demonstrated to be subject to the laws of physics; their orbits could be calculated and their return predicted years in advance [18]. Comet 1P/Halley approached the Sun again in 1835, 1910, and 1986 (see Section 1.4, which discusses five space probes that are approaching the nucleus of comet 1P/Halley) and will next appear in 2061. Before the epochal discovery of Edmond Halley, the appearance of comets was entirely unpredictable. In 1720, Edmond Halley, who also described and catalogued the orbital elements of 24 comets [18], became the Royal astronomer and director of the Royal Greenwich Observatory<sup>8)</sup> in London.

Until the 1990s,  $\sim 10$  new comets were discovered each year. This number recently increased to 20–30 because of automated cometary research and space telescopes. Most of the newly found comets are only visible with telescopes. As they approach the Sun, comets appear brighter; however, comets' increase in brightness and development of tails remain very difficult to predict. Impressively, bright comets appear  $\sim 10$  times per 100 years. Comets Ikeya-Seki (1965) and Hale-Bopp (1997) belong to the group of impressively bright comets that have been visible to the naked eye.

A number of comets exhibit orbital periods that are not constant. Their orbital periods can decrease or increase. This variation is due to the loss of material coupled with the rotation of the cometary nucleus. If the rotation of the cometary nucleus causes mass loss in the forward direction with respect to the comet's motion, the generated force decelerates the comet and decreases its orbital period. If the mass loss is in the backward direction, the comet becomes accelerated and its orbital period increases [18]. Variations in cometary orbits can also be caused by planets, which can perturb cometary orbits; the reverse effect is negligible [14].

**1.3.2.2 Periodic and Nonperiodic Comets**

Comets are traditionally classified according to their orbital characteristics. We distinguish between periodic comets, such as comet Halley, which orbit on a stable elliptical orbit around the Sun (orbital eccentricity  $e < 1$ ) and nonperiodic comets, which are on a nonstable parabolic ( $e = 1$ ) or hyperbolic trajectory ( $e > 1$ ). Nonperiodic comets on hyperbolic trajectories will not re-approach the Sun. They pass

8) Today, the Royal Greenwich Observatory is known for its position being used as the prime meridian, which serves as the reference line for longitude and for setting Greenwich Mean Time (GMT).

once through the inner Solar System before entering interstellar space. Comets exhibit wide variations in their orbital periods that range from several years to hundreds of millions of years. They are traditionally classified as long-period and short-period comets [35].

### 1.3.2.3 Long-Period Comets and the Oort Cloud

Long-period comets have orbital periods  $P$  that range from 200 years to as much as 100 million years and orbital eccentricities that are  $\sim 1$ . They are believed to originate mainly from the Oort cloud, which is a spherical cloud that is located beyond the outer Solar System and extends halfway to the Sun's nearest neighbor, alpha Centauri [36]. The Oort cloud is named after the Dutch astronomer Jan Hendrik Oort, who developed the concept in 1950 by suggesting that many comets originate in a region of space that extends from 20 000 to 150 000 AU from the Sun [37]. Although this distance extends halfway to the nearest star, Oort noted that comets are *not* interstellar objects and inferred that comets have always been members of the Solar System [18]. Based on the known population of long-period comets, Oort estimated the number of comets in the cloud to be approximately  $10^{11}$  [37]. More recent estimates obtained using numerical simulations propose the distinction between a disk-like massive inner Oort cloud and an isotropic outer Oort cloud [38], with a boundary between two at  $\sim 20\,000$  AU [18]. Estimates suggest that the inner Oort cloud contains approximately  $10^{13}$  comets and the outer Oort cloud  $\sim 10^{12}$  comets [39].

As a consequence of the spherical size of the Oort cloud, long-period comets exhibit orbital inclinations that are statistically distributed, and they can enter the Solar System not only in the same direction of circulation as the planets (prograde comets) but also in the inverse direction of circulation (retrograde comets). Orbital eccentricities of long-period comets that are slightly greater than 1 (which indicates a hyperbolic trajectory) have also been observed, but they are rare and caused by perturbations from large planets. Long-period comets remain, by definition, influenced by the gravitational force of the Sun. By entering the inner region of the Solar System, the trajectory of long-period comets often becomes influenced by giant planets, especially Jupiter. Because of these influences, these comets are either ejected to interstellar space or are captured into more tightly bound orbits and become long-period comets [18]. A long-period comet can modify its orbital parameters and become a short-period comet. Consequently, it is difficult to identify some of the short-period Jupiter-family comets as ancient members of the Oort cloud after they have undergone a few perihelion passages.

### 1.3.2.4 Short-Period Comets and the Kuiper Belt

Short-period comets exhibit a periodicity of  $P < 200$  years. They are concentrated in a rather narrow interval because 60% of short-period comets have periods of between 5 and 6.5 years [35]. Short-period comets are assumed to primarily

originate from the Kuiper belt [40, 41],<sup>9)</sup> which is a disk of objects that is located beyond the orbit of Neptune at a distance of 30–50 AU from the Sun. Between 1940 and 1990, there was considerable speculation about the existence of the Kuiper belt, and in 1990, the first Kuiper belt objects (KBOs) were discovered [42]. Since 2000, hundreds of KBOs became known, and hundreds of thousands are believed to exist [18]. Short-period comets usually exhibit the same direction of circulation as the planets. In contrast with long-period comets, the orbital inclination of short-period comets is  $\sim 13^\circ$  [35]. Short-period comets are therefore close to the ecliptic. For many short-period comets, the aphelion, which is furthest distance of their elliptical trajectory from the Sun, is  $\sim 5$  or 6 AU, corresponding to the orbit of the planet Jupiter. Jupiter-family comets may have originally been long-period comets with trajectories that were altered by the gravitational force of Jupiter.

### 1.3.2.5 Jupiter-Family Comets and Halley-Type Comets

As indicated earlier, it has become common to subdivide the short-period comets into two groups: Jupiter-family comets and Halley-type comets. Jupiter-family comets include a number of well-known comets, such as 2P/Encke, 9P/Tempel 1, 10P/Tempel 2, 19P/Borrelly, 21P/Giacobini-Zinner, 46P/Wirtanen, 67P/Churyumov-Gerasimenko, 81P/Wild 2, and 103P/Hartley. Often, they originate in the Kuiper belt [43] and exhibit orbital periods of less than 20 years and a median inclination of  $\sim 11^\circ$  [3]. In contrast, Halley-type comets have orbital periods  $P$  that range between 20 and 200 years, exhibit a distribution of inclinations that is not isotropic, and can move in either a prograde or retrograde sense [18]. The Halley family is a relatively small group, with approximately a dozen known members [18].

Carusi and Valsecchi proposed a distinction between Jupiter-family comets and Halley-type comets based on the Tisserand parameter  $T$ , which is calculated on the basis of Jupiter's and the comet's orbit, eccentricity, and inclination [44]. Here, Jupiter-family comets are characterized by  $T > 2$  [18], whereas Halley-type and long-period comets have  $T < 2$ . A more precise classification scheme for Jupiter-family comets proposed by Horner *et al.* [45] distinguishes between transition-type ( $2.0 < T < 2.5$ ), loosely bound ( $2.5 < T < 2.8$ ), and tightly bound ( $T \geq 2.8$ ) Jupiter-family comets.

Brandt and Chapman [18] pointed out that members of the three families of comets, that is, long-period comets, Jupiter-family comets, and Halley-type comets, can originate in either the Oort cloud or the Kuiper belt. It is important to note that knowledge of a comet's orbital period does not necessarily indicate its origin. A computer simulation code that numerically integrates the orbits of the known short-period comets to predict their long-term evolution has revealed

9) The Kuiper belt is sometimes named the Edgeworth–Kuiper belt to honor the work of the Irish astronomer Kenneth E. Edgeworth, who proposed the existence of a disk of bodies beyond Neptune's orbit.

that most comets move between Jupiter-family ( $P < 20$  years) and Halley-family (200 years  $> P > 20$  years) orbits many times in their dynamical lifetimes [46].

Jupiter-family comets have lifetimes in the inner Solar System that are typically limited to  $\sim 10\,000$  years because of both solar heating effects and gravity-driven orbital changes [15]. Although short-lived, Jupiter-family comets are ancient bodies whose history is believed to typically include important information about the formation of the Solar System [15].

Among 660 investigated comets, 43% exhibit a parabolic trajectory ( $e = 1$ ), 25% have orbits that are long-period ellipses with periods of more than 200 years, 17% orbit on short-period ellipses with periods of less than 200 years, and 15% exhibit hyperbolic trajectories. The large number of parabolic trajectories is most likely due to the short observation times for many comets, which do not allow one to distinguish between long-period ellipses and parabolic trajectories. Longer observation times of 240–500 days have revealed that only 3% of comets exhibit parabolic trajectories. Consequently, comets with long-period-ellipse trajectories are most abundant.

The Oort cloud and Kuiper belt are considered to be the primary reservoirs of most comets today. They might contain billions of comets. Tidal forces of nearby stars or the gravitational forces of large trans-Neptunian objects can cause slight modifications to the trajectories of cold cometary nuclei and inject them toward the Sun. Each year, this gravitational perturbation results in the discovery of new comets. However, the precise mechanism by which comets are released from the Oort cloud toward a Sun-directed trajectory is not yet known. The appearance of new comets that originate in the Oort cloud is therefore unpredictable.<sup>10)</sup>

### 1.3.2.6 Where Did the Oort Cloud and Kuiper Belt Comets Originate?

There is a consensus that the place where comets – kilometer-sized bodies that consist of ice–dust mixtures – formed must have been cold enough to allow for the existence of frozen water [8]. If comets originated in the Solar System, only the region in the vicinity of Jupiter's orbit and beyond guarantees permanent water ice. Condensation of molecules from the gas phase requires sufficient gas density, which too distant regions of the solar nebula do not provide. It was therefore classically assumed that comets originated at the birth of the Solar System, in much the same manner and in the same regions in which the planets

10) Comets continue to be discovered in an irregular manner by both amateur and professional astronomers. Some of the brightest recent comets, such as Hyakutake, which was discovered using the naked eye in 1996, have been discovered by amateurs (Hyakutake was discovered by a Japanese amateur [18]). Once a new comet is discovered, it is to be communicated to the Central Bureau for Astronomical Telegrams (CBAT) at the Smithsonian Astrophysical Observatory in Cambridge, Massachusetts. The most

successful discoverers of comets were Charles Messier (1730–1817), who found 21 comets; Jean Pons (1761–1831), who found 37 comets; Caroline Herschel (1750–1848), who found 8 comets; Lewis Swift (1820–1913), who found 11 comets; Giovanni Donati (1826–1873), who found 6 comets; William Brooks (1844–1921), who found 20 comets; E. E. Barnard (1857–1923), who found 19 comets; and Carolyn Shoemaker, the widow of Eugene Shoemaker, is still active and found 32 comets [18].

were formed, and that they were transported to their present large distances through perturbations from Jupiter and other large planets [8, 35]. The present large-distance reservoirs are the Oort cloud and the Kuiper belt. The temperature at which comets formed is assumed to be greater than 25 K because highly volatile species such as helium and the other noble gases, along with molecular nitrogen, methane, and carbon monoxide, exhibit very low abundances [8].

Recent studies and observations have complicated the simple classical picture by distinguishing between Oort cloud and Kuiper belt comets, thereby emphasizing that both the Oort cloud and Kuiper belt are *today's* reservoirs of cometary nuclei.

Michael A'Hearn [36] reasons that the scattered disk feeds comets into both the Jupiter family *and* the Oort cloud, thereby contributing to a mixing of cometary families. In 2005, Alessandro Morbidelli of the Observatoire de la Côte d'Azur in Nice, France, and colleagues [47] presented the NICE model, which was based on numerical simulations of the orbits of planetesimals and planets. Morbidelli *et al.* [47, 48] found that an outer disk of icy planetesimals (15–35 AU) disrupted and ejected comets into both the Oort cloud and Kuiper belt. It is assumed today that icy bodies were scattered into Oort cloud and Kuiper belt from a range of nebular distances and that the comets from both reservoirs at least partially share common origins [48]. More recent numerical simulations from Levison *et al.* [49] have led astronomers to question the assumption that Oort cloud comets formed in the Sun's protoplanetary disk because the Oort cloud appears to contain too many cometary nuclei. Levison's simulations suggest that more than 90% of the Oort cloud comets originated in the protoplanetary disks of other stars [49]. If this is the case, such comets should exhibit chemical, isotopic, or mineralogical signatures of their natal heritage [48].

### 1.3.3

#### **Nomenclature of Comets and Orbital Elements**

The systematic nomenclature of comets is assigned using a well-defined method. After the discovery of a new comet, the International Astronomical Union (IAU), which is headquartered in Paris, France, designates a name that is composed of the year of discovery, a capital letter, and a number. The capital letter A is assigned to a discovery in the range of 1–15 January, B is assigned to a discovery in the range of 16–31 January, and so forth. The final number is used to distinguish among comets that were identified in the same half-month.

Once the orbital elements of the newly discovered comet are known, a letter is assigned as follows: P indicates that the period is less than 200 years and that at least two observations of the perihelion have been confirmed. C indicates that the period is greater than 200 years. X indicates that the orbital elements are undefined. D indicates that a periodic comet no longer exists. A indicates that further investigation revealed that this near-Earth object is not a comet but rather an asteroid. For example, comet C/1996 B2, which is also named Hyakutake, had a

period longer than 200 years and was the second comet discovered in the second half of January 1996.

Usually, a newly discovered comet also obtains the name of its discoverer. In this case, the P/ (or D/) prefix is preceded by an official sequential number. For example, Halley's comet is 1P, Encke's comet is 2P, Biela's comet is 3D, and so forth [18].

To fully specify the size and shape of a cometary orbit, the orbit's orientation in space, and the position of the comet in the orbit, six constants are used. These constants are the perihelion distance in astronomical units  $q$ , the eccentricity  $e$ , the time of perihelion passage  $T$ , the inclination of the orbital plane relative to the plane of the ecliptic  $i$ , the longitude of the ascending node as measured east from the vernal equinox  $\Omega$ , and the angular distance of the perihelion from the ascending node, which is also called the *argument of perihelion*,  $\omega$  [18]. Once the six orbital elements of a comet are known, the position in space can be calculated. To identify the position of the comet on the plane of the sky, one must furthermore know the Earth's position in space [18]. The orbital elements can be used to determine whether comets are members of comet groups. The Kreutz group (see Section 1.3.1.7) of sungrazing comets, for example, is characterized by the orbital elements  $e = 1$ ,  $q = 0.0062 \pm 0.0015$ ,  $\omega = 77.95^\circ \pm 9.84^\circ$ ,  $\Omega = 357.95^\circ \pm 11.90^\circ$ , and  $i = 143.17^\circ \pm 2.52^\circ$  [18].

#### 1.4

##### Space Probes Vega, Sakigake, and Suisei: Observations of Comet 1P/Halley

Comet 1P/Halley approached the Sun in February 1986. At that time, it was the best known and brightest short-period comet. It exhibited an orbital period of  $\sim 76$  years. During perihelion passage, comet 1P/Halley is – because of its brightness – visible with the naked eye (naked-eye comets are those that become brighter than  $5^m$  [4]). Its orbital parameters are unique [14]. The orbital period is not constant but varies between 75 and 77 years because the trajectory of 1P/Halley – a long ellipse with a perihelion at 0.586 AU and an aphelion at 35.082 AU, which is close to Neptune's orbit – is considerably influenced by the planet Jupiter. This gravitational influence causes slight variations in the orbital period. 1P/Halley is emblematic because its name and parameters are used for the classification and characterization of Halley-type comets. 1P/Halley's orbital inclination is  $162.3^\circ$ , and its trajectory is oriented *against* the ecliptic in a retrograde direction so that 1P moves retrograde with respect to the motion of the planets. The ideal mission would have been a rendezvous in which a spacecraft flew with low relative velocity information with the comet and made measurements over a long period of time [18]. However, spacecraft launched from Earth on direct orbits use the orbital velocity of the Earth to provide the necessary velocity to the spacecraft [18]. Because of comet 1P/Halley's retrograde orbit, it was decided to visit this comet by using fast flyby maneuvers [18]. Because the comet orbits in a direction that is opposite to that of Earth, the close



**Figure 1.10** Comet 1P/Halley as observed on 19 May 1910 by the Lowell Observatory. The original photographic plate was digitized at the Kitt Peak National Observatory. When the photograph was taken in 1910, the comet had passed through perihelion 1 month earlier. It was at a distance of 0.9 AU from the Sun and 0.3 AU from the

Earth. During Halley's 1910 perihelion passage, the closest approach to Earth was  $\sim 0.15$  AU, which is a distance that is less than the length of the dust and plasma tail. Consequently, Earth is believed to have passed through the outer parts of 1P's tail, with some dust and gases surely entering the Earth's atmosphere [18].

encounters with the spacecraft were exceedingly brief –  $\sim 10$  min [50]. In 1986, comet 1P/Halley was on its 30th known and 29th recorded return to the inner Solar System [14]. Images of 1P/Halley taken during its 1910 perihelion passage are presented in Figures 1.10 and 1.11.

The brightness of comet 1P/Halley decreases with the number of perihelion passages. This decrease is due to the mass loss associated with the formation of a crust on the cometary nucleus. The mass loss of comet 1P/Halley during perihelion passage is estimated to be  $\sim 50 \text{ t s}^{-1}$ , which corresponds to 2.5% of its mass.

All nations with significant space flight programs anticipated the perihelion passage of comet 1P/Halley in 1986 as an opportunity for close flyby maneuvers. Comet 1P/Halley was the selected target comet for five different international cometary missions. These Halley Armada missions were Vega 1 and Vega 2, Saki-gake, Suisei, and Giotto. Comet 1P/Halley was selected because of its high activity, which is an effect of its high gas and dust production rates, comparable to those of new comets, and because of the requirement that a target comet has a precisely known orbital trajectory, which rules out new comets and leaves only the short-period and a few intermediate-period comets as potential targets [7]. Moreover, a mission to comet 1P/Halley requires one of the lowest launch energies of all possible cometary missions. Finally, Halley could be observed from Earth during the flyby, thus enabling correlation of the *in situ* measurements with remote



**Figure 1.11** Comet 1P/Halley as observed on 6 June 1910 by the Yerkes Observatory. The 1910 appearance of 1P led to the first worldwide observation campaign, which provided a large amount of data, the assessment of which was not completed until 20 years after the perihelion passage [4]. (Image credit: Yerkes Observatory; the image was purchased by the New York Times for publication in June 1910.)

ground-based observations [7]. The four participating space agencies, ESA, Soviet Intercosmos, Japanese Institute of Space and Aeronautics (ISAS), and NASA, were coordinated by the Inter-Agency Consultative Group [51]. The period of the 1980s during which comet 1P/Halley occupied the attention of researchers was called the *Halley era* because it provided so much new knowledge [18].

#### 1.4.1

##### The Vega Mission to Comet 1P/Halley

The Soviet Vega mission, which was one of the most elaborate of the Soviet space missions and was initially planned to precede a series of Soviet planetary space missions, was composed of two independent, identical, and unmanned spacecraft, Vega 1 and Vega 2. The name Vega is derived from the first two letters of Венера Venera = Venus and Галлей = Gallej = Halley. Vega 1 and Vega 2 were successfully launched on a Proton rocket from the Baikonur Cosmodrome in December 1984 to visit planet Venus and later comet 1P/Halley. Joint international contributions from east- and west-European countries enabled the technical and scientific realization of the missions. For the observation of Venus, both Vega space probes contained a landing probe and a Helium-filled balloon that was 3.4 m in diameter and constructed in France. In June 1985, the lander and balloon were effectively deposited on the surface and in the atmosphere of Venus, respectively, to study the temperature, pressure, wind, and ultraviolet irradiation and for the detection

of lightning phenomena. The balloons collected data for 47 and 60 h, respectively, and transmitted them to Earth [52]. In March 1986, after the observations of the surface and the carbon dioxide atmosphere of Venus, the Vega space probes reached comet 1P/Halley. A relatively safe trajectory was chosen for the Vega spacecraft [11]. On March 6, Vega 1 passed the comet at a distance of 8890 km and with a relative velocity of  $79.2 \text{ km s}^{-1}$ ; its sister probe, Vega 2, passed on March 9 at a distance of 8030 km and with a relative velocity of  $76.8 \text{ km s}^{-1}$  [53]. The flyby speed was extremely high because the direction of orbital motion of 1P is retrograde and thus opposite to the direction of motion of the spacecraft [53]. The high speed required that parts of the spacecraft were protected from dust [53]. At the time of the encounter, 1P/Halley was at a distance of 0.8 AU from the Sun. Measurements were taken to study the dimensions, shape, temperature, and surface properties of the cometary nucleus of comet 1P/Halley. Moreover, the Vega mission, with a scientific payload of 14 instruments [53], aimed to study the structure and dynamics of the near-nucleus coma and its chemical and dust composition. The Vega mission sent approximately 1500 images of comet Halley to Earth [11]. However, it was not possible to determine the contour and shape of the comet nucleus: the interpretation of the images was not conclusive because the contrast between scattered light from the dust near the nucleus and the light reflected directly from the surface was low [4]. Two well-separated broad maxima were the only discernible 1P features.

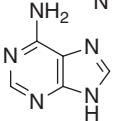
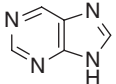
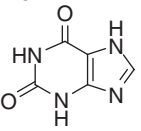
#### 1.4.1.1 Physical and Chemical Properties of Cometary Dust

In 1980, Grün and Kissel *et al.* [54], gained significant experience with dust detectors because of their work on the Helios mission, which provided the required knowledge for the design of a new type of dust-analyzing instrument [19]. Based on this experience, Kissel and colleagues [55] developed the dust impact mass analyzers (PUMAs) that were carried by Vega 1 (PUMA-1) and Vega 2 (PUMA-2). These instruments acted as a reflectron time-of-flight mass spectrometer to analyze dust particles in the cometary coma (or in interplanetary space) that struck the target in front of the spectrometers. The collisions caused ions to form, and those with a positive charge were mass analyzed (later versions of this type of dust analyzer also allowed for the detection of negatively charged ions; examples include the cometary and interstellar dust analyzer (CIDA) instrument on the Stardust Mission, which is discussed in Section 1.7). The PUMA instruments onboard Vega 1 and Vega 2 provided the first direct measurements of the physical and chemical properties of cometary dust. PUMA-1 successfully returned data for more than 1000 cometary dust particles to Earth because Vega 1 flew through the dustiest environment of Halley's comet and suffered no instrumental problems [56]. PUMA-2 provided a few hundred mass spectra. Most of the detected particles were demonstrated to be rich in light elements such as C, H, O, and N. Because the PUMA mass analyzers were sensitive to both molecular *and* atomic ions [56], in addition to these light elements, the masses of the positively charged Mg ( $m/z = 24$ ), Si ( $m/z = 28$ ), Ca ( $m/z = 40$ ), and Fe ( $m/z = 56$ ) ions were determined. Based on these data, the Mg/C and Si/C

ion ratios were calculated and found to range over more than four orders of magnitude, which demonstrates the highly variable proportions of the C, H, O, and N and silicate components [19]: 72% of the particles are CHON-dominated, with a mean (C + O) to (Mg + Si + Fe) ratio of about 5, whereas 28% of the particles are dominated by Mg, Si, and Fe, with (C + O) to (Mg + Si + Fe) ratios of  $\sim 0.1$ . The reader should note that oxygen may stem not only from the CHON component but also from the inorganic silicate material [19].

Despite the inhomogeneous composition of the captures, the obtained data about the dust particles were reported to support models that describe cometary material as consisting of radiation-processed ices [55]. The authors concluded that the high contents of C and N in the analyzed samples do not hint at type C1 carbonaceous chondrites being the sole chemical model for cometary dust particles. The data support the Greenberg model (see Section 2.4), in which comets are aggregates of interstellar dust particles consisting of a silicate core embedded into a nonvolatile organic mantle, which were produced from ices by ultraviolet radiation before condensation of the solar nebula [55]. A more detailed study of the PUMA-1 data revealed that most of the analyzed cometary dust particles consisted of a predominantly chondritic core and an organic mantle composed mainly of highly unsaturated compounds [57]. Jessberger *et al.* concluded that the samples of Halley's dust collected by the Vega 1 spacecraft were a mixture of a refractory organic components and unequilibrated silicates. More exhaustive chemical information about individual cometary dust particles was difficult to extract from PUMA's mass spectra because of the complexity of the impact-ionization process [58]. After subtracting singly charged ions as identified by isotopic abundances from the PUMA-1 mass spectra, the remaining spectra enabled the use of coincidence diagram analyses to access, in particular, lower mass lines (mass < 50  $m/z$ ). The presence of many types of organic molecules was thereby inferred, as depicted in Table 1.1 [19, 57]. The authors distinguished between CH-, CNH-, and COH-, and CNOH-compounds. A comparison of these compounds with the species that were produced in a simulation of interstellar ice photoprocessing (in which many saturated and unsaturated *N*-heterocyclic molecules were identified [59]), as presented in Figure 3.1 and Table 3.1, is striking. Krueger and Kissel emphasized that in addition to formic acid and formaldehyde, the presence of biologically important precursors of nucleobases in cometary dust particles was highly probable, whereas no indications have been found for, for example, amino acids, which would also form molecular ions if present [56]. PAHs and polyoxymethylene (POM) (see Section 2.5.6, which is about extended sources) populated rather small areas in the PUMA mass spectra [19]. Prior to further interpretation of these data, the reader should note that in the PUMA-1 mass spectra of the CHON-rich particles, the intensities of the  $m/z = 1, 12, 14,$  and  $16$  atomic species were reported to be more than 100 times greater (!) than the intensities of possible molecular species because most of the projectile molecules decompose into their atomic constituents upon impact [19]. The PUMA instruments were not designed for the detection and identification of molecular species.

**Table 1.1** Types of organic molecules that were inferred to be present in the captured dust particles analyzed using the PUMA-1 instrument onboard Vega 1.

	Chemical structure <sup>a)</sup>	Chemical name
CH compounds	$\text{HC}\equiv\text{C}(\text{CH}_2)_2\text{CH}_3$	Pentyne
	$\text{HC}\equiv\text{C}(\text{CH}_2)_3\text{CH}_3$	Hexyne
	$\text{H}_2\text{C}=\text{CH}-\text{CH}=\text{CH}_2$	Butadiene
	$\text{H}_2\text{C}=\text{CH}-\text{CH}_2-\text{CH}=\text{CH}_2$	Pentadiene
		Cyclopentene
		Cyclopentadiene
		Cyclohexene
		Cyclohexadiene
		Benzene
		Toluene
	CNH compounds	$\text{H}-\text{C}\equiv\text{N}$
$\text{H}_3\text{C}-\text{C}\equiv\text{N}$		Acetonitrile
$\text{H}_3\text{C}-\text{CH}_2-\text{C}\equiv\text{N}$		Propanenitrile
$\text{H}_2\text{C}=\text{NH}$		Iminomethane
$\text{H}_3\text{C}-\text{CH}=\text{NH}$		Iminoethane
$\text{H}_2\text{C}=\text{CH}-\text{NH}_2$		Aminoethene (tautomer)
$\text{H}_2\text{C}=\text{CH}-\text{CH}=\text{NH}$		Iminopropene
		Pyrroline, pyrrole, imidazole
		
		
		Pyridine, pyrimidine (and derivatives)
		
		
		urine, adenine
COH compounds	$\text{H}_2\text{C}=\text{O}$	Formaldehyde
	$\text{H}_3\text{C}-\text{CHO}$	Acetaldehyde
	$\text{HCOOH}$	Formic acid
	$\text{CH}_3-\text{COOH}$	Acetic acid (?)
	CNOH compounds	$\text{N}\equiv\text{C}-\text{OH}, \text{O}=\text{C}=\text{NH}$
$\text{N}\equiv\text{C}-\text{CH}_2-\text{OH}$		Methanolitrile
$\text{HN}=\text{CH}-\text{CH}=\text{O}$		Methanolimine (tautomer)
		Oxyimidazole
		Oxypyrimidine
		Xanthine

a) Constitutional isomers are also possible. Several types may form tautomers, mesomers, and conformational isomers. Thus, the molecules given here serve only as examples of the classes of substances that are possibly present in the organic component of the dust. The authors were not certain whether oxygen-containing species were present.

Adapted from [19, 57].

#### 1.4.1.2 Vega's Infrared Investigations and the Temperature of the Cometary Nucleus

The IKS (InfraKrasnoi Spectromètre) infrared spectrometer onboard Vega 1 and Vega 2 was designed for the detection of the emission bands of cometary parent molecules in the inner part of the coma and to measure the temperature of the cometary nucleus. The recorded IKS signals on Vega 1 (the cryogenic system of IKS on Vega 2 failed) were attributed to the vibrational bands of  $\text{H}_2\text{O}$  ( $\nu_3 = 2.7 \mu\text{m}$ ) and  $\text{CO}_2$  ( $\nu_3 = 4.25 \mu\text{m}$ ) and potentially to CH-bearing molecules ( $\nu = 3.2\text{--}3.5 \mu\text{m}$ ) [60]. The  $7.5\text{-}\mu\text{m}$  feature could be related to the presence of carbonaceous material that includes C–C bonds [60]. Marginal features were recorded at  $4.85$  and  $4.45 \mu\text{m}$  and tentatively attributed to OCS- and CN-containing molecules, respectively [61]. The IKS-determined temperature of the nuclear surface was measured to be  $300\text{--}400 \text{ K}$  [60], which is much greater than previously thought [53]. Other references suggest a surface temperature of  $\sim 330 \text{ K}$  [1]. This temperature was also much greater than the expected  $215 \text{ K}$ , which is necessary to sublimate water ice [18]. The apparently contradictory presence of ice in the cometary nucleus and the comet's high surface temperature can be explained by the assumption that the nucleus is covered by a thin insulating layer [60] (or mantle) of a black, porous, refractory substance with a thickness of  $\sim 1 \text{ cm}$ . There can be ice on the lower boundary of this layer at a temperature of  $\sim 200 \text{ K}$ , whereas the external boundary is  $100\text{--}150 \text{ K}$  warmer [53]. The sublimation is thought to occur a few centimeters below the cometary surface, and the gases pass through the porous dust layer to escape. Energy for the sublimation is transported down to the ice [18]. Molecules sublimate in the cometary interior; they are believed to flow to the cometary surface and be driven by a pressure gradient. This complex process is key for the understanding of cometary activity and was modeled by calculations for which parameters such as the porosity, pore size, permeability, surface-to-volume ratio, and thermal conductivity must be well estimated. What makes the system even more complicated is that the liberated gases may recondense during the outward flow [18]. Entrained dust particles that are larger than the critical pore size cannot be carried in the flow and will be trapped in the near-surface layers and thus form the dust mantle.

The *interior* temperature of the nucleus of 1P was derived via remote observation of the ratio of the nuclear spin isomers, as represented in ortho-water and para-water. These remote recordings deserve particular attention and will be described in Section 2.5.8. Regarding the *evolution* of the interior temperature of comets, we will see later in this book that some comets are thought to have heated their interior through radioactive decay processes, which are primarily due to the short-lived radioisotope  $^{26}\text{Al}$ . According to this assumption, such heating can result in the formation of liquid water in the interior of cometary nuclei.

The three-channel spectrometer (TKS) onboard Vega 1 and Vega 2 was designed for recording spectra in the infrared, visible, and ultraviolet domains. On Vega 1, the TKS failed completely, but the Vega 2 TKS measured spectra in the infrared and visible ranges; the UV channel did not function well [62]. TKS spectra were recorded at a distance of  $300 \text{ km}$  from the cometary nucleus. They provide information about the presence of OH, CH,  $\text{C}_2$ ,  $\text{C}_3$ , CN, and NH

species in comet 1P/Halley's dust [62]. TKS also observed various  $\text{NH}_2$  bands at  $\sim 560$  nm and signatures of diatomic  $\text{S}_2$  between 280 and 300 nm [63]. The claimed tentative finding of the PAH phenanthrene in the near-ultraviolet spectra of comet 1P/Halley based on the lines observed by Vega 2 TKS at wavelengths of  $\lambda = 347, 356, 364,$  and  $374$  nm [64] was later questioned [65] because of the rather low resolution of the spectra and the lack of confirmation of PAH bands in observations of other comets, such the observations of Hale-Bopp performed in 1997 [66]. In 2008, new laboratory spectra of anthracene were recorded under laser-induced fluorescence conditions in a jet-cooled molecular beam, and it was found that 1P/Halley's spectral features as recorded by TKS in the form of four main peaks at 363, 367.5, 373, and 382.5 nm are consistent with the laboratory fluorescence spectrum [67]. The detection of the PAH anthracene was thus reported. In 2004, this technique was applied to the three peaks at 371, 376, and 382 nm to suggest a tentative detection of the PAH pyrene in the coma of comet Halley [68]. The identification of PAHs in cometary comae was newly discussed in the light of data from samples of comet Wild 2 that were returned to Earth in 2006 by the Stardust mission (see Section 1.7).

#### 1.4.1.3 Vega's Analyses of Cometary Dust

Vega's dust particle counter SP-1 recorded the spectral and spatial distributions of dust grains. Masses of dust particles were measured down to  $10^{-16}$  g, and the dust production rates for different particle mass ranges were determined, with a total dust production rate of  $4 \text{ t s}^{-1}$  [69]. The dust coma was found to be quite inhomogeneous and to include strong, narrow jets [69]. In parts of these jets, heavier particles were observed before lighter particles [69]. The SP-2 data suggest a high density of submicrometer-sized particles in the cometary dust [70]. Vega's dust counter and mass analyzer (DUCMA) revealed that 1P/Halley's coma is highly dynamical on all spatial and temporal scales and exhibits remarkable quasiperiodic intensity fluctuations, thus suggesting a complex structure of localized regions of dust emission from the nucleus [71].

Further measurements from the scientific instruments of the Vega payload were used to study the neutral gas [72], plasma [73, 74], energetic ion [75], and electric [76] and magnetic field environment [77] of comet 1P/Halley. Vega's data that contributed to our current understanding of the cometary plasma tail were of particular importance. Therefore, cometary plasma tails will be introduced here; particular attention will be paid to the interpretation of Vega data.

#### 1.4.1.4 Solar Wind-Cometary Ion Interaction: the Plasma Tail

Usually, plasma tails, which are composed of molecular ions such as  $\text{CO}^+$  [78],  $\text{H}_2\text{O}^+$ ,  $\text{OH}^+$ ,  $\text{CO}_2^+$ ,  $\text{CH}^+$ , and  $\text{N}_2^+$  along with protons, other atomic ions, and electrons (see Section 1.3.1), are observed for comets at a heliocentric distance less than 1.5–2.0 AU. Comets at greater heliocentric distances and comets such as Ikeya-Seki that pass too close to the Sun may not exhibit plasma tails, the reason for which is not understood [18]. The plasma tail is electrically neutral. Electrons provide the negative charge.

The formation of the plasma tail is assumed to occur because of the interaction of cometary charged particles with the solar wind, which is an interplanetary gas that flows away from the Sun. Observations of cometary plasma tails were used by Ludwig Biermann from the Max Planck Institute of Physics in Göttingen to provide evidence for the existence of the solar wind [79]. In his original publication, Biermann did not use the phrase “solar wind”; instead, he referred to the solar corpuscular radiation (“Korpuskularstrahlung” in German) that accelerated the ions in cometary plasma tails. Biermann supported his predictions using the example of comet Whipple–Fedtke (1942g) [80]. His description introduced the concept of the solar wind. A typical aberration angle  $\varepsilon$  between the solar wind and plasma tail of  $5^\circ$  was determined; this value corresponds to a solar wind speed of  $\sim 450 \text{ km s}^{-1}$  and provided the required evidence for the existence of the solar wind [18]. We note that both the cometary dust tail and cometary ion tail point away from the Sun but not *exactly* in the anti-sunward direction.

It is evident that understanding the cometary plasma tail requires profound knowledge about the solar wind. Because many comets exhibit rapidly changing turbulent or disrupted plasma tails – some comets even exhibit plasma tails that turn at a rate of  $\sim 22^\circ$  per hour [18] – we anticipate that the interaction between the solar wind and cometary ions is often complex. The solar wind is composed of electrons, protons, alpha particles ( $\text{He}^{2+}$  ions), and heavier ions. It is affected by solar rotation and exhibits time-variable phenomena. A large bend that was visible in the plasma tail of comet Kohoutek on 20 January 1974 was attributed to a  $30 \text{ km s}^{-1}$  change in the solar wind speed [81].

The solar wind does *not* interact with the cometary nucleus, and its interactions with cometary dust and neutral molecules and atoms are limited [18]. The solar wind interacts with ionized molecules and electrons in the cometary plasma. Ionization of cometary molecules and atoms occurs because of photoionization by solar ultraviolet radiation; impact ionization from cometary and solar wind electrons; and charge exchange between solar wind protons and cometary molecules and atoms [18]. The solar wind has a high velocity of  $450 \text{ km s}^{-1}$ , which is much greater than the velocity of ions in the cometary plasma ( $1\text{--}2 \text{ km s}^{-1}$ ). The interaction between the solar wind and cometary ions is such that the velocity of the solar wind decreases [18] as the wind entrains cometary ions that contribute to heating [13].

#### 1.4.1.5 Bow Shock, Cometopause, and Contact Surface

In the vicinity of the comet, the deceleration of the solar wind is stronger than in regions that are far from the nucleus. Here, the velocity of the solar wind flow changes from supersonic to subsonic, thereby creating a bow shock or outer shock [13], which develops over a distance of  $\sim 10^6 \text{ km}$  sunward from the cometary nucleus [18]. In 1964, Axford correctly predicted that a comet with ionized expanding coma gas should act as an obstacle to the supersonic solar wind, and he expected a bow shock to form  $10^4\text{--}10^5 \text{ km}$  upstream of the comet [82]. Ip and Axford emphasized that at the bow shock, the thermal pressure rapidly increases by a factor of 30, whereas the flow speed decreases

by  $\sim 25\%$  [17]. The evolution and bow shock formation of a comet *approaching* the Sun [83, 84] will be described in Section 5.4 using the example of comet 67P/Churyumov-Gerasimenko, which is the target of the Rosetta mission.

After crossing the bow shock, the incoming flux of solar wind particles enters the cometopause. The cometopause is a unique feature and was first observed by the Vega plasma instruments at a distance of  $\sim 10^5$  km from the 1P nucleus. The cometopause is the boundary that separates the fast-moving solar wind plasma from the cold, slow plasma flow of cometary origin [17]. It describes the region in which cometary ions picked up by the solar wind add significantly to the wind's mass [13]. The flux of solar wind ions thus decelerates to a velocity of a few tens of kilometers per second, and it deeply penetrates the comet coma [13]. In the cometopause, solar wind protons and  $\text{He}^{2+}$  particle intensities decrease suddenly, whereas the comet ion density – including  $\text{H}_3\text{O}^+$  and cold  $\text{O}^+$  ions – increases rapidly with a radial dependence of  $1/R^2$  [17]. At a distance from the cometary nucleus of  $\sim 6-8 \times 10^4$  km, the solar wind protons and hot oxygen ions were observed to disappear completely [85]. For mass ratios ranging from 1 to  $85 m/z$ , the Vega plasma analyzer delivered data to deduce the main parts of the ionospheric composition. In addition to signals at  $m/z = 18, 28, \text{ and } 44$ , broad count rate maxima were found at  $m/z = 56, 70, \text{ and } 85$ , thereby revealing for the first time the presence of ions more massive than  $\text{CO}_2^+$  [17] in the comet's ionosphere. The general processes that are associated with the expansion of the neutral coma gas, followed by photodissociation, photoionization, and then charge exchange with the solar wind ions at different regions in the coma, are depicted in Figure 1.12 [17].

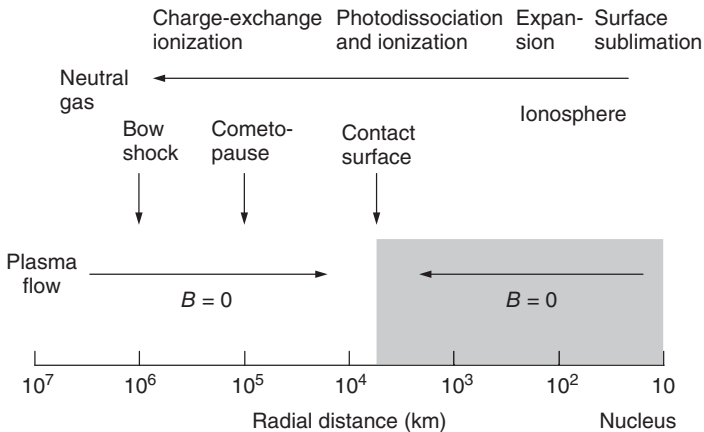


**Figure 1.12** The physical processes are associated with the interaction of the expanding cometary ionosphere with the fast-moving solar wind plasma and cause the formation of the bow shock, cometopause,

and contact surface. There is no intrinsic magnetic field that acts on the expanding gas that results from sublimation processes on the cometary nucleus. (Adapted from [17].)

The contact surface, which is the boundary that separates the inner pure cometary plasma close to the nucleus from the mixed cometary and solar wind plasma [18], follows. As stated by Ip and Axford, the contact surface divides the plasma of the mass-loaded solar wind from the plasma that is associated with the cometary ions [17]. The magnetized solar wind does not penetrate the contact surface [18]. Between the cometopause and the contact surface, solar wind particles can interact directly with cometary molecules, with which they undergo multiple charge-exchange reactions [13]. The reader should note that at distances greater than 5 AU, a typical cometary nucleus does not emit enough water molecules to provide a protective atmosphere; thus, the nucleus is directly exposed to the solar wind and solar ultraviolet radiation [19]. Consequently, the surface of the nucleus becomes electrically charged, mainly by the photoelectric effect, which provides a surface potential of  $\sim +5$  V [19].

We conclude that the cometary ion tail is composed of a mixture of cometary and solar wind ions. These ions are deviated around the comet's contact surface by the resistance offered by the escaping cometary ions [13]. Accelerations of up to 1000 times that of solar gravity have been measured in the tail. The radiation pressure that produces the dust tail is known to produce minor accelerations on the order of 1–200 times that of solar gravity on light atoms and on fine dust particles [13]. More detailed information about the large-scale processes of the solar wind–comet interaction, the plasma tail ion composition, ionospheric processes, the thermal structure of the ionosphere, plasma wave turbulence, ion acceleration, and the International Cometary Explorer (ICE) mission that passed through the onset of the ion tail region of a comet (21P/Giacobini-Zinner), thereby indicating ion acceleration processes in the vicinity of a comet for the first time, can be found in Ref. [17].

The results of the joint NASA–ESA Ulysses space probe revealed that the solar wind emitted from the Sun is not constant [86]. The solar wind emitted from the polar regions exhibits small variations and a speed of  $750 \text{ km s}^{-1}$ , whereas the solar wind emitted at equatorial latitudes exhibits large variations and a speed of  $450 \text{ km s}^{-1}$  [18]. As a consequence, comets that pass the polar region of the Sun are exposed to a faster and relatively constant solar wind, whereas comets that pass the equatorial region of the Sun are exposed to a slower and gustier solar wind [18]. In the polar region of the Sun, the cometary plasma tail points close to the antisolar direction because of the high solar wind speed. The fine structure expressed in plasma tails implies that magnetic fields exist in comets [18].

#### 1.4.1.6 Plasma Tail Disconnection Events

As depicted in Figures 1.11 and 1.13, plasma tails may undergo spectacular phenomena in which the entire plasma tail detaches from the cometary head and a new tail forms. These phenomena are called *disconnection events*.

The solar wind exhibits a feature called the *heliospheric current sheet* (HCS). The HCS is caused by the rotation of the Sun and provides information about the morphology of the magnetic field that surrounds the Sun, which is known to exhibit two hemispheres of opposite magnetic polarity [18]. The HCS, which



**Figure 1.13** A disconnection event of the plasma tail observed for comet Borrelly on 24 July 1903. The photographic observation was performed at Yerkes Observatory [87].

surrounds the Sun like the brim of a hat, represents the magnetic equator. If a comet, with its cometary plasma, crosses the HCS, a magnetic field of opposite polarity is pressed into the comet, and reconnection of the plasma tail occurs, as first proposed by Niedner and Brandt [88].

From 1985 to 1986, 19 ion tail disconnection events were observed for comet 1P/Halley, one of them during the time of passage of the Halley Armada. Brandt *et al.* [89] associated all of these 19 disconnection events with crossings of the HCS, and Vega 1 and Vega 2 data confirmed the reversal of the polarity of 1P's magnetic field [89]. Vega 1 passed prior to the disconnection event, and Vega 2 passed comet 1P/Halley after the disconnection event. Because of the Vega missions' observations of the cometary ionosphere, for the first time, the existence of an HCS-triggered disconnection event could be demonstrated. It should be

noted that the fascinating Niedner–Brandt model for the explanation of ion tail disconnection events was called into question because of data obtained from the Sakigake spacecraft (see later). Saito *et al.* [90] compared Sakigake’s plasma data with ground-based observations and found that *no* distinct disconnection event was observed for comet 1P/Halley’s ion tail even though Sakigake crossed the HCS at least four times. Ip and Axford concluded that the generation of plasma structures, such as disconnection events, in ion tails could be a complicated process that does not necessarily conform to the simple Niedner–Brandt scenario and proposed alternative explanations [17].

The data from the Vega mission enabled the European mission Giotto to optimize its comet-approaching navigation because the two Vega spacecraft reached comet 1P/Halley a few days before Giotto and the Vega trajectories were precisely known through the use of very long-baseline interferometry [91]. The Vega 1 and Vega 2 space probes were the last successful planetary space probes of the Soviet Union.

#### 1.4.2

#### The Japanese Spacecraft Suisei and the Cometary Hydrogen Corona

The 1986 Armada of space probes to comet 1P/Halley included two Japanese spacecraft, Sakigake (Japanese for “forerunner”) and Suisei (Japanese for “comet”). These interplanetary missions were a new experience for the ISAS [51]. Both spacecraft were almost identical, except for the scientific payload. Due to strict weight constraints, both Japanese spacecraft were – in contrast to Vega – not protected against cometary dust impacts [51]. Sakigake and Suisei were launched with M-3SII launchers from the Kagoshima Space Center in Uchinoura, Japan, on 8 January 1985 and 18 August 1985, respectively. The closest cometary flybys of Sakigake and Suisei were on 11 March 1986 and on 8 March 1986 at a high relative velocity of  $\sim 73 \text{ km s}^{-1}$  [51].

The Suisei space probe was designed to explore the plasma environment and hydrogen corona of comet 1P/Halley from a distance of 200 000 km on the sunward side. At this position, few dust particles were expected [51]. Later, Suisei was maneuvered to a closer distance of 150 000 km to measure cometary ions. The hydrogen corona that surrounded the cometary coma was observed by Suisei’s ultraviolet imager. The hydrogen cloud that is now known to surround a comet was predicted in 1968 by Biermann, who assumed a total production rate of  $10^{30} - 10^{31} \text{ atoms s}^{-1}$  [92]. Suisei’s ultraviolet imager instrument recorded the time variation of the Lyman- $\alpha$  intensity of the coma of comet 1P/Halley and found that the total brightness of the hydrogen coma changed rhythmically or periodically [93] and exhibited pulsations [14]. The obtained data revealed that 1P’s hydrogen corona has a shell structure [51] due to periodic cometary outbursts [93]. It is believed that periodicity in the brightness of the hydrogen coma is caused by outbursts or jets from nuclear surface features, such as fractures or holes, that are activated when rotation of the nucleus brings it into a position in which it is illuminated by the Sun [93]. The periodicity cannot be

caused by continuous sublimation from the entire cometary surface. Today, it is known that the hydrogen cloud that surrounds a comet contains H, O, and OH, with H<sub>2</sub>O being the parent molecule [18].

Solar wind and cometary ions were observed by a charged-particle energy analyzer. The instrument allowed for the identification of not only proton ions but also ions of water, carbon monoxide, carbon dioxide [51], and CH<sup>+</sup> [94]. The data revealed the existence of an assimilation process of cometary ions in the solar wind flow [94], and shell structures in the velocity space of cometary protons and water-group ions were detected [94].

### 1.4.3

#### The Japanese Spacecraft Sakigake

The scientific payload carried by Sakigake was developed to characterize the solar wind by measuring its bulk velocity ( $v \approx 450 \text{ km s}^{-1}$ ), flow direction (determined in degrees), ion density (up to  $30 \text{ cm}^{-3}$ ), and ion temperature ( $T \approx 10^5 \text{ K}$ ) [95] before and on the day of the encounter with comet Halley. The obtained data hint at a deceleration of the solar wind due to its interaction with the cometary atmosphere. This assumption remained hard to verify because it was difficult to isolate the effect of the comet on solar wind parameters from background disturbances [95]. Moreover, the interaction of the interplanetary magnetic field with the comet was analyzed by Saito *et al.* [90], who provided data to interpret possible origins of the ion tail disconnection events, and plasma waves in the low-frequency and extremely low-frequency ranges were recorded [51]. These waves are thought to at least partially originate from plasma instabilities that are associated with the pickup of cometary ions by the solar wind [96].

Ip and Axford describe Sakigake's discovery of cometary kilometric radiation (CKR) as somewhat surprising: discrete radio emissions in the frequency range of 30–195 kHz were recorded by the plasma wave experiment. These emissions may result from conversion of the electrostatic plasma waves to electromagnetic waves in the turbulent plasma environment of comet Halley [17].

### 1.5

#### The Giotto Spacecraft and the First Image of a Cometary Nucleus

ESA's mission Giotto, which was named after the medieval Italian painter Giotto di Bondone (1267–1337), who in 1304 depicted comet Halley as the “star of Bethlehem” in one of the frescoes in the Scrovegni chapel in Padua (Figure 1.14) [7], appeared to be the most sophisticated of the five great 1986 cometary missions [50]. ESA originally planned to contribute a satellite to a US mission to comet 1P/Halley, which was planned to approach the comet at a shorter distance than its mother US space probe. This collaboration between NASA and ESA was initially formed to realize the International Comet Mission (ICM) [18]. Because of problems with a solar–electric ion propulsion system (IPS), the US space



**Figure 1.14** The interior of the Scrovegni Chapel in Padua is decorated by a fresco cycle that includes the “Adoration of the Magi” fresco, which is depicted here. The Florentine master Giotto di Bondone painted the fresco, most likely in 1303 and 1304.

Giotto di Bondone was most likely inspired to depict the Star of Bethlehem as a comet because comet 1P/Halley had appeared in 1301. ESA’s spacecraft Giotto was named after the artist Giotto di Bondone. (Image credit: ESA.)

probe to comet Halley was never realized and ESA developed the cometary probe Giotto independently.

### 1.5.1

#### The Passage through a Cometary Coma

The Giotto spacecraft was successfully launched on 2 July 1985 using an Ariane-1 rocket from Kourou, French Guyana. It encountered comet 1P/Halley on 14 March 1986, as depicted in the artist’s illustration presented in Figure 1.15. At that time, 1P had passed perihelion [97]. The Vega and Giotto encounter parameters are summarized in Table 1.2. The Giotto space probe passed through 1P’s coma and encountered only  $\sim 10^{14}$  molecules  $\text{m}^{-3}$ , which corresponds to less than  $10^{-12}$  times the density of air at sea level [14]. The Giotto spacecraft and its instruments were protected from the impact of cometary dust particles. A cometary dust particle with a mass of 0.1 g and a velocity of  $68 \text{ km s}^{-1}$  can penetrate an 8-cm-thick solid aluminum sheet. Protection of the Giotto spacecraft against high-velocity dust particle impacts was essential for the spacecraft to

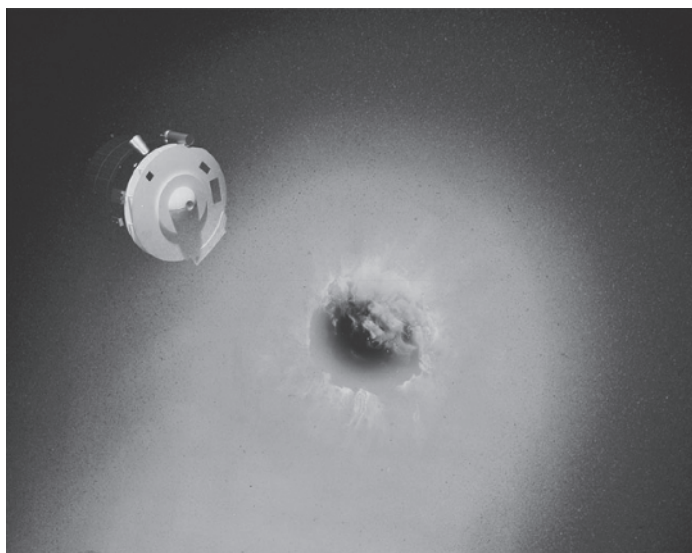


**Figure 1.15** Artist's illustration of Giotto's encounter with comet 1P/Halley on 14 March 1986. The Giotto space probe is protected by its white dust shield. In the center of the dust shield, white shells are visible; these shells closed the nozzle of the solid propellant boost motor after firing. Giotto's cylindrical Halley Multicolor Camera (HMC) is located on top of the space probe, and the starmapper is on its left. (Image credit: ESA.)

**Table 1.2** Vega and Giotto encounter parameters. (Adapted from [4].)

	Date 1986	Time (UTC)	Distance of closest approach (km)	Relative velocity ( $\text{km s}^{-1}$ )	$r$ (AU)	$\Delta$ (AU)
Vega 1	6 March	07:20:06	8889	79.2	0.7923	1.153
Vega 2	9 March	07:20:00	8030	76.8	0.8341	1.073
Giotto	14 March	00:03:01.84 $\pm$ 0.20	596 $\pm$ 2 <sup>a)</sup>	68.4	0.9023	0.960

a) Determined by HMC.

approach to within a few hundred kilometers of the nucleus, where dust fluxes are high [7]. Because it was out of the question to equip the Giotto space probe with a 600-kg aluminum shield, Giotto was protected by a dual-sheet bumper shield that could withstand the impact of dust particles of masses up to  $\sim 1$  g [7]. In Figure 1.16, the dual-sheet bumper shield can be observed on the bottom of the image. The closest approach of the Giotto space probe to the nucleus of comet 1P/Halley, which occurred on 14 March 1986, was rather spectacular because, 14 s before its closest approach, Giotto was hit by a “large” dust particle of size 1–10  $\mu\text{m}$  [7]. Another deceleration was reported 7 s prior to Giotto's closest cometary approach and was caused by an impacting particle with a mass of  $\sim 0.4$  g [19]. Because of these impacts, the spacecraft angular momentum vector was

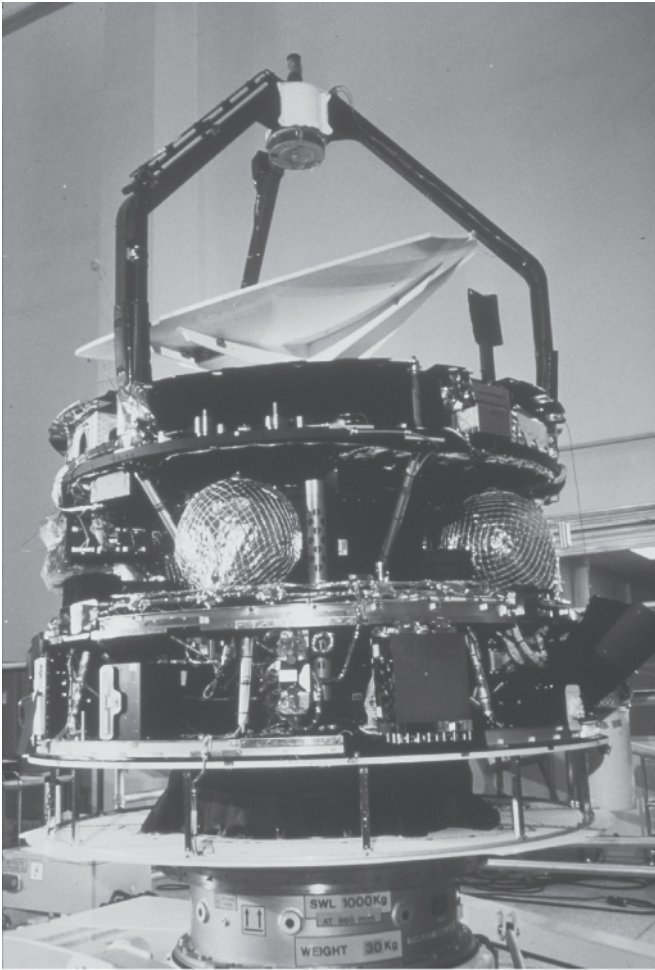


**Figure 1.16** The Giotto space probe depicted in May 1985 prior to launch during the integration phase in Toulouse. The two protective 1-mm-thick aluminum and 12-mm-thick Kevlar Whipple-type sheets, which were 23 cm apart, are visible on the bottom of the image. The aluminum vaporized incoming dust particles, whereas the protecting Kevlar sheet absorbed the debris; the energy of the vaporized dust particles was thus dissipated over a large area. The cylindrical white instrument on the right that is pointed downward toward the comet is the HMC. The starmapper is pointing upward and located to the left of the HMC. The two

visible silver spheres on the main platform belong to the four tanks that contained the hydrazine  $N_2H_4$  fuel for orbit and attitude correction. The high-gain dish antenna on the top of the image had a diameter of 1.47 m and points toward Earth. The low-gain cardioid antenna, through which the first contact was made with the spacecraft for reactivation, was located on top of the high-gain dish antenna. The Giotto space probe was mantled by solar cell arrays, which are not depicted here. The total mass of the Giotto spacecraft was 584 kg. (Image credit: ESA.)

shifted by  $0.9^\circ$ , and the spacecraft performed a nutation around the new axis with a period of 16 s [7]. This impact complicated telecommunication between Giotto and Earth, and some instruments and experiments suffered.

### 1.5.2

#### Imaging a Cometary Nucleus

The Giotto spacecraft succeeded at directly observing the cometary nucleus from the sunward side. The Sun–comet–Giotto angle was  $107^\circ$  [4]. The most important finding of Giotto was the clear identification of the cometary nucleus made by the Halley Multicolor Camera (HMC) [7]. At that time, the existence and size of cometary nuclei were unknown [7]. Giotto's HMC camera was designed to take pictures of the cometary nucleus by approaching to a closest approach distance of 600 km. However, the Giotto spacecraft, on which the HMC was mounted, rotated with a 4-s rotation period [4]. Comet 1P/Halley could only be observed by HMC for a few milliseconds at a certain phase during each spin period [10]. It could not be followed continuously. The position and exact moment of the next image had to be predicted using a complicated tracking program [10]. It was particularly difficult to obtain high-resolution images from a spinning spacecraft.

The HMC could be operated in single detector mode (SDM) and multidetector mode (MDM). For calibration and test purposes, the HMC recorded images of the planet Jupiter in September 1985, 2 months after launch. In October 1985, the HMC took MDM images of the planet Earth, thereby demonstrating that the HMC was fully operational [10]. On 14 March 1986, the HMC took the first image of comet 1P/Halley 3:06 h before closest approach, when the distance to the nucleus was greater than 773 000 km [10]. The camera operated in SDM. A total of 2043 images were taken in SDM before switching to MDM 6 min before closest approach [10]. The first MDM image was taken 295 s before closest approach at a distance of 20 200 km [10]. Data transmission was interrupted shortly before closest approach, and the last transmitted HMC frame was taken 15 s before closest approach [10]. The last useful image that shows details of the cometary nucleus was taken from a distance of 1680 km [4, 10, 98]. A composite image is given in Figure 1.17. The HMC operation was interrupted by a reset of one of the microprocessors [10]. The resolution of the recorded images varies from 50 m/pixel near the bright, top end of the nucleus to 320 m/pixel near the dark, bottom end [99].

As the Giotto space probe passed the cometary nucleus at a distance of 602 km<sup>11)</sup> [10], the encounter velocity between the probe and the cometary nucleus was very high ( $68.4 \text{ km s}^{-1}$ ) compared with the speed of the ejected cometary gas and dust particles, which is a few hundred meters per second [7]. Giotto thus observed an essentially static situation as it traversed the coma, and all dust particles struck the spacecraft from the forward direction [7]. Pictures taken by Giotto's HMC

11) The closest approach distance of 602 km was determined in real time by Giotto's onboard software, which analyzed the images. An Earth-based analysis provided a value of  $591.5 \pm 2 \text{ km}$  [10].



**Figure 1.17** The nucleus of comet 1P/Halley as imaged by the HMC camera onboard ESA's Giotto spacecraft on 14 March 1986. The figure, which shows considerable detail, is a 68-image composite. The distance from the cometary nucleus at which the HMC took the images was  $\sim 2000$  km. The Sun is on the left at  $\sim 17^\circ$  behind the image plane [4] and caused outbursts on the dayside of

comet 1P/Halley. Because of the  $107^\circ$  phase angle, most of the nuclear surface that faces the observer is not illuminated. The terminator – the line that separates the illuminated side from the dark side – is observed from the northern tip to the southern sunward limb [4]. (Image credit: ESA and Max Planck Institute for Solar System Research.)

show the irregular nonspherical shape of the cometary nucleus, which was visible in the reflected sunlight [98], and its size of  $15.3 \times 7.2 \times 7.2$  km, which represents a 2:1 elongation. The size was much larger than the anticipated 6 km [4], and the nucleus was aspherical. The minor axis of the comet was directed sunward. The 2:1 elongation ratio represented a much greater deviation from a spherical nucleus than had been anticipated [1]. For the first time, the existence of a solid, single cometary nucleus, as predicted by Whipple [9], was proven beyond any doubt [4].

#### 1.5.2.1 Topographic Structures on a Cometary Nucleus

The HMC revealed the topographic structures, morphology, and color of the nuclear surface for the first time [4]. The surface of Halley's nucleus was found to be irregular and exhibit spherical structures, which were interpreted as impact craters, valleys, hills [7], and chains of hills [10]. A circular shape ("crater")

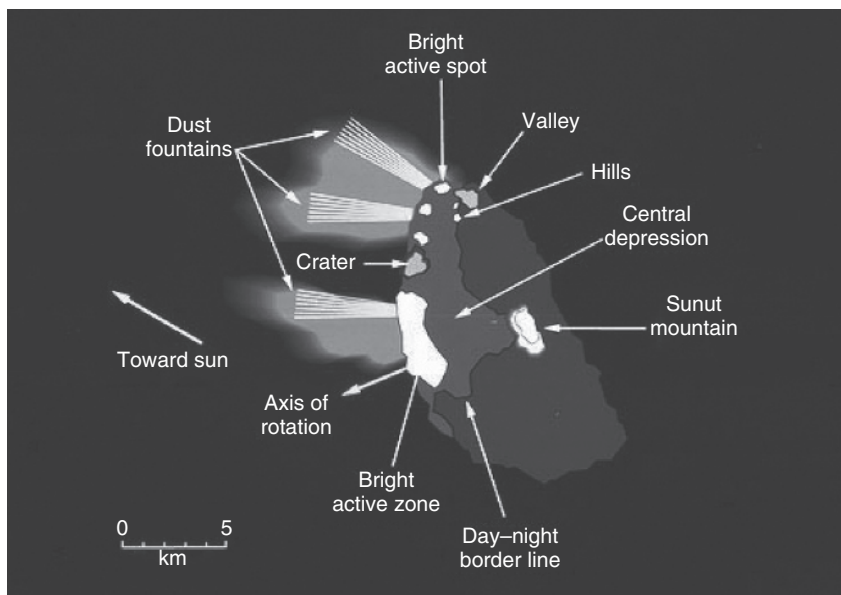


**Figure 1.18** The principal features identified on the nucleus of comet 1P/Halley. Valleys, hills, depressions, a crater, and a mountain are visible, as are the comet's active areas and the day–night borderline. The scattered light from the dust fountains at a  $107^\circ$  phase angle was redder than the reflected light from the nucleus. Keller argued that the chemical composition of the dust grains, with their high content of organic material, caused this effect [4]. (Image credit: ESA.)

with a diameter of 1600 m and a minimum depth of 100 m was identified on the cometary nucleus, and other circular features seemed to be visible [10]. A mountain less than 1000 m in height was observed to be located at the center of the nucleus [4]. The principal features identified on the surface of comet 1P/Halley are indicated in Figure 1.18. The considerably less precise Vega images of the nucleus of comet 1P/Halley taken between 4 and 11 March 1986 [18] were used to estimate the size of the “irregular potato-shaped” cometary nucleus to be  $14 \times 7.5 \times 7.5$  km. A rotation period of 53 h was obtained from a comparison of the images obtained by Vega 1 and Vega 2 [11, 53], and a period of 54 h was determined by including the Giotto data [10]; these periods correspond to approximately 2.2 days. However, until 1990, it had *not* been possible to accurately determine the rotational position of the nucleus [4]. In 1991, the value for 1P's rotation period was simultaneously correctly determined by Belton *et al.* [100] and Samarasingha and A'Hearn [101] to be 7.3 days, who determined that the originally assumed orientation of the large end of 1P's long axis during the Vega 1 encounter had to be reversed. Note that the spin axis is not perpendicular to the comet's orbital plane; moreover, the spin axis is neither the long nor the short axis of the cometary nucleus. The volume of 1P/Halley's nucleus was determined to be  $420 \text{ km}^3$ , and its density was determined to have the quite low

value of  $0.55 \pm 0.25 \text{ g cm}^{-3}$ , perhaps only  $0.2 \text{ g cm}^{-3}$  [10]. Comets are thus the lowest density bodies in the Solar System. They are very fragile. Cometary nuclei are expected to exhibit low heat conductivity and heat capacity, which prevents cometary activity from continuing on the night side [10].

### 1.5.2.2 The Albedo of the Cometary Nucleus

Giotto's measurement of the geometric albedo  $p$  of the cometary surface was a tremendous scientific surprise. Estimations for  $p$  varied; some values were as high as  $p = 0.6$  [18].<sup>12)</sup> Giotto observed that the surface of 1P/Halley's nucleus is dark and exhibits a very low geometric albedo of  $p = 0.04$ , thereby indicating that the comet's nucleus at full phase has about one-third the reflectivity of the moon [10, 98]. The albedo value is one of the lowest of all known objects in the Solar System [98]: only some C-type asteroids and Saturn's moon Iapetus exhibit smaller values as low as  $p = 0.01$  [102]. Keller *et al.* [98] concluded that most of the surface of the nucleus of comet 1P/Halley must be covered by a nonvolatile insulating crust of dark material that traps light in tiny cavities between fluffy dust particles because of its high porosity. The temperature of the crust must become much hotter than the equilibrium temperature for the sublimation of water ice [98]. Keller *et al.* [10] suggests that the crust or mantle is more than several centimeters thick. Furthermore, the Giotto images of the cometary nucleus indicate that main parts of the surface of the cometary nucleus are inactive. Thus, models that describe the nucleus as uniform were found to be inadequate [98].

### 1.5.2.3 Gas- and Dust-Emitting Areas on the Nucleus of 1P/Halley

Giotto observed that the gas and dust emissions from 1P/Halley were not uniform over the entire cometary surface [18]. Gas and dust were only emitted into space in an anisotropic manner in the form of discrete jets from specific cometary regions. The regions were typically kilometer sized and pointed toward the Sun. In his seminal work of 1950, Whipple had already noted that the sunward ejection of material from cometary nuclei had long been recognized for the bright comets [9]. In the near-source region, the acceleration zone, the dust accelerates through interaction with the gas that streams away from the surface [4]. Nevertheless, the active areas account for approximately 10% of the entire cometary surface [98]. Seven main jets were observed and were labeled with the letters A through G [98]. There was an attempt to correlate the observations of the jets with ground-based observations of comet 1P/Halley [103]. A more precise analysis of Giotto's HMC data revealed two areas of major activity and at least 13 faint, narrow jets [10]. Most of the cometary activity appeared to originate from only a few discrete sources [7, 98] on the afternoon hemisphere of the cometary nucleus [10],

12) The albedo (Latin: white color; German: *Die Albedo*) is a quantification of the backscattering of light by diffuse reflecting surfaces. The geometric albedo is the ratio of the amount of irradiating light over the diffuse light that is re-emitted into a half-sphere. The spherical

albedo is the ratio of the irradiating light over the light that is re-emitted into all directions of space. Usually, a given surface exhibits a slightly higher value for the spherical albedo than for the geometrical albedo.

and active areas did not seem to exist on the nighttime side [98]. The nighttime region of the cometary nucleus appeared on the HMC images as a dark silhouette against the background dust [10]. If evaporation of the ice continues into the cometary evening, recondensation and freezing may occur in the crust, thereby causing subsequent cracking under thermal stresses [98]. The surface crust that prevents free sublimation of the icy conglomerate must thus have a variable thickness [98]. Giotto determined the gas production rate to be  $3.1 \times 10^6 \text{ g s}^{-1}$  [104], which had been estimated from ground-based experiments in November 1985, when the comet was in a distance of 1.75 AU from the Sun to be  $1.5 \times 10^6 \text{ g s}^{-1}$  [105]. Giotto's observed gas production rate agrees with observations of the International Ultraviolet Explorer (IUE), which observed comet 1P/Halley while all Giotto Armada spacecraft passed the comet [106]. The gas production rate of the nucleus of comet 1P/Halley correlates to an approximately 6-m-thick lost layer per orbital revolution [10]. Assuming 30 revolutions of the short-period comet 1P/Halley, this rate amounts to less than 200 m [10]. Others assume hundreds, if not thousands, of passages of comet 1P/Halley through the inner Solar System [99].

#### 1.5.2.4 The Formation of the Nonspherical Nucleus of 1P/Halley

How did the shape of comet Halley's nucleus develop? Keller *et al.* concluded from the HMC data that it is improbable for the nucleus of comet 1P/Halley to have formed as a spherical body because the ellipsoidal shape could not be formed by preferential sublimation over long time intervals [10]. A nonuniform sublimation process that yielded the observed shape of the cometary nucleus starting from a spherical body could have occurred if sublimation was suppressed by a crust on both ends of the nucleus. This model clearly disagreed with the strong activity level observed during the Vega 1 flyby, when an end of the cometary nucleus pointed toward the Sun [10]. The ellipsoidal "potato-like" shape of the cometary nucleus had to be formed during the creation process due to either a collision of two subnuclei or the breakup of a larger body during the early period of formation [10]. Inhomogeneities in the cometary coma – such as in the grain sizes and chemical composition – and also the variability in cometary activities could be explained by the nucleus of comet 1P/Halley being formed by different subnuclei of as much as a few kilometers in diameter [10]. The accumulation of only very small subnuclei of a meter or less in size was ruled out by the extremely nonspherical shape of the nucleus and the morphology of its surface [1].

Keller *et al.* [10] furthermore concluded from Giotto's HMC data that a large body, such as the cometary nucleus, cannot form easily because of its low density, particularly if collisions of subbodies are involved. In 1987, the authors wrote that laboratory experiments with low-density icy materials and extremely low temperatures were "urgently needed" [10] to better understand the formation of low-density cometary nuclei.

In addition to the camera for imaging the cometary nucleus and inner coma, Giotto's scientific payload comprised nine experiments: three mass spectrometers for analyzing the elemental and isotopic composition of cometary neutrals,

ions, and dust particles; various dust-impact detectors; a photopolarimeter for measuring the coma brightness; and a set of plasma experiments for studying the interaction processes between the solar wind plasma and the cometary ionosphere [7].

### 1.5.3

#### The Chemical Composition of Cometary Dust

Giotto intensively analyzed the chemical composition of the emitted jets. The jets were found to be composed of 80% water (v/v) [107], carbon monoxide (10%), carbon dioxide, formaldehyde, methanol, methane, ethane, ethylene, acetylene, ammonia, hydrogen sulfide, and hydrogen cyanide [108]. Ions such as  $\text{H}_2\text{O}^+$ ,  $\text{C}^+$ ,  $\text{CO}^+$ , and  $\text{S}^+$  were identified in the cometary atmosphere [109]. The occurrence of some ions was associated with the presence of hydrocarbons [110], and classical CN and  $\text{C}_2$  emission bands were observed in the spectra 1P/Halley's coma [111].

Data of outstanding scientific importance were provided by performing chemical analyses of cometary dust particles: Giotto contained the Dust mass spectrometer onboard Giotto (PIA), which was the counterpart of the PUMA instruments onboard Vega 1 and Vega 2 [55]. PIA was a time-of-flight mass spectrometer for positively charged ions produced from solid cometary dust particles that hit the target in front of the spectrometer. The instruments differed conceptually in that PIA used a silver-doped platinum foil as the target material to provide the ionization, whereas PUMA-1 used a corrugated silver plate and PUMA-2 used a flat, solid-silver plate [19]. PIA was thus designed to study the chemical and physical nature of cometary dust particles. Its spectacular and unexpected data revealed that cometary particles contain not only hydrogen (with its isotopes, deuterium and tritium) and oxygen but also carbon and nitrogen atoms. One of the significant surprises of the Halley encounters was the detection of large amounts of carbonaceous dust that was rich in H, C, O, and N, the so-called CHON particles [1]. The observation of CHON particles by PIA agrees with PUMA data (see Section 1.4.1) and suggests the presence of organic molecules on the cometary nucleus. In addition to these elements, metal ions of Na, Mg, Si, and Fe were found [112]. Comet 1P/Halley's total content of organic material was greater than the mineral content by a factor of 3–10 [113]. The PIA observations indicated some variations in the particle composition, number density, and density as function of the location within the coma, thereby suggesting compositional heterogeneity of the source region and, hence, of the nucleus [4]. This result is another important finding. However, the PIA mass spectrometer was not sensitive to the direct detection and identification of intact organic molecules. Organic molecules – if present in the surrounding ices of cometary dust particles – would not entirely survive the impact of the solid cometary particles onto the ionizing target of the PIA mass spectrometer, which occurred with an impact velocity of  $\sim 68 \text{ km s}^{-1}$ .

In addition to PIA, Giotto's Neutral Mass Spectrometer (NMS) allowed for the precise identification of carbon monoxide and water molecules and hydrogen and oxygen isotopes in the cometary coma [114]. These data will be

presented in detail in Section 2.5.6, which discusses potential extended sources of volatiles in cometary comae, and in Section 3.1, which addresses isotopic water fingerprinting.

#### 1.5.4

##### The Radio Science Experiment and Cometary Ionosphere

The Giotto Radio Science Experiment (GRE) recorded a deceleration of the Giotto spacecraft because of drag effects in the cometary atmosphere. The change in the velocity of the spacecraft was determined to be  $16.7 \text{ cm s}^{-1}$ , which corresponds to a Doppler frequency of 4.7 Hz. Edenhofer *et al.* [115] estimated, through knowledge of the total mass of the spacecraft (573.7 kg) and the encounter velocity ( $68.37 \text{ km s}^{-1}$ ), that the total mass of cometary material that struck the spacecraft was 0.1–1 g.

Energetic ions in the environment of comet 1P/Halley were investigated by McKenna-Lawlor and colleagues [116]. As outlined earlier, the ionosphere of a comet is assumed to originate from the sublimation of atoms and neutral molecules from the cometary nucleus into the inner coma of the comet. Due to the low gravitational force of a typical comet, the escape velocity is  $\sim 1 \text{ km s}^{-1}$  [14]. In the inner coma, atoms and neutral molecules are subjected to various chemical reactions. Farther out, they are subjected to a variety of photodissociative and ionizing processes. The ionized particles are then entrained by the solar wind and gain energy, and are convected away in the anti-sunward direction. The predominant species in the outer atmosphere of comet Halley were recorded to be  $\text{O}^+$ ,  $\text{OH}^+$ , and  $\text{H}_3\text{O}^+$ , the so-called water-group ions [116]. However, the pickup process by the solar wind was found to be insufficient to account for the high energies observed for these and other typical ions in the cometary ionosphere, and other acceleration mechanisms were postulated by the McKenna–Lawlor team.

Giotto precisely investigated the interaction between the solar wind plasma, including its protons and  $\alpha$ -particles [117], electrons [118], and magnetic field [119], and the cometary ionosphere. As illustrated in Figures 1.12 and 1.19, these interactions are characterized by two distinct boundaries, the bow shock and the contact surface [7]. The bow shock was encountered by the Giotto space probe at a distance of  $1.15 \times 10^6 \text{ km}$  from the nucleus. At a distance of 16 400 km from the nucleus, the magnetic field strength attained a maximum value of 57 nT [7]. The contact surface was crossed by the spacecraft at a distance of 4700 km, where the magnetic field decreased to essentially zero [7, 118]; this decrease had been theoretically predicted. The existence of the bow shock, contact surface, and magnetic cavity had been predicted before the comet encounters, but new insight was gained through detailed *in situ* investigations of the plasma features and the regions between them, including the discovery of the cometopause (see Section 1.4.1) [1].

The interaction between the solar wind and cometary ionosphere involves the loading of the solar wind by cometary ions. At large distances from the comet,

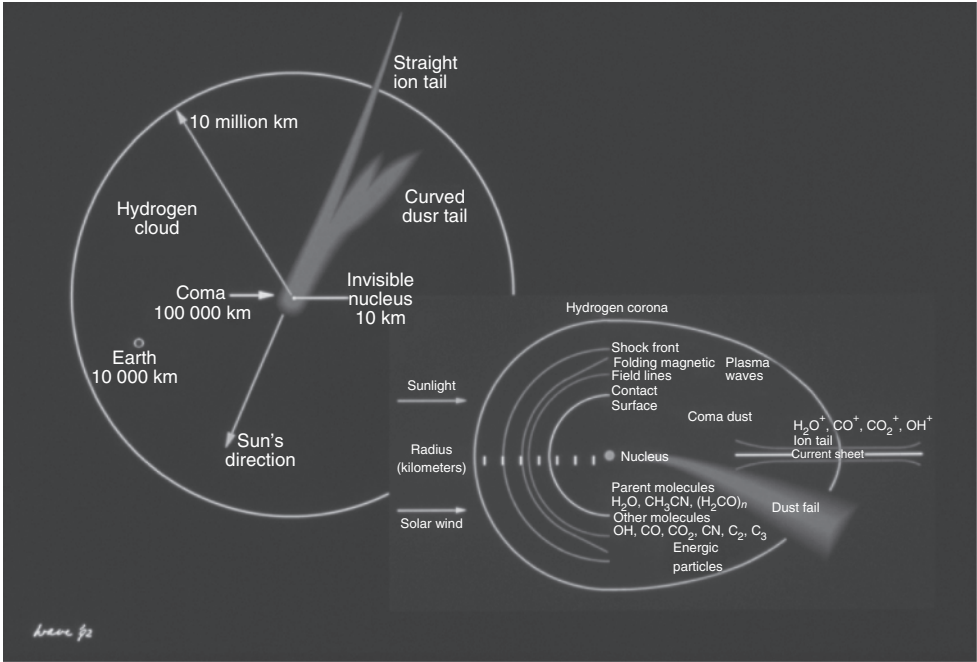


**Figure 1.19** The main cometary features, including the hydrogen corona, shock front, contact surface, and nucleus. The interaction of the nucleus and coma with the solar wind causes the formation of a straight, thin plasma tail (type I) that is composed of molecular ions and points away from the Sun. By interacting with the cometary coma, radiation pressure from the Sun generates

the dust tail (type II), which is curved and usually broad and diffuse. The dust tail exhibits the spectrum of the reflected sunlight, thereby indicating that it is not composed of atoms and molecules that absorb and emit their characteristic light but rather of dust grains that only scatter sunlight. (Image credit: ESA.)

neutral molecules of cometary origin are ionized by the solar wind. The energy and momentum given to the cometary ions originate from the solar wind, which is therefore thought to decelerate by increasing amounts as the cometary nucleus is approached [117]. By yielding more precise data than that obtained by the Saki-gake spacecraft (see Section 1.4.3), the Johnstone Plasma Analyzer (JPA) onboard Giotto revealed that as the cometary nucleus was approached, the speed of the solar wind reduced gradually and its temperature increased gradually, with no major discontinuity [117].

### 1.5.5

#### Overview, Summary, and Current Status

The 1986 missions to comet 1P/Halley, as summarized in Figure 1.20, were the first close and exciting encounters with a comet [50]. The data obtained by those missions influenced our understanding of cometary nuclei more strongly than any

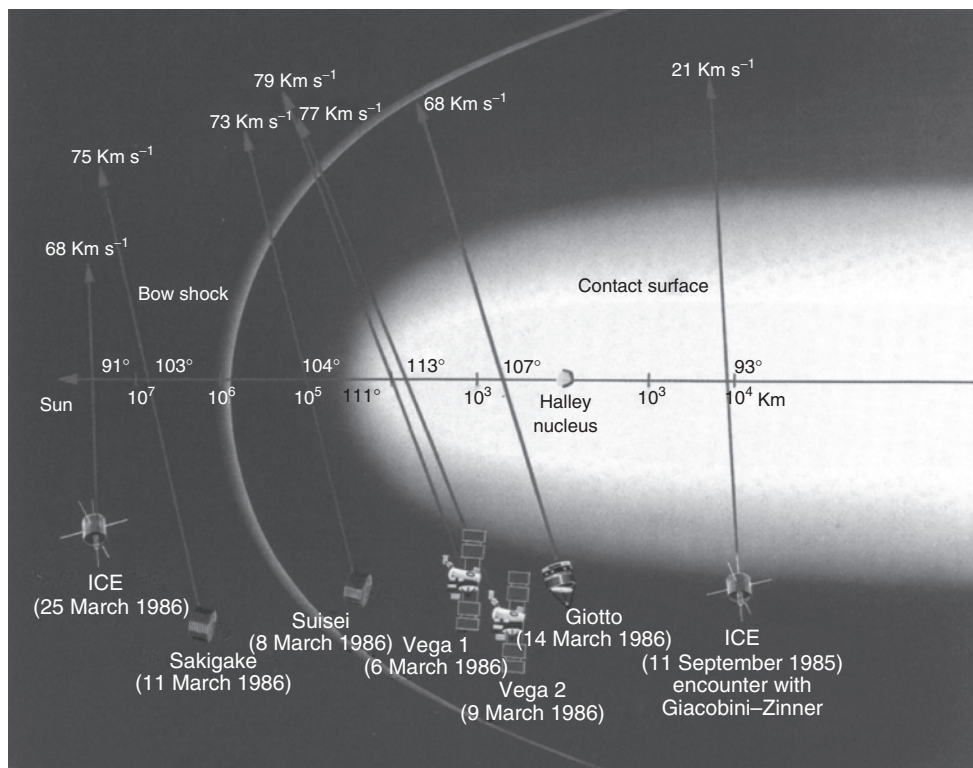


**Figure 1.20** Spacecraft encounters with comets 1P/Halley and 21P/Giacobini-Zinner; the dates and distances of closest approach are provided. (Image credit: NASA.)

other comet physics studies [4]. The recorded data revealed that the visible surface of the nucleus is relatively hot (300 K) and black, thereby absorbing visible light. According to the data provided by these missions, there is nothing that sharply contradicts the Whipple theory of how comets are made: that they consist of dust particles held together by ice [50]. However, comet nuclei do not look like “snowballs”, not even like “dirty snowballs” [4]. A cometary nucleus can be characterized as an asymmetric, kilometer-sized solid object with an irregular tar-type crust that contains dirty ices in a porous matrix of refractory material and that rotates toward the Sun. In 1990, Rickman and Huebner stated that even after the Halley encounters, we are still far from being able to specify the place of origin of Halley’s comet, let alone that of comets in general [8].

After the encounter with comet 1P/Halley, the Giotto spacecraft – with most of the instruments and solar cell arrays still intact – was retargeted to the neighborhood of Earth. An Earth-gravity-assist maneuver enabled the redirection of Giotto toward comet 26P/Grigg–Skjellerup for an encounter on 14 July 1992 [7]. Giotto passed the nucleus of comet 26P/Grigg–Skjellerup at a distance of 100–200 km, which is closer than Giotto’s minimum distance to comet 1P/Halley, 600 km, and

the closest ever cometary flyby [18]. However, pictures of 26P could not be taken because the cameras were damaged after their approach to comet 1P/Halley. Giotto's still successfully operating Dust Impact Detection System observed that for comet 26P/Grigg–Skjellerup, the mass distribution of the cometary dust was dominated by larger particles compared with that of comet 1P/Halley [120]. McBride *et al.* [121] identified one event at a distance of approximately 1000 km from the nucleus, which suggested the existence of a 10–100 m nucleus fragment that produced its own dust coma. This is a considerable finding, particularly in consideration of the new data pertaining to the cometary environment obtained by the Deep Impact spacecraft that visited comet 103P/Hartley and provided high-resolution images of the close environment of a cometary nucleus (see Section 1.8.4). 26P/Grigg–Skjellerup's magnetic field was also investigated [122].

## 1.6

### Comet 19P/Borrelly as Observed by Deep Space 1 and the Contour Comet Nucleus Tour

#### 1.6.1

##### The Deep Space 1 Spacecraft Accelerated by Ion Propulsion

Twelve years after the spectacular encounter of a flotilla of spacecraft with comet 1P/Halley, the NASA-JPL DS1 space probe was launched on 24 October 1998. Equipped with cutting-edge technology, such as an ion propulsion system (IPS) – instead of classical chemical propulsion – and another 11 advanced technologies that were important for future space and Earth science programs, DS1 was part of NASA's New Millennium Program (NMP), which tested high-risk technologies in operational spaceflight (Figure 1.21). The most important innovation [123], the solar electric propulsion (SEP) system of DS1, was based on the ionization of the noble gas Xenon (Xe) by electrons to form  $\text{Xe}^+$  ions. The  $\text{Xe}^+$  ions were then electrostatically accelerated by a potential of 1280 V through a pair of molybdenum grids [124] and emitted from the spacecraft to accelerate it. A separate electron beam was emitted from DS1 to avoid the accumulation of negative charges on the spacecraft. SEP was believed to offer significant mass savings for future space missions. In October 1998, the first attempt of DS1 to thrust with the IPS failed, and after operating for 4.5 min, IPS shifted to a standby mode [124]. It is thought that a contaminant caused a short between the two molybdenum grids, and a restart of the thruster on that day remained unsuccessful. During the following 2 weeks, the IPS underwent thermal cycling that changed the spacing between the grids and enabled the IPS to be restarted and its desired operation achieved [124].

DS1 also had initial problems with its star tracker, but these problems did not hinder its approach to comet 19P/Borrelly, although DS1 had not been designed for a comet encounter [123]. DS1 had no protection against cometary dust, and the end of its fuel supply was immanent [18].

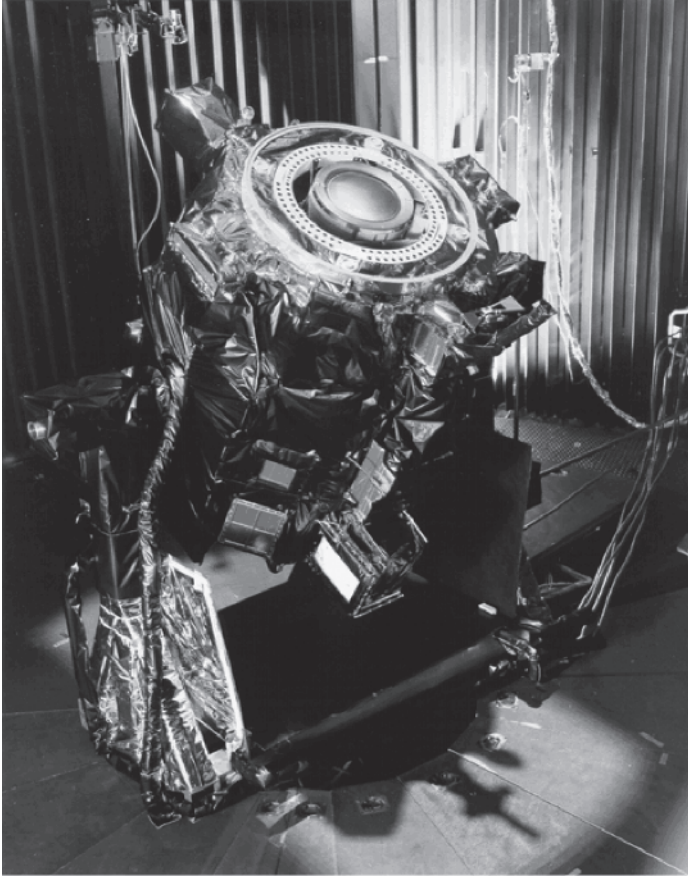


**Figure 1.21** The Deep Space 1 spacecraft pictured during ground tests, with its innovative ion propulsion system on the top. The ion drive's generated thrust corresponds to the force required to hold a piece of paper on Earth. (Image credit: Deep Space 1 team, JPL, and NASA.)

## 1.6.2

### Encounter, Nucleus Images, and Properties of Comet 19P/Borrelly

“The encounter did not go the way we expected,” said project manager Marc Rayman of Jet Propulsion Laboratory (JPL), “It went perfectly” [125]. Nearly 3 years after launch, on 22 September 2001, DS1 traveled at a velocity of  $16.5 \text{ km s}^{-1}$  on the sunward side through the coma of comet 19P/Borrelly. Its distance to the cometary nucleus during closest approach was 2171 km [102]. In contrast with comet 1P/Halley, which is thought to originate in the Oort cloud [102], comet 19P/Borrelly belongs to the Jupiter-family comets, which are believed to originate in the Kuiper belt [102]. Its orbital period is 6.9 years [99], and it has an orbital inclination of  $30.3^\circ$  and a perihelion distance of 1.358 AU.

DS1 passed the nucleus of comet 19P/Borrelly 8 days after the comet's perihelion passage [102]. The encounter velocity of Giotto as it passed the nucleus of comet 1P/Halley was much higher ( $68.4 \text{ km s}^{-1}$ ), and its distance during closest approach was much shorter (602 km). DS1 took high-resolution black-and-white images of the surface of the nucleus of comet Borrelly that were sharper than any of the images taken by the Giotto and Vega missions to comet 1P/Halley [125]. The DS1 spacecraft returned pictures to Earth that revealed for the first time recognizable geology on a comet nucleus [125]; consequently, DS1 was a great success. The nucleus of comet 19P/Borrelly was described as a bowling-pin-shaped object of size  $8.0 \times 3.2 \times 3.2 \text{ km}$  [99] that exhibited rugged terrain and towering jets of dust and vaporized ice [125]. Its nucleus rotation period was measured to be 26 h. In 1999, using remote observations from the Hubble Space Telescope (HST), Lamy *et al.* predicted that 19P/Borrelly's semi-axes have lengths of  $4.4 \pm 0.3 \text{ km}$  and  $1.8 \pm 0.15 \text{ km}$ ; the authors inferred a rotational period of 25 h [126]. This prediction is important to note because – as we will see in Section 5.4 – Lamy and colleagues also predicted the size and shape of the nucleus of comet 67P/Churyumov-Gerasimenko [127], the knowledge of which will be crucial for the cometary nucleus landing and scientific operations of the Rosetta mission.

DS1 was equipped with the Miniature Integrated Camera and Spectrometer (MICAS) instrument, which contained two visible-wavelength cameras and ultraviolet and infrared spectrometers [102]. The UV spectrometer failed soon after launch. Comet 19P/Borrelly was thus observed by the charge-coupled device (CCD) camera<sup>13</sup>, which delivered 52 images in the visible wavelength region, and the IR spectrometer, which delivered 45 short-wavelength IR spectra in the 1.3–2.6- $\mu\text{m}$  spectral region [102]. The highest resolution of the images was  $\sim 45 \text{ m/pixel}$ ; these images were obtained 160 s before closest approach at a distance of 3417 km. MICAS provided superb images, such as that of the nucleus of comet Borrelly depicted in high resolution in Figure 1.22, and spectral information [18]. A variety of terrain and surface textures, including mountains, fault structures, and dark material, are visible over the nucleus's surface.

Soderblom and colleagues divided the Borrelly nucleus into two main terrain units, smooth terrain and mottled terrain. The smooth terrain in the central part of the cometary nucleus included several mesa-like features, which may be associated with active jets. The mottled terrain occurs at both ends of the elongated cometary nucleus and seems rougher because it exhibits irregular pits, bumps, troughs, and ridges [102]. The mottled terrain, with its strong albedo variation, appeared to be largely inactive and not associated with jet sources of gas and dust. It was assumed to represent an older surface lag. The shape of comet 19P/Borrelly's nucleus and its structure are evidence for its formation by the coalescence of multiple bodies [102]. Fractures on the cometary nucleus were

13) CCD cameras, which are often used in conjunction with specialized filters, became popular in applications that require high photometric precision because they are highly linear and have large dynamic ranges [18]. Moreover, CCD cameras deliver a digital signal.



**Figure 1.22** The nucleus of comet Borrelly depicted at a high resolution of  $\sim 45$  m/pixel. The image exhibits a variety of terrain and surface textures, such as mountains, fault structures, and dark material. A map sketch that indicates the identified morphological units and features was published by Soderblom and colleagues [102]. (Image credit: NASA.)

observed by the MICAS camera, several of which were located right at the thin neck of the bowling-pin shape, which caused Laurence Soderblom of the U.S. Geological Survey to suggest that it is quite possible that Borrelly could break into two or more fragments [125]. Soderblom *et al.* [102] identified no fresh impact craters of diameter greater than 200 m, which hints at a young and active surface.

The surface of comet 19P/Borrelly was found to be covered by dark material. The geometric albedo of  $p = 0.04$  observed for the nucleus of comet 1P/Halley by Giotto was surprisingly low, but the geometric albedo of the nucleus of comet 19P/Borrelly was determined to be even lower, with  $0.01 < p < 0.03$  [18, 102]. The geometric albedo of  $p = 0.03$  was found for the smooth terrain, and the darker spots had values that ranged down to  $p = 0.01$ ; the variations could be evidence for differences in the composition, particle size, or compaction effects [102].

The short-wavelength IR spectrometer of MICAS onboard DS1 performed a 28-s long-exposure observation just before its closest approach to the nucleus of comet Borrelly. Somewhat surprisingly, the spectrometer recorded an absorption feature at  $2.39 \mu\text{m}$  with a width of  $0.02 \mu\text{m}$  in the nucleus reflectance spectrum. Soderblom and colleagues suggested that this feature may be evidence for

hydrocarbons such as POM (see Section 2.5.6), which exhibits absorption features in this region [102]. Bands of water ice or hydrated minerals were not identified in the cometary crust.

Temperatures on the sunward side of the surface of the cometary nucleus ranged from 300 to 345 K, thereby indicating a hot and dry surface [18]. These temperatures and the lack of water IR bands are consistent with the estimates that only  $\sim 10\%$  or less of the nucleus surface is active [102]. Regions of actively sublimating ice are believed to reach temperatures of approximately 200 K [102].

The data provided by MICAS indicate two main features that contribute to the coma of comet 19P/Borrelly: collimated jets and fans [18]. Two sets of bright collimated dust jets were identified, the  $\alpha$  jet and the  $\beta$  jet, which exhibit cylindrical cores and are offset by  $15^\circ$ . The less bright fans originate from spatially extended sources. Typical fans exhibit a  $1/R$  decrease in brightness in the image, where  $R$  is the distance from the nucleus. Collimated jets produce a much shallower decrease in brightness than  $1/R$ : they can retain roughly constant brightness out to  $\sim 5$  km, after which the brightness decreases in the conventional  $1/R$  manner [102]. Soderblom and colleagues interpret this behavior as evidence that the narrow collimated jets contain relatively coarse icy dust particles with diameters of  $\sim 10$   $\mu\text{m}$ . Once ejected from the nucleus, these traveling icy dust particles fragment by sublimation. Assuming a speed for the icy dust particles of approximately  $0.4 \text{ km s}^{-1}$  and a length for the collimated jet of approximately 4 km, their time of flight is  $\sim 10$  s. The sublimation lifetime of a 10- $\mu\text{m}$  particle was also estimated to be 10 s, which led Soderblom *et al.* [102] to conclude that coarse particles sublimate and fragment, thereby dispersing into a cloud of fine dust particles. In Section 2.5.6, we will discuss this fragmentation and gas release in the general context of extended sources in cometary comae.

Investigations by the Plasma Experiment for Planetary Exploration (PEPE) onboard DS1 revealed the chemical composition of the cometary plasma to be approximately 63%  $\text{OH}^+$ , 25%  $\text{H}_2\text{O}^+$ , 8%  $\text{CH}_3^+$ , 2.5%  $\text{C}^+$ , and 2%  $\text{N}^+$ ; the abundances of the ions  $\text{O}^+$ ,  $\text{H}_3\text{O}^+$ , and  $\text{CH}^+$  were less than the detection limits [18].

In summary, the data obtained by DS1 provided unique information about the surface of comet Borrelly's nucleus, which is hot, dry, and extremely dark.

### 1.6.3

#### The Cometary Nucleus Probe CONTOUR

Comet 2P/Encke is a short-period comet that exhibits the shortest orbital period of all known comets (3.3 years). Because of its both low inclination and short orbital period, 2P/Encke has often been perturbed by interactions with the inner planets. Because of fragmentation of the cometary nucleus, comet 2P/Encke is believed to be the origin of near-Earth object 2004 TG<sub>10</sub> and the Taurid meteor

shower, and it may also be the origin of the ancient symbol of the swastika<sup>14)</sup>. After comet 1P/Halley, comet 2P/Encke was the second comet for which a periodicity was determined in 1819. Comet 2P/Encke is a highly evolved comet [18].

Similar to 2P/Encke, 73P/Schwassmann-Wachmann 3 is a short-period comet with an orbital period of 5.36 years, but comet 73P/Schwassmann-Wachmann is thought to be less evolved [18]. As indicated in Section 1.3.1, 73P is of particular scientific interest because during perihelion passage, its nucleus broke into five fragments, labeled A–E, in 1995. In 2001, three of these fragments, B, C, and E, were found again. In 2006, further spectacular fragmentation processes of the cometary nuclei were observed; these events drastically increased the brightness of 73P because of the release of gas and dust in the cometary atmosphere. To date, more than 60 different cometary nuclei fragments have been described.

The unmanned NASA-CONTOUR cometary nucleus probe was designed to closely approach the nuclei of comet 2P/Encke in 2003 and 73P/Schwassmann–Wachmann in 2006 at a distance of only ~100 km during the phase of maximal cometary activity. High-resolution images of fresh cometary nuclei were expected to provide pictures of the surfaces of cometary nuclei with unprecedented detail. CONTOUR stands for Comet Nucleus Tour. Sadly, this rendezvous with cometary nuclei did not occur due to the failure of CONTOUR in 2002, shortly after it was launched into the Earth orbit. The precise origin of CONTOUR's explosion into three pieces remains unknown; possible explanations include problems with the solid-rocket motor and a collision with space debris.

## 1.7

### The Stardust Sample Return Mission to Comet 81P/Wild

The international cometary flotilla in 1986 and DS1 in 2001 provided a fair understanding of the morphology of the nuclei of comets 1P/Halley and 19P/Borrelly, their crust, the formation of cometary comae, and the processes that yield cometary dust and plasma tails. It became evident that cometary nuclei contain not only water but also carbon and nitrogen, which are the fundamental elements of organic chemistry. Consequently, the state of cometary carbon and its potential occurrence in cometary organic molecules began to attract tremendous scientific interest.

#### 1.7.1

##### Conceptual Remarks

Vega's PUMA and Giotto's PIA mass spectrometers were designed to detect the elemental composition of cometary dust after dust particles from the cometary

14) In various cultures across the world, the swastika appeared at a similar time. The symbol of the swastika might have been inspired by a rotating comet that emitted gas and dust jets in four different spatial directions.

nucleus impacted the targets in the mass spectrometers. These instruments were not conceptually designed for the detection and identification of individual and intact organic molecules in cometary ices because the mass spectra were recorded from a *mixture* of molecular and atomic ions. For the identification of individual organic molecules, it is convenient to separate these molecules from other molecules and atoms prior to their mass spectrometric analysis. The obtained fragmentation pattern then often allows – comparable to a fingerprint – for unambiguous identifications.

The cometary Stardust mission, which was part of the NASA Discovery Program, heralded a new era in space research: the Stardust discovery mission aimed to approach the coma of a cometary nucleus and to collect samples to be transported to Earth, where samples of cometary origin can be analyzed using highly sophisticated and dedicated instruments in selected suitable laboratories.

### 1.7.2

#### Encounter with Comet 81P/Wild 2 and Sample Collection

In January 2004, the Stardust spacecraft – which had been launched in 1999 – encountered comet 81P/Wild, which is also known as *Wild 2* or *81P/Wild 2*. This encounter occurred at a “breathlessly” short distance of 236 km and a velocity of  $6.1 \text{ km s}^{-1}$  [128] during the comet’s approach to the Sun at a distance of 1.86 AU [113].<sup>15)</sup> Never had a space probe approached a cometary nucleus at such a close distance (except for Giotto’s post-1P/Halley encounter with comet 26P/Grigg–Skjellerup) and, in particular, at such a low relative velocity, which is still six times faster than the velocity of a bullet [129]. The “low” velocity was important because the Stardust probe passed through the cometary coma and was constructed to retrieve samples. The low velocity required a special design of the orbital trajectory that included three loops around the Sun [18]. The orbital trajectory was developed by Chen-Wan Yen of the JPL [130]. By flying through the cometary coma, dust particles could be collected for further analyses: particles of cometary dust of submillimeter sizes were collected in a special aerogel, which is an extremely low-density sponge-like microporous silica (Figure 1.23) [128] that provided a relatively “soft” catcher for impinging dust particles [99].

The aerogel was developed by Peter Tsou of JPL [130]. The aerogel cells mounted on the Stardust spacecraft were able to capture both particles and cometary gases during the cometary flyby [131]. The challenge was to capture the dust particles without destroying both the dust and the spacecraft in the capturing process [130]. The aerogel cells were lined with aluminum foils that composed approximately 15% of the total collection surface [132], in which hypervelocity craters were later

15) On 2 January 2004, the encounter between NASA’s Stardust mission and comet Wild 2 passed virtually unnoticed by most of the public [99], partly because the rover Spirit aimed to land on Mars the next day.

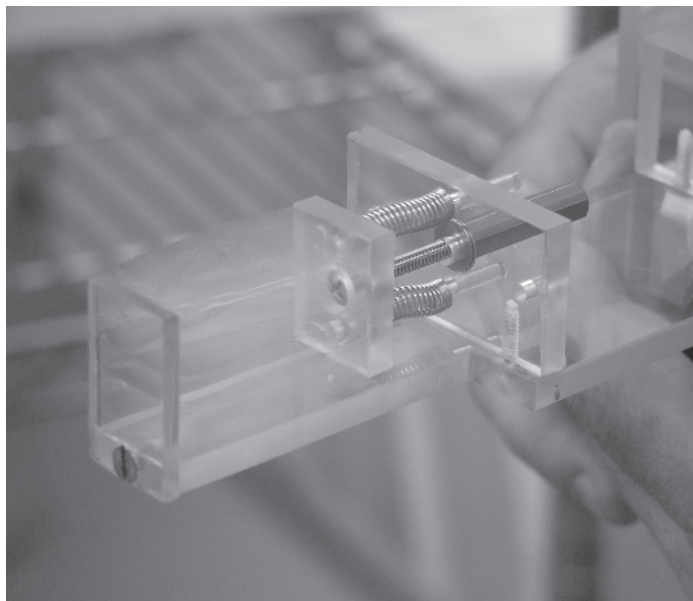


**Figure 1.23** Block of silica aerogel pictured in the Stardust Cleanroom at Johnson Space Center (prelanding). The silica aerogel has the density of air [129, 130]. (Image credit: NASA.)

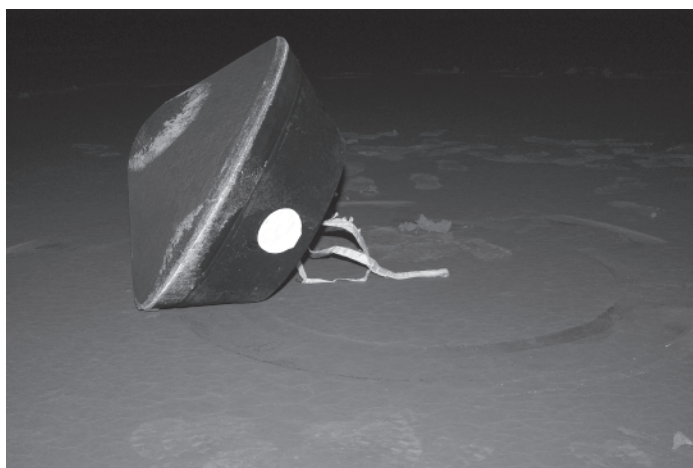


**Figure 1.24** NASA's Stardust sample return capsule successfully landed at the U.S. Air Force Utah Test and Training Range on 15 January 2006. (Image credit: NASA.)

observed and analyzed [133, 134]. The density of the silica aerogel exhibited a gradient that varied from  $< 0.01 \text{ g cm}^{-3}$  at the impact surface to  $0.05 \text{ g cm}^{-3}$  at a depth of 3 cm [132].

The obtained sample that contained nanoscopic cometary dust particle material was the first Solar System sample returned to Earth (Figures 1.24 and 1.25)



**Figure 1.25** In a laboratory at the Johnson Space Center, Stardust material is inspected soon after investigators from the University of Washington, Johnson Space Center, and

Lockheed Martin Missiles and Space, Denver, Colorado, opened a container that included the sample collector. (Image credit: NASA.)

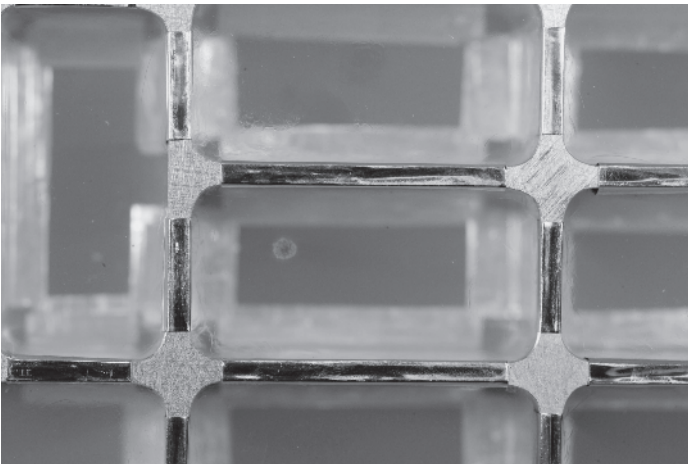


**Figure 1.26** Close-up view of a cometary impact (center) into aerogel as observed at the Johnson Space Center hours after the Stardust sample return canister was delivered to the Johnson Space Center from the spacecraft's landing site in Utah. (Image credit: NASA.)

since the samples taken and returned from the Moon, and it was the first sample ever returned from deep space [132, 135]. The Dust Flux Monitor Instrument (DFMI) onboard the Stardust space probe estimated from data taken during cometary flyby that ~2800 particles with diameter  $>15\ \mu\text{m}$  impacted the aerogel collectors (Figures 1.26 and 1.27) (2300 particles collected in the inner coma plus 500 particles from the postencounter swarm), and the largest particle had

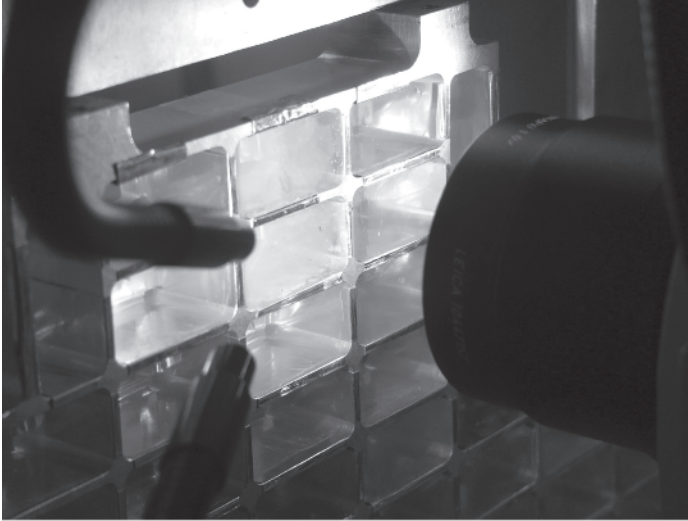


**Figure 1.27** Close-up of prelanding camera scanning in the Stardust Cleanroom at Johnson Space Center. (Image credit: NASA.)

a mass of  $\sim 0.6$  mg and diameter of  $\sim 1.3$  mm [136]. Two years after the cometary encounter, the protective capsule with the loaded aerogel collectors was dropped off during Stardust's swing by the Earth on January 2006. It was expected to land in the Utah desert in January 2006 [99] via a parachute landing, which proceeded successfully. Approximately 200 investigators around the world – an “incredible array of analytical firepower” [130] – participated in the analysis of the returned samples, which consisted of more than 10 000 particles with sizes in the range of 1–300  $\mu\text{m}$  [132]. The science project Stardust@home involved  $\sim 30$  000 volunteers who participated in the identification of tiny dust deceleration tracks.

### 1.7.3

#### **The Hot Origin of Selected Cometary Grains Provides Evidence for Radial Mixing of the Solar Nebula**

It had been widely believed that comets – during their formation and evolution – were isolated from inner Solar System materials [132]. In 2006, microscopic and X-ray analyses of Stardust's impacted dust particles (Figures 1.28 and 1.29) demonstrated, somewhat surprisingly, that the impacted particles were *not* exclusively interstellar grains of submicron size. Abundant high-temperature minerals, such as forsterite ( $\text{Mg}_2\text{SiO}_4$ ), which has a condensation temperature of 1400 K, enstatite ( $\text{MgSiO}_3$ ), and calcium- and aluminum-rich inclusions (CAIs), were identified in the impacted cometary particles; such materials must have formed in the *hot* and innermost regions of the solar nebula, well inside the orbit of Mercury [132]. These mineral grains and components clearly did not form in the environment in which they were found [132]. Radial large-scale mixing



**Figure 1.28** Visible track of a particle captured in the Stardust aerogel. The impacts of cometary dust particles into the silica aerogel produced deep (>1 mm) tapered cavities called *deceleration tracks* [132], which exhibited a large variety of morphologies [133]; some individual grains were well preserved, whereas others melted [137]. Often, the particles consisted of aggregates that separated into fragments during impact, and some of these fragments left bifurcated tracks [132]. The smaller fragments stopped

in the upper region of the tracks, whereas the larger fragments traveled deeper into the aerogel [132]; most cometary material was observed to be left as fragments along the walls of the deceleration tracks, usually with an intact terminal particle [130]. The deceleration tracks of particles collected from Wild-2 were approximately perpendicular to the aerogel surface, whereas interplanetary particles, which were also collected, arrived with a wide range of orientations [134]. (Image credit: NASA.)

in the solar nebula was proposed by Brownlee and colleagues, who suggested that these inner Solar System materials – which account for ~10% of the comet’s mass – must have been transported beyond the orbit of Neptune, either by ballistic transport above the nebular midplane or by turbulent transport in the midplane [132]. This transport corresponds to abundant radial transport of solids on the largest spatial scales [132]. Furthermore, Michael F. A’Hearn from the University of Maryland concluded from the Stardust data that even more extensive and earlier mixing of the material took place in the disk in which the planets of the Solar System formed [36].

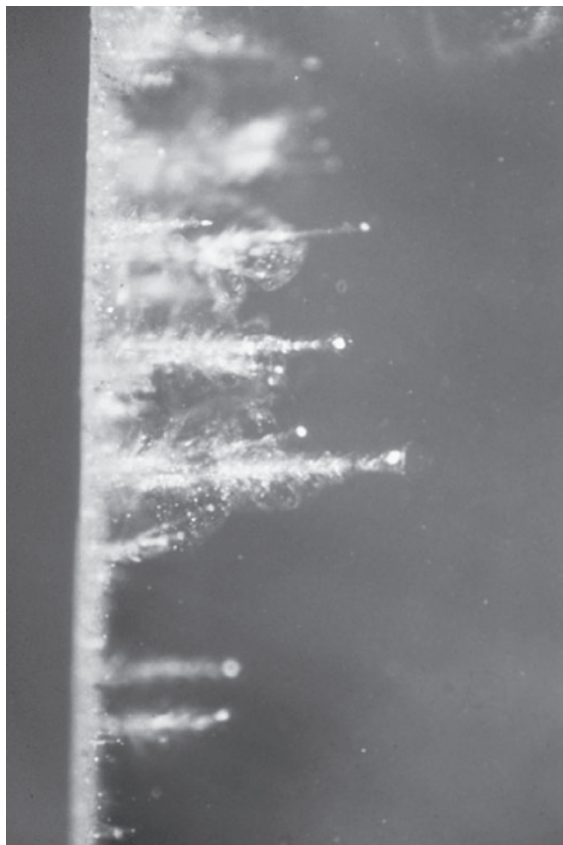


**Figure 1.29** NASA photo of an aerogel being tested during the prelaunch phase of the Stardust Mission. Laboratory simulation studies were difficult to perform because of the technical challenge of accelerating loosely bound aggregates to  $6.1 \text{ km s}^{-1}$  [132]. Particles that impacted Stardust's aerogel at velocities of  $6.1 \text{ km s}^{-1}$  were decelerated on timescales that ranged from  $1 \mu\text{s}$  to less than  $1 \text{ ns}$  depending on the particle size. It was

estimated that the thermal wave produced by the particle–aerogel contact reached temperatures above  $2000 \text{ K}$  but did not penetrate deeply into the captured particles on ns interaction times [132]. Brownlee *et al.* [132] believe that the smallest dust particles were often strongly heated, whereas those that were larger than a micron in size appeared to have been protected by their own thermal inertia. (Image credit: NASA.)

A detailed analysis of the elemental composition, including the abundances of Mg, Si, Mn, Fe, Ni, Ca, Ti, Cr, S, Cu, Zn, Ga, Ge, and Se, of comet Wild 2 samples was provided by Flynn and colleagues [134]. A study of the mineralogy of the particles captured by Wild 2 performed by Zolensky *et al.* revealed the presence of primarily silicates [129, 130], such as olivine  $[(\text{Mg,Fe})_2\text{SiO}_4]$ , and low-Ca pyroxene  $[(\text{Mg,Fe})\text{SiO}_3]$  and also ubiquitous Fe–Ni sulfides, including troilite (FeS) [130] and Fe–Ni metal; these compounds require a wide range of formation conditions [137]. In agreement with the data provided by Brownlee *et al.* [132], these data strongly

support the formation of mineral cometary constituents at very different locations in the protoplanetary disk [137]. The identification of such minerals would be common for planetary materials; however, their identification in cometary grains was somewhat surprising because it was commonly expected that cometary material would be similar to interstellar material, in which most silicates are believed to be amorphous [130]. Amorphous material in the returned samples was rare or nonexistent [130]. It should be noted in this context that impact-triggered melting of aerogel produces silica glass, which, mixed with cometary materials, renders the identification of cometary amorphous material difficult [130]. Sulfides were identified in restricted compositional ranges, whereas silicates were identified in a very wide range, which suggests that comet Wild 2 experienced little or no aqueous alteration [137].

#### 1.7.4

##### Isotopic Analyses of Returned Wild 2 Samples

The new belief that comet 81P/Wild 2 contains material from the inner Solar System that formed at high temperature and was transported to the Kuiper belt before comet accretion was supported by isotopic analyses of Wild 2 samples. McKeegan *et al.* [138] quantified the hydrogen and deuterium isotopes in five dust particles captured by Stardust. The D/H values obtained were reported to range from typical terrestrial values up to moderate D/H enhancements of approximately three times the D/H value of mean ocean water. The D enrichments were associated with carbon, and it is important to note that these enrichments might have been modified during impact and cannot be ascribed to Wild 2 water [138].

In two sections of an impact track called *Thera 1* and *Thera 2*, the noble gases helium, neon, and argon were analyzed, and the  $^{20}\text{Ne}/^{22}\text{Ne}$  and  $^{21}\text{Ne}/^{22}\text{Ne}$  ratios were calculated. To do so, the aerogel was melted using a  $\text{CO}_2$  laser, and the released gases were analyzed for noble gas abundances and isotopic ratios by performing static mass spectrometry after specific purification [139]. Helium-4 ( $^4\text{He}$ ) was found with an abundance of as much as  $23.6 \pm 7.6 \times 10^{-15}$  mol, and  $^{20}\text{Ne}$  had an abundance of as much as  $2.58 \pm 0.19 \times 10^{-15}$  mol [138]. McKeegan and coworkers [138] argued that these noble gases were captured in the aerogel as cometary volatiles and found  $^{20}\text{Ne}/^{22}\text{Ne}$  ratios of up to  $12.86 \pm 3.20$ , ratios that are significantly higher than that of air.

Carbon and nitrogen isotope analyses were performed on the impacted cometary dust particles by performing isotopic mapping on the nanometer scale with secondary ion mass spectrometry (NanoSIMS). No circumstellar dust grains that contained C- and N-rich inorganic phases, such as graphite, SiC, and  $\text{Si}_3\text{N}_4$ , could be definitively identified [138]. On the micrometer scale, all studied samples were found to be homogeneous in terms of both the C and N isotope composition. Carbon exhibited “normal”  $\delta^{13}\text{C}$  values, expressing the ratio of the  $^{13}\text{C}/^{12}\text{C}$  isotopes of carbon in the sample as compared to a standard of  $-20\text{‰}$  to  $-50\text{‰}$  (for comparison with the cometary isotope ratios obtained via remote spectroscopy, see Section 2.5.8). Nitrogen isotopes were characterized

by more widespread and somewhat high  $\delta^{15}\text{N}$  values between 0‰ and +500‰ [138]. Interpretations of these observations suggest that organic matter did not necessarily survive the high-velocity impact capture process in Stardust's aerogel [138].

Moreover, oxygen isotope measurements that were performed on 24 particle fragments of comet Wild 2 exhibited a wide variety of different  $\delta^{18}\text{O}$  and  $\delta^{17}\text{O}$  values that are similar to those of materials from carbonaceous chondrites and indicate that the dust of Wild 2 is a nonequilibrated aggregate of material from different sources [138] that originated in the Solar System [130].

### 1.7.5

#### **Infrared Analyses of Returned Wild 2 Samples: Hints at Aliphatic Hydrocarbons**

Wild 2 particles captured in Stardust's aerogel were analyzed using Fourier transform infrared (FTIR) spectroscopy. Analysis of extracted grains and *in situ* measurements from individual deceleration tracks revealed infrared absorption features in the C–H stretching region, which are consistent with long-chain aliphatic hydrocarbons [140]. The observed characteristic infrared  $\text{CH}_2/\text{CH}_3$  band depth ratio was  $\sim 2.5$  and thus larger than that of carbonaceous chondrite meteorites, such as Orgueil and Murchison, which exhibit  $\text{CH}_2/\text{CH}_3$  values of  $\sim 1.1$  [140]. These infrared data indicate that the aliphatic hydrocarbons in Wild 2 are longer or at least less branched than those of carbonaceous chondrites. A more precise molecular identification of the hydrocarbon structures in Wild 2 samples cannot be achieved using infrared spectroscopy. Furthermore, in some cometary grains, weak carbonyl C=O and C–C bending vibrations were observed [140]. The reader should note that the blank silica aerogel that had not been exposed to the comet also contained symmetric and asymmetric hydrocarbon bands; however, according to Keller and colleagues [140], these infrared bands were distinct from those of the Wild 2 organic matter. Amorphous silicates are known to be the dominant silicate in the interstellar medium. FTIR studies confirmed the presence of *crystalline* silicates in the Wild 2 samples, thereby indicating that this comet is a mixture of presolar and Solar System materials [140]. This finding agrees with both the mineralogical and isotopic analyses of the returned Stardust Wild 2 samples. Michael A'Hearn concluded from these data that nearly all of the crystalline silicate must have formed in the Solar System, very close to the proto-Sun, rather than being circumstellar or other presolar grains that were transported from the interstellar medium and directly incorporated [36].

### 1.7.6

#### **Organic Molecules, PAHs, and an Amino Acid in Returned Wild 2 Samples**

Particular attention was paid to the analysis of amino acids and their chemical precursor molecules in the valuable and unique Wild 2 samples collected by the Stardust spacecraft. The reason for this interest is that amino acids are considered of crucial importance in the initial processes of chemical evolution that triggered

the appearance of life on Earth, and there is reason to assume that at least some of the molecular inventory necessary for the origin of life was delivered by comets to Earth. Twenty amino acids are the molecular building blocks of proteins. Furthermore, many amino acids are chiral and thereby related to the phenomenon of homochirality of biomolecules [141].

Several organic compounds of different chemical nature that are rich in oxygen and nitrogen atoms, including the amines methylamine and ethylamine and the amino acid glycine, were reported by Sandford *et al.* [142] to be detected in Stardust's samples by the Stardust Organics Preliminary Examination Team (PET), with its kernel located at NASA's Goddard Space Flight Center. A wide diversity of chromatographic and spectroscopic analytical instruments<sup>16)</sup> was employed for the analysis of such organics in the cometary dust particles that were captured by the Stardust space probe. The 55 authors from 31 different institutions who wrote the key 2006 publication in *Science* indicated that some of the identified organic molecules were generated or altered during the impacts of the cometary dust particles with the aerogel. Furthermore, the authors specified that the silica aerogel itself employed in the Stardust collector contained "a few weight percent carbon" [142], largely in the form of Si-CH<sub>3</sub>, that – according to the authors – should be easily distinguishable from cometary organics. Moreover, Sandford *et al.* [142] stated that the locations in the aerogel visualized near particle impact tracks exhibited no deficit in the original methyl groups, thereby implying that the original carbon had not been substantially converted to other forms. For space experiments and sample return missions of such outstanding importance, it might have been useful to isotopically mark the carbon atoms in the aerogel, for example, by <sup>13</sup>C-labeling. This isotopic labeling of the synthetic aerogel would significantly facilitate the determination of the origin of organic molecules – aerogel constituents versus analytes – if identified. This comments holds true not only for the cometary Stardust mission but also for many other space missions that are intended to perform molecular analysis, including the Mars Science Laboratory (MSL) onboard the Curiosity rover, the Philae lander onboard the Rosetta cometary probe (see Section 7.3), the ExoMars mission (see Section 8.3), and others.

As indicated earlier, the amines methylamine and ethylamine and the amino acid glycine were reported to be detected in Stardust's samples [142]. In this context, it is important to note that many amines and amino acids were also present in the witness coupon aerogel sample (*sic*) that had not been comet-exposed [142]. A detailed chemical analysis revealed that a suite of amines, including ethanolamine and methylamine, ethylamine, and the amino acids glycine, L-alanine, β-alanine, γ-amino-*n*-butyric acid, and ε-amino-*n*-caproic acid

16) The analytical techniques employed by the PET included laser desorption laser ionization mass spectrometry (L<sup>2</sup>MS), liquid chromatography with UV fluorescence detection (LC-FD), and time-of-flight mass spectrometry (TOF-MS), scanning transmission X-ray microscopy (STXM), X-ray absorption near-edge spectroscopy (XANES),

IR and Raman spectroscopy, ion chromatography with conductivity detection (IC), secondary ion mass spectrometry (SIMS), and time-of-flight SIMS (TOF-SIMS). These methods provided a wealth of information about the chemical nature and relative abundance of the organics in the samples [142].

were identified in the Stardust aerogels and also in the flight aerogel witness tile that was not exposed to the comet [143]. This is important knowledge. Moreover, the proteinogenic aspartic and glutamic amino acids, as well as serine and alanine, were detected in the comet-exposed Stardust aerogel samples; in this case, the low D/L enantiomeric ratios (see Chapter 4) found for these chiral amino acids provided additional evidence that these amino acids did not originate from Wild 2 [143] but rather originated from terrestrial contamination. The amines methylamine and ethylamine exhibited significantly greater abundances in the comet-exposed aerogel compared with the preflight aerogel, thereby suggesting that these two amines were cometary in origin [142]. According to the authors, the same argument holds for the amino acid glycine, which was found in comet-exposed aerogel samples in higher quantities than in the nonexposed blank controls, thus indicating its cometary origin [142]. In later studies, the amino acid glycine, which was identified in Stardust's aerogel samples, was subjected to isotopic analysis to reveal its stable isotopic carbon ratio. The  $\delta^{13}\text{C}$  value was  $+29 \pm 6\%$ , which is well outside the terrestrial range of  $-6\%$  to  $-40\%$  expected for organic carbon and which falls in the previously reported range for glycine that was detected in the Murchison carbonaceous chondrite ( $+22\% < \delta^{13}\text{C} < +41\%$ ), thereby strongly suggesting an extraterrestrial origin for glycine [131]. In the case of  $\epsilon$ -amino-*n*-caproic acid, the  $\delta^{13}\text{C}$  value was determined to be  $-25 \pm 2\%$ , thereby indicating terrestrial contamination (by Nylon-6 storage and shipping bags, which have  $\delta^{13}\text{C} = -26.8\%$ ) as its origin [131]. However, the obtained isotopic glycine data do not allow the exclusion of amino acid formation during high-velocity dust particle impacts into the silica aerogel. Glycine might have formed from cometary carbon and provided the  $\delta^{13}\text{C} = +29 \pm 6\%$  during impact within the deceleration track.

The amines and amino acids had been predominantly identified in hot-water extracts of the Stardust particles that were acid hydrolyzed [143]; in nonacid-hydrolyzed aerogel extracts, no amines or amino acids were identified [142]. This phenomenon is similar to that observed in analyses of carbonaceous chondrite meteorites and samples of simulated interstellar ices (see Section 3.3), in which the quantity of amino acids drastically increases after an acid hydrolysis step. It is assumed that the amines and amino acids were present in the Stardust samples in an acid-soluble bound form rather than as free amines and amino acids [142]. Furthermore, Raman spectroscopy, XANES, and isotopic data indicated that the identified organic molecules were distributed in an inhomogeneous manner both within particles and between particles, thus suggesting that cometary organics do not represent an equilibrated reservoir of material [142].

Sandford and colleagues also reported the L<sup>2</sup>MS and TOF-SIMS identification of PAHs, such as naphthalene, phenanthrene, and pyrene, including their alkylated homologs, in the Stardust Wild 2 samples [142]. This finding was supported by Raman spectra acquired for 12 Stardust particles, which revealed graphite-like sp<sup>2</sup>-bonded carbon in the form of condensed carbon rings. This is an important finding because the presence of PAHs in comets has been an open issue: the identification of phenanthrene was claimed based on the near-ultraviolet spectra of

comet 1P/Halley recorded by the TKS instrument onboard the Vega 2 probe [64] but was called into question because of the low resolution of the TKS ultraviolet spectra [65], and there was no evidence of PAH bands in other comets such as Hale-Bopp [66].

### 1.7.7

#### Hoodoos and the Surface Morphology of the Wild 2 Nucleus

The Stardust mission provided the opportunity to combine information from the returned samples with information obtained through remote sensing [132]. In addition to the collection of cometary dust particles, the Stardust space probe used its scientific payload to obtain highly spatially and temporally resolved images of the cometary nucleus [128].

Comet Wild 2 was of particular interest and was selected for the Stardust Discovery Mission because it is a *young* Jupiter-family comet that has spent nearly all of its billions of years of life in the outermost Solar System. Wild 2 was captured only 40 years ago through a perturbation from Jupiter [99] on 10 September 1974 [132], which injected it into an orbit of the Jupiter-family comets [15]. It exhibits a relatively short orbital period of 6.4 years [99], which brings it within the reach of spacecraft [129]. Since then, the comet's mass loss has been estimated to correspond to  $\sim 1$  m over its total surface area [15]. During the Stardust encounter, comet Wild 2 was on its fifth passage through the inner Solar System [18]. As it approached the nucleus of comet Wild 2, the optical navigation camera took 72 images of the nucleus in steps of 10 s and with a maximal resolution of 14 m/pixel [15]. The shape of comet Wild 2 was found to be oblate and much more spherical and round compared to the "potato-shaped" nucleus of 1P/Halley and the "bowling pin" shape of 19P/Borrelly. Its size is  $5.5 \times 4.0 \times 3.3$  km [99], and it has a geometric albedo of  $p = 0.03$  [15]. Features with geometric albedo values that differed by a factor of 3, as observed for 19P/Borrelly [102], were not found on Wild 2 [15]. The surface on the dayside of the cometary nucleus was reported to be devoid of ice and have a temperature of  $\sim 300$  K [15].

Stardust principal investigator Donald Brownlee of the University of Washington, Seattle, and his colleagues identified circular depressions in the surface of the nucleus of Wild 2. They distinguished two different morphologies: "pit-halo" features, which have a rounded central pit surrounded by an irregular and rough region of partially excavated material, and "flat-floor" features, which lack halo regions and are bounded by steep cliffs [15, 99]. Among the three identified pit-halo features, one, which was called *Rahe*, was surrounded by sharp ragged cliffs with heights up to 200 m [15]. A flat-floor feature called *Left Foot* was surrounded by a nearly vertical wall of height 140 m. The flat-floor features seem to be inactive because none of them has been associated with observed jets [15]. Both pit-halo features and flat-floor features are believed to be craters that resulted from impacts. In addition to *Rahe* and *Left Foot*, the Stardust team named other the impact features – as depicted in Figure 1.30 – *Right Foot*, *Shoemaker Basin*, *Mayo*, *Hemenway*, and *Walker* [15]. Later Earth-based hypervelocity

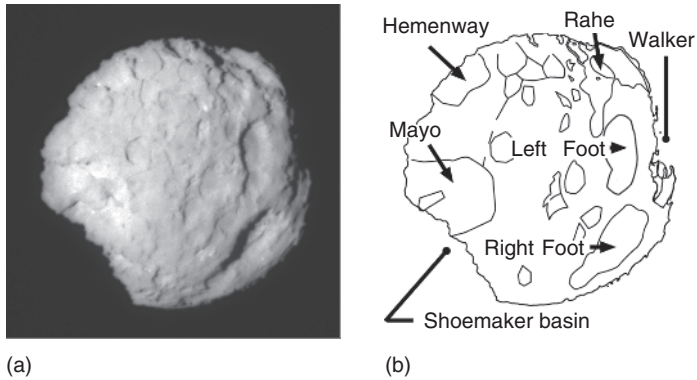


**Figure 1.30** Image (a) and diagram (b) of the nucleus of comet Wild 2 as taken by the optical navigation camera onboard NASA's Stardust space probe during flyby on 2 January 2004. The features on the diagram were named by the Stardust team for identification purposes. The word "basin" does not imply an impact origin. (Image credit: NASA.)

impact experiments used ceramic projectiles that impacted a porous target at  $2 \text{ km s}^{-1}$ ; these experiments, performed for comparison purposes, revealed that the pit-halo versus flat-floor features on Wild 2 are controlled by the strength properties of the surface, with almost no influence of gravity [15]. The implication is that the nucleus of Wild 2 has substantial strength and that gravity plays a minor role in shaping these features, which contradicts to conventional wisdom [99].

Deposits of ejecta due to impacts were not detected on the surface of Wild 2. This result was somewhat surprising and explained by the assumption that cometary ejecta are so porous, fine-grained, weak, and charged with volatiles that they disintegrate into fine powder and are blown away with the required escape velocity of  $\sim 1 \text{ m s}^{-1}$  [15]. Smaller ( $< 500 \text{ m}$ ) and irregular depressions in the surface of Wild 2 were not associated with impacts; rather, they were related to cometary sublimation processes [15]. Mesas with typical heights of  $\sim 100 \text{ m}$  above the local terrain were identified on the surface of comet Wild 2 by the optical navigation camera onboard Stardust; even larger flat-topped mesas bounded by cliffs had been previously observed on the surface of comet 19P/Borrelly by DS1 [15]. Mesas had not been identified in the images of comet 1P/Halley, most likely because of the limited resolution of the camera [15]. Lineaments were observed to be rare on Wild 2; the most prominent large-scale examples are scarps from Rahe to Hemenway [15].

Brownlee and colleagues attracted attention because of the highly speculative but intriguing possibility that cometary equivalents of hoodoos, upward-pointing spires sometimes observed in volcanic ash, exist on Wild 2 [15]. If the cometary nucleus contains conduits of escaping water vapor with entrained molecules of limited volatility, those molecules may freeze out on the conduit walls. After sublimation of the cometary surface, the conduit lines could be resistant and form a pinnacle [15].

Stardust's cameras observed that most of the comet's original surface has been preserved, thus exhibiting impact craters [135]. Comets 1P/Halley and 19P/Borrelly exhibited different surface morphologies because they often passed inside the orbit of Mars at perihelion, leaving them as remnants of the pristine balls of ice, rock, and organic matter that formed in the outer Solar System 4.5 billion years ago and resembling a dirty snowbank after a few warm rains [135]. Harold A. Weaver from Johns Hopkins University believes that comet 1P/Halley has made hundreds, if not thousands, of passages through the inner Solar System, which have caused its highly evolved surface to be smoothed by sublimation processes [99]. Comet Wild 2 appears to be in the early stages of its degradation [15]. According to planetary geologist Daniel Britt of the University of Central Florida in Orlando, who had previously studied the 19P/Borrelly images taken by DS1, the nucleus of comet Wild 2 looked like a very old surface that was just beginning to sublimate [135]. Britt believes that the spherical shape of the nucleus of comet Wild 2 and its impact-cratered surface hint at its direct formation from the dust and gas of the presolar disk. Wild 2 lacks major structural discontinuities and heterogeneities, suggesting that it did not form from the juxtaposition of large blocks of physically dissimilar materials acquired either by the accretion of various planetesimals or by extensive collisional processing [15]. In contrast with Wild 2, the ellipsoidal "potato-like" shape of the cometary nucleus of 1P/Halley was assumed to be formed either through a collision of two subnuclei or due to the fragmentation of a larger body during the early period of formation [10]. The nucleus of comet 19P/Borrelly was interpreted to have formed by the coalescence of multiple bodies [102]. The unique and preserved surface of the nucleus of Wild 2 made analysis of its physical and chemical composition particularly important.

### 1.7.8

#### Chemical Composition and *In Situ* Analyses of Wild 2 Dust Particles

The scientific payload of Stardust included the Cometary and Interstellar Dust Analyzer (CIDA), which was built by von Hoerner und Sulger GmbH, Schwetzingen, Germany, and which is – similar to PUMA onboard Vega and PIA onboard Giotto – a time-of-flight mass spectrometer that detects the atomic and molecular ions formed when fast dust particles strike the instrument's silver target [113]. At the relatively low speed of "only"  $6.1 \text{ km s}^{-1}$  of the Stardust space probe relative to the cometary dust particles, Kissel *et al.* expected that complex molecular ions would form; this formation had previously not been observed with PIA and PUMA, which approached comet 1P/Halley at  $v > 68 \text{ km s}^{-1}$ . The relatively low speed between the dust particles and CIDA's silver target implied that the formed ions originated from the uppermost few hundred monolayers of the dust particles, in which organic phases should be present [113]. It is important to note that the main parts of the volatile and refractory organic molecules that are believed to stick to the solid cometary dust grains with mineral kernels (see Chapter 2) will – according to Kissel *et al.* – be lost in the 20–60 min that it takes

for a dust particle that leaves the cometary nucleus to reach CIDA [113]. CIDA provided – in contrast with PIA and PUMA – both positive- and negative-ion modes, with the negative-ion mass spectra providing much more chemical information than the previously recorded positive-ion mass spectra [113]. A total of 29 impact events occurred during the flyby of comet Wild 2 and thus provided 29 mass spectra. These spectra confirm the presence of organic matter [113].

The negative-ion mass spectra of dust particles that originated from comet Wild 2 were dominated by ions with  $m/z = 26$ , which were interpreted as cyanide  $CN^-$  ions, providing evidence for a nitrogen-rich organic chemistry [113]. Cyanide anions had not been detected in the dust grains of comet 1P/Halley by the PIA and PUMA mass spectrometers, most likely because the PIA and PUMA instruments were limited to the positive-ionization mode. Kissel *et al.* suggest that such cyanide ions might have been formed from nitriles and polymerization products of hydrocyanic acid that struck CIDA's silver target and became ionized [113].

Kissel *et al.* [113] noted that the signals observed by CIDA at  $m/z = 33$  and 35 in the negative-ion mode could be attributed to  $SH^-$  ions, which had not been identified in interstellar dust during the Stardust cruise phase and hint at a sulfur-rich chemistry in cometary grains.  $S^-$  ions were not detected by CIDA but had been identified as positive ions in 1P/Halley.

CIDA's positive-ion mass spectra revealed typical peaks for  $CH^+$  ( $m/z = 13$ ),  $N^+$  (14),  $NH^+$  (15),  $O^+$  (16), and  $OH^+$  (17), along with lines of unsaturated organic species [113]. The surprising and most prominent signal in the positive-ion spectra at  $m/z = 90$  was more difficult to understand. Kissel *et al.* proposed that the  $C_6NH^+$  ion originated from methylpyridine-like alicyclic structures.

Mass signatures of water ice, POM, and aminonitriles were not present in CIDA's mass spectra; no traces of free amino acids were found [99, 113]. The CIDA mass spectra of Wild 2 dust grains are similar to the spectra obtained from comet 1P/Halley, thereby indicating that the two comets have similar chemistry even though they have different ages [113].

### 1.7.9

#### Gas and Dust Jets Emitted by the Wild 2 Nucleus

Comet Wild 2 contains dozens of regions that emit jets of gas and dust (Figure 1.31) [15], including collimated jets that are similar to those observed from Halley and Borrelly. Sekanina and colleagues [144] systematically assigned the Greek letters from  $\alpha$  to  $\psi$  to 20 of these jets and identified the location of the parent emission sources on the surface of the nucleus. It became apparent that the largest depressions on the surface of Wild 2 are devoid of activity, most likely because these zones were exhausted during previous passages of Wild 2 through the inner Solar System. Most of the jets originate near the latitude of the subsolar point, and it seems that one of the outstanding unresolved issues in cometary science [99] is to connect the jets of dust to particular surface features in the cometary nucleus. Tuzzolino *et al.* [136] used the DFMI onboard Stardust

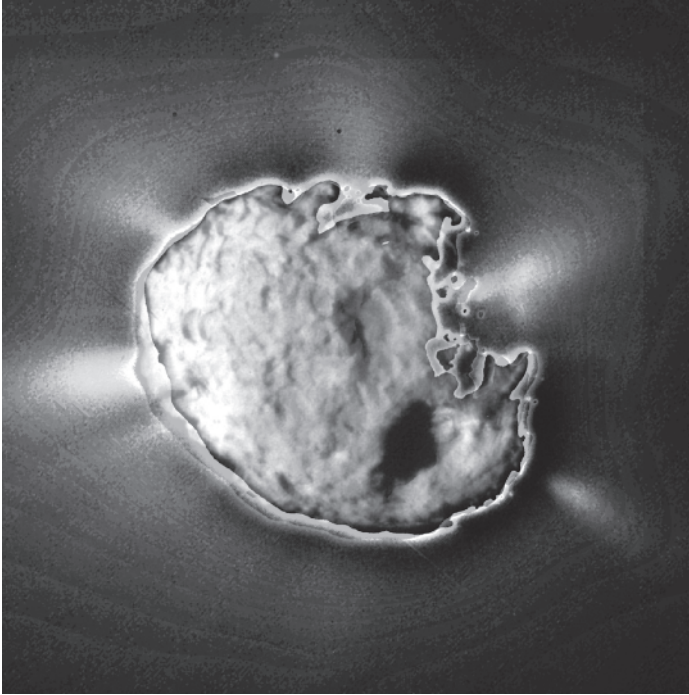


**Figure 1.31** Comet Wild 2 and its jets, which are visible because of reflected sunlight. On the shadowed night side of the nucleus depicted on the right, unusual jets that originated from Walker and from a region below Walker are visible. (Image credit: NASA.)

to determine the dust particle flux and recorded very large variation [145] in the mass distribution during flyby. The authors note that the Stardust space probe flew slowly through clouds of particles that were only a few hundred meters across, which originated in a burst of cometary activity.

In short, the nucleus of comet Wild 2 was found to be a microporous aggregate of very small grains of frozen volatiles and dust [15]. Sophisticated laboratory analyses of returned dust particle samples from Wild 2 revealed that many of the silicate grains are high-temperature minerals that formed in the inner regions of the solar nebula; this result considerably modified our understanding of the formation of comets [132]. Organic molecules such as methylamine, ethylamine, and glycine seem to be present in the returned samples from comet Wild 2.

## 1.8

### The Deep Impact Mission's Excavation of Comet 9P/Tempel 1

Deep Impact is a cometary space mission that belongs to NASA's Discovery Program. Its main scientific objective is to reveal the interior structure and physical and chemical compositions of a cometary nucleus. Comet 9P/Tempel, which

is also called *Tempel 1*, was chosen as the target. 9P/Tempel was discovered in 1867, and its orbital history is complex, with varying perihelion distances due to close approaches to Jupiter [18]. The design and concept of Deep Impact were unique: Deep Impact consisted of two independent unmanned parts, an impacting spacecraft to collide with and excavate the nucleus of comet 9P/Tempel and a flyby spacecraft to observe the impact and collect data. The response of the targeted comet 9P/Tempel was unclear: (i) a low-density nucleus composed of a fluffy agglomeration of ice and dust might swallow the impactor without leaving a trace, (ii), the impactor might leave a fairly conventional crater, or (iii), the nucleus of comet 9P/Tempel would completely disintegrate into pieces [146].

### 1.8.1

#### Observations of Comet 9P/Tempel Prior to the Impact

Deep Impact was launched in January 2005 so that it would reach comet 9P/Tempel in July 2005. On 3 July 2005, the impacting spacecraft depicted in Figure 1.32 separated from the mother spacecraft, and 24 h later, it effectively and successfully collided with the nucleus of comet 9P/Tempel with an impact speed of  $10.3 \text{ km s}^{-1}$ , an incidence angle of  $34^\circ$  to the local horizon [147], and an energy of  $\sim 2 \times 10^{10} \text{ J}$  [148].

The impactor spacecraft had a mass of 370.5 kg,<sup>17)</sup> and it used an autonavigation system to guide it to an impact location on the sunward side of the cometary nucleus, an impact location that also had to be visible to the scientific payload onboard the flyby spacecraft [147]. The impactor spacecraft was made of 49% copper to minimize chemical reactions with water in the comet, which would cause bright emission features [147]. The impactor itself was equipped with a camera that provided spectacular and scientifically important images of the cometary nucleus until  $\sim 4 \text{ s}$  prior to impact.

Because of the slow 40.7-h rotation period of the nucleus of comet 9P/Tempel, its dimensions could not be determined with very high precision; the mean radius was determined to be 3.0 km [147]. In 2001, Lamy *et al.* [149] reported 1997 observations of comet 9P/Tempel that were performed using the HST. Based on remote data, the authors predicted the semi-axes of the nucleus to be 3.9 and 2.8 km and a rotational period in the range of 25–33 h. Remote HST data recorded by the authors and reported in 2007 after the Deep Impact encounter with comet 9P/Tempel indicated even more accurate values for size (effective radius of 3.01 km) and rotational period ( $41.27 \pm 1.85 \text{ h}$ ) [150].

The Deep Impact data indicated that the nucleus of 9P/Tempel provided signs of past geological activity; it is much more than a primordial “dirty snowball” [146]. Several regions of distinct morphology were identified on the nucleus of 9P/Tempel: the top half differs from the bottom half, as shown in Figure 1.33, and

17) Often, the literature refers to a mass of 364 kg for the impactor spacecraft. However, the 6.5 kg of unused  $\text{N}_2\text{H}_4$  hydrazine fuel at the time of impact caused the total impactor mass to be 370.5 kg.

each half displays several dozen circular features that range from 40 to 400 m in diameter and are most likely impact craters [147]. The size distribution and morphology of the 9P/Tempel craters are distinct from the Wild 2 features observed by Stardust [147]. Unsurprisingly, the surface of comet 9P/Tempel is homogeneous in its geometric albedo, which has a value of  $p = 0.04$  [147]; this value is very similar to the albedo of the 1P/Halley and Wild 2 nuclei. The infrared spectrometer of Deep Impact enabled a precise measurement of the surface temperature of the nucleus of 9P/Tempel. The temperature varied from  $260 \pm 6$  K on the night side to  $329 \pm 8$  K on the comet's day side [147]. The observed temperatures were well matched with the topography of the nucleus: shadows corresponded the coolest places, whereas the hottest places were close to the subsolar point [147], that is, the point at which the Sun is at the zenith. A'Hearn and colleagues concluded from the observed temperatures that the thermal inertia of the cometary nucleus is low, most likely less than  $100 \text{ W K}^{-1} \text{ m}^{-2} \text{ s}^{-1/2}$  [147]. According to the temperature maps yielded by Deep Impact's infrared spectrometer, the surface of comet 9P/Tempel warms and cools quickly, which means that the surface must be porous, like loose sand or granular snow, rather than a solid block of ice [146]. The surface temperatures, colors, albedos, and spectra indicate no water ice on the cometary surface [147].

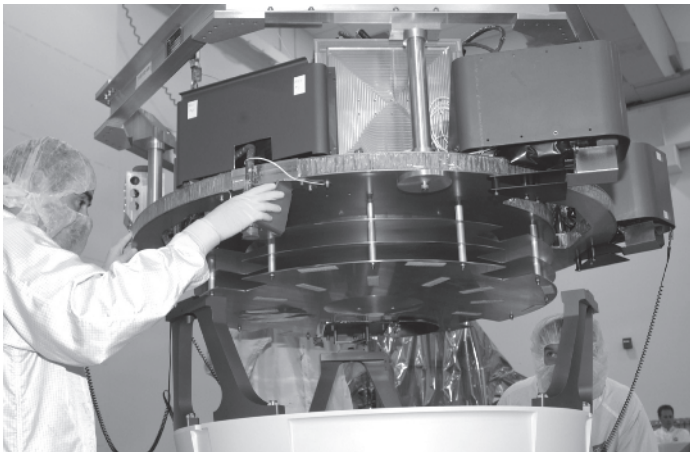


**Figure 1.32** The impactor spacecraft, with a mass of 370.5 kg, during attachment to the mounting ring, which is the white ring at the bottom of the figure with three titanium bipods. The mounting ring was used to fix the impactor spacecraft to the launch vehicle. Three parallel thin sheets made of copper protected the spacecraft from impacting cometary dust particles. Similar

Whipple-type aluminum and Kevlar sheets were used in 1986 to protect the Giotto space probe from impacting dust particles (see Figure 1.16). Just above the technician's right hand, the spacecraft's large, circular, aluminum main deck is visible; on top of this deck, the spacecraft control systems are mounted. (Image credit: NASA.)



**Figure 1.33** Composite of several images of comet 9P/Tempel 1 taken from the impactor-targeting sensor (ITS) installed onboard the impactor spacecraft. The highest resolution images are in the vicinity of the impactor site in the lower part of the image because images were recorded until  $\sim 4$  s prior to impact, which corresponded to a distance of  $\sim 40$  km from the surface. The Sun is on the right. Two large and particular smooth areas – which are similar to the plateau observed on comet Borrelly – appear in the upper right and the lower left on the image. The lower-left smooth terrain, which was recorded at higher resolution, is surrounded by a visible and Sun-illuminated bright scarp; the smooth area is elevated above the extremely rough terrain [147]. A'Hearn and colleagues suggested that the nucleus is layered in its structure and that the terrain outside the scarps was removed, thereby leaving an exhumed rough surface

that contains circular features [147]. Richard A. Kerr described this finding by saying that “one smooth area appears eaten away at its edges, revealing an older layer beneath with its own muted impact craters.” No one is willing to say whether the layers formed when Tempel 1 did or much later [146]. If 9P/Tempel loses  $10^9$  kg of material per perihelion passage, this mass would lower the surface – if lost from 10% of the  $100 \text{ km}^2$  area of the comet – by 10 cm (assuming a density of  $1000 \text{ kg m}^{-3}$ ) [147]. Alternatively, the lost mass per perihelion passage could have been provided by a material retreat of a 1-km-long and 20-m-high scarp of thickness 50 m. Because the nucleus of 9P/Tempel possesses several kilometers of such scarps, the mass loss was proposed to originate from a few meters of retreat of scarps per perihelion passage [147]. (Image credit: NASA/JPL/UMD.)

Prior to the collision between the impactor spacecraft and the nucleus, A'Hearn and colleagues aimed to link the coma phenomena observed for 9P/Tempel with remote instruments to specific locations on the nucleus. The coma was observed to be fainter than that of Wild 2, which made study of small outbursts easier but study of the coma harder [147]. Many of the frequent small outbursts were associated with an area located near local sunrise, and two active areas on the nucleus were successfully identified to have triggered two outbursts. For many well-observed outbursts, the duration was estimated to  $\sim 1$  h, and large outbursts were observed for a considerable portion of a day. A'Hearn and coworkers concluded from the time-resolved outburst observations that cometary outbursts occur nearly instantaneously, in a few minutes or even less [147].

### 1.8.2

#### Postimpact Observations of Comet 9P/Tempel

On 4 July 2005, the Deep Impact projectile spacecraft hit the nucleus of comet 9P/Tempel in its southern terrain. The magnificent impact was observed not only by the Deep Impact flyby spacecraft but also by nearly all of the entire world's ground- and space-based observing facilities in an unprecedented coordinated observational campaign [151]. It was also observed by instrumentation on the impactor itself, such as the impactor-targeting sensor (ITS). The optical system on the impactor was hit by large cometary dust particles at  $\sim 20$  and  $\sim 10$  s prior to impact, and the last image of the impact site exhibited a high resolution of  $\sim 3$  m/pixel (see Figure 1.33) [147]. The material released by the impact was estimated to have a mass of  $\sim 10^6$  kg [132, 152], which was removed from the comet in a "gentle fashion," thereby preserving the mineralogical nature of the component material at the micrometer-scale level, although the deaggregation of large ( $>100 \mu\text{m}$ ) fractal particles clearly occurred [153].

During the impact event, the Deep Impact mother spacecraft passed the cometary nucleus at a distance of 500 km. It decelerated to a velocity of  $100 \text{ m s}^{-1}$  to provide a 800-s viewing window after the impact [147]. Immediately after the impact, an initial flash of less than 200 ms in duration was observed; this flash was caused by the vaporization of the impactor and part of the comet. The second flash was associated with the first eruption of material from the cometary surface [147]. The velocity of this material was estimated to be  $7\text{--}10 \text{ km s}^{-1}$  [98]. The collision between the impacting spacecraft and the cometary nucleus excavated a large volume of very fine particles of microscopic size (Figure 1.34), most likely more than what could have been pulverized by the impact itself [147]. Dynamic ejecta flow properties allowed for an elegant calculation of the local gravitational acceleration at the impact site, which yielded a value of  $50 (+34/-25) \text{ mGal}$ , where the unit of acceleration (1 Gal) corresponds to  $1 \text{ cm s}^{-2}$  [147]. This value for the local gravitational acceleration requires the total mass of the nucleus to be  $7.2 \times 10^{13} \text{ kg}$  and the bulk density to be  $620 \text{ kg m}^{-3}$  [147], which corresponds to two-thirds the density of pure water ice [146]. The authors noted that the



**Figure 1.34** Comet 9P/Tempel as observed by the high-resolution camera on the Deep Impact flyby spacecraft 67 s after the impactor collided with the southern part of the cometary nucleus. (Image credit: NASA/JPL/UMD.)

calculated bulk density may very well differ from the density of the surface layers [147].

After impact, the mother spacecraft imaged an expanding cone of ejecta [146]. Infrared spectral analyses of the excavated cometary ejecta revealed emission features, including those of  $\text{H}_2\text{O}$ ,  $\text{HCN}$ , and  $\text{CO}_2$ . These data indicate that even if no water ice is found on the cometary surface itself, ices are located near the surface [147]. Moreover, infrared bands that correspond to the C–H vibrational stretching mode, which is often called the *organic feature* and typically occurs in molecules such as formaldehyde and methanol, were identified in the cometary ejecta [147]. Spectral analysis at various times, including pre-impact spectra, revealed a strong “organic feature,” thereby indicating that the impact might have vaporized organic molecules that would not normally be vaporized in comets [147]. A  $\nu_2 = 4.40\text{-}\mu\text{m}$  feature in the cometary ejecta was tentatively attributed to a CN stretching band in methyl cyanide ( $\text{CH}_3\text{CN}$ ), as confirmed by the  $\nu_1 = 3.38\text{-}\mu\text{m}$  feature of the CH stretching band [147].

Postimpact observations of comet 9P/Tempel from an Earth-based campaign that was unprecedented in size and scope (it involved 73 Earth-based telescopes at 35 observatories [151]) provided supplementary and complementary information. These data confirm the observation of new material after impact that was

compositionally different from that observed prior to impact. As an example, the Keck-1 telescope observed that the CN  $\Delta\nu = 0$  emission bands increased in brightness by more than a factor of 5 after impact [151]. At 1.5 h after impact, the CN emission began to decrease [151]. Compounds such as H<sub>2</sub>O, C<sub>2</sub>H<sub>6</sub>, CH<sub>3</sub>OH, C<sub>2</sub>H<sub>2</sub>, and HCN that were not directly detectable before impact were identified by near-infrared spectroscopy after the impact [151]. HCN (88.6 and 265.9 GHz) and CH<sub>3</sub>OH (145 GHz) were also monitored by ground-based radio telescopes for a few days after impact [151].

Mumma and colleagues [154] used the Keck-2 telescope in Hawaii to quantify volatile organic molecules such as C<sub>2</sub>H<sub>6</sub>, CH<sub>3</sub>OH, CO, CH<sub>4</sub>, C<sub>2</sub>H<sub>2</sub>, and HCN, and also water before, during, and after the impact using high-dispersion near-infrared spectroscopy. Interestingly, these authors found that the abundance ratio of ethane relative to water increased after impact by a factor of 1.8, whereas the abundance ratios for methanol and hydrogen cyanide remained unchanged. The data hint at the possibility that the nucleus of 9P/Tempel is inhomogeneous in its composition [154]. Mumma *et al.* [154] speculate that the impactor spacecraft hit a region on the cometary surface located between two circular features that might be exposed rims of primordial cometesimals; if so, the impact ejecta might represent material from those cometesimals. In contrast with the results of Mumma *et al.*, data taken by the optical, spectroscopic, and infrared remote imaging system (OSIRIS) camera onboard the Rosetta spacecraft found a cyanide-to-water production ratio that was slightly enhanced in the impact cloud, with hydrogen cyanide as the suggested parent molecule [155].

Ground-based spectroscopy of the cometary postimpact ejecta in the mid-infrared range often exhibited superb signal-to-noise ratios [132]. These spectra revealed the presence of submicrometer-sized dust grains because of an increase in the brightness of the 8- to 13- $\mu\text{m}$  silicate emission feature [151]. This emission feature was dominated by signals that originate from amorphous pyroxene, amorphous olivine, and magnesium-rich crystalline olivine [43]. Observations of the emission features by NASA's Spitzer Space Telescope were used to determine the mineralogical composition of the comet. With the help of the spectra of 11 laboratory standard minerals, the presence of amorphous and crystalline silicates, amorphous carbon, carbonates, phyllosilicates, PAHs, water gas and ice, and sulfides in the cometary ejecta was identified [153]. The relative atomic abundances, compared with Si = 1.0, in the ejected dust were determined to be H = 15, C = 0.53, O = 11, Si = 1.0, Mg = 0.88, Fe = 0.74, S = 0.28, Ca = 0.054, and Al  $\leq$  0.085 [153]. Mg-rich forsterite and Fe-rich fayalite were found to be the dominant olivine species in a 3.9 abundance-ratio-by-mole fraction, suggesting that the temperature for the incorporation of olivine into the comet was between 1100 and 1400 K [153]. The mean temperature of the icy grain particles in the cometary ejecta was estimated to be 220 K. The presence of high-temperature crystalline silicates (olivines) was surprising and requires thermal heating of material near the young Sun, where temperatures  $>1000$  K were reached only inside the present orbit of Mercury [153]. A method for efficiently transporting the silicates out to the formation region of the comet, such as strong mixing

of material in the proto-solar nebula, is required [153]. However, in view of the mineralogical composition proposed by Lisse *et al.* for the dust of comet 9P/Tempel, Brownlee and colleagues [132], who had examined the Stardust data, point to the fact that the model composition chosen to match cometary and laboratory infrared data is not at all consistent with the Stardust sample return data: no compelling evidence for either the presence of the proposed mineral phases or their thermal decomposition products has been observed in the Stardust samples. Only forsterite was found in Wild 2 at abundances above a few percent [132]. FeMg-sulfides, carbonates, amorphous olivine, pyroxene, and hydrated silicates were not observed in Wild 2 [132]. To provide an explanation for the observed differences in the Deep Impact and Stardust data, Brownlee and colleagues argue that the comets 9P/Tempel and Wild 2 might be different but also that the laboratory materials that were chosen to match the infrared observations may not be appropriate analogs for submicron cometary materials that are both ancient and complex [132]. Furthermore, Zolensky and coworkers point to the fact that the mineralogy reported by Lisse *et al.* for comet 9P/Tempel is in clear contrast with the lack of aqueous alteration products in Wild 2 that was demonstrated by the Stardust mission [137]. This mineralogical difference could be due to differences in the geological histories of Jupiter-family comets [137].

The dust distribution in the inner part of the ejected plume was found to be inconsistent with a purely gravitational origin, thereby implying that the evaporation and expansion of volatiles accelerated the dust [156]. The implication that sublimating water molecules accelerate dust particles in the cometary coma was confirmed by observations of comet 9P/Tempel performed using the OSIRIS camera system<sup>18)</sup> onboard the Rosetta spacecraft, which was, at the time of impact, located at a distance of 0.53 AU from 9P/Tempel [148]. The kinetic energy of the impactor spacecraft, which was  $\sim 2 \times 10^{10}$  J, was estimated to be insufficient to provide the required energy to sublime the observed amount of water [148, 155]. The energy for the sublimation of water and the acceleration of dust in the coma was provided by sunlight [148]. Moreover, Sugita and colleagues [156] found that the high mass ratio of crystalline silicates compared with amorphous silicates demonstrates that comet 9P/Tempel, which is a Jupiter-family comet, contains many high-temperature components of the solar nebula, similar to Oort-cloud comets.

Spectroscopic signatures of organic refractory material were not found in the mid-infrared emission bands [151]. The ratio of the dust mass of the cometary ejecta to the gas mass increased because of the forced impact [151]. Because the ejected dust came from a deeper surface layer than normal, the volatile content of the material several meters below the surface of the nucleus seems to be depleted

18) OSIRIS stands for Optical, Spectroscopic, and Infrared Remote Imaging System. The OSIRIS camera is onboard the European Space Agency's Rosetta spacecraft, which will reach its target comet 67P/Churyumov-Gerasimenko in August 2014. According to Egyptian mythology, Osiris (which is ancient

Greek for "place of the eye") is also the name of an Egyptian god that was murdered, cut into pieces, and distributed over the country by his brother Seth. Isis found the heart of her husband Osiris on an island on the Nile River called *Philae Island*.

[151]. Observations of comet 9P/Tempel performed by the OSIRIS camera system onboard the Rosetta spacecraft provided estimates of the quantity of the water vapor content,  $4.5 \times 10^6$  kg – this value corresponds to 20% of the water molecules that were present in the cometary coma as a result of normal activity – and the cross section of the ejected dust,  $330 \text{ km}^2$  [148]. Küppers, Keller, and colleagues [155] concluded that the dust/ice mass ratio is most likely  $>1$ , thereby suggesting that comets are “icy dirtballs” rather than “dirty snowballs,” as is commonly believed [148].

The activity increase caused by the impact lasted for only a few days; on 9 July 2005, the comet's behavior was indistinguishable from its pre-impact behavior, and no new long-lived jet or fan has been identified as resulting from the newly excavated crater [151]. The reason why a major jet did not occur after the excavation of a volatile-rich layer remains unknown [156]. The lack of a major jet suggests that, in general, impacts of meter-sized meteoroids are not the cause of the frequently observed outbursts of comets [148].

The Deep Impact data about comet 9P/Tempel modified our view about comets and, in particular, cometary nuclei. After Borrelly and Wild 2, comet 9P/Tempel was the third Jupiter-family comet whose surface was imaged at high resolution. The shapes and topographies of these three comets are very different from one another, which raised the question of whether any comet can be considered typical when examined closely [147]. The comets Borrelly and 9P/Tempel are believed to have performed many perihelion passages and thus spent a long time in the inner Solar System, whereas comet Wild 2 did not. However, the differences between Borrelly and 9P/Tempel are as great as the differences between either of them and Wild 2 [147]. Comet 9P/Tempel exhibits morphological evidence for classical impact craters, which were the first to be observed on a cometary nucleus [157].

### 1.8.3

#### **Postimpact Observations of Comet 9P/Tempel by Stardust-NExT: Impact Site and the Actively Eroding Scarp**

NASA's Stardust spacecraft, which took dust samples from the cometary tail of Wild 2 in 2004 that were successfully returned to Earth in 2006, where they were distributed for detailed analysis to laboratories [132], obtained an important extension of its scientific mission in 2007. The new mission phase was named Stardust-NExT, the Stardust New Exploration of Tempel 1, and Joe Veverka of Cornell University became the principal investigator. On 4 February 2011, during its extended mission, the Stardust spacecraft encountered comet 9P/Tempel [158]. 9P is the comet onto which the NASA's Deep Impact mission's projectile impactor crashed in July 2005 [147], and 9P remains the only cometary nucleus that was visited by two spacecraft; the visits were separated by a cometary year. Table 1.3 compares the 9P/Tempel encounter characteristics for the Stardust-NExT spacecraft with those of the Deep Impact mother spacecraft.

One of the crucial objectives of the Stardust-NExT mission was to use the spacecraft camera, NAVCAM, to record images of the crater produced by the impactor

**Table 1.3** Characteristics of the 9P/Tempel encounters. (Adapted from [158].)

	Deep Impact	Stardust-NExT
Encounter time	1 day before perihelion	34 days after perihelion
Flyby distance (km)	500	178
Flyby speed (km s <sup>-1</sup> )	10.2	10.9
Activity (H <sub>2</sub> O) (mol s <sup>-1</sup> )	5 × 10 <sup>27</sup>	3 × 10 <sup>27</sup>

in 2005 [158]. During its flyby maneuver in 2005, the Deep Impact mother spacecraft was not able to capture images of the crater [147] because a cloud of dust that resulted from the impact obscured the surface of the impact site and made it invisible from a distance of 500 km. Estimates of the size of the crater suggested that it was a few hundred meters in diameter and 25 m in depth, but they were highly uncertain and depended on the density and strength of the cometary nucleus [18]. The initial impact point was precisely determined to lie in a 20–40 m area on the surface of 9P [159]. Due to the 34° inclination of the impactor trajectory, this area is elliptic and not circular. Figure 1.35 depicts the impact side prior to impact and postimpact. The diameter of the minimally observed crater was estimated to be  $49 \pm 12$  m [160].

The Stardust-NExT camera, which was considerably improved during inflight calibration [162], provided 72 images during the closest cometary approach phase, and the best images exhibited a resolution of 11 m/pixel [158]. Deep Impact provided images of approximately one-third of the cometary nuclear surface. Together with Stardust-NExT, ~70% of the nuclear surface was imaged [163] and ~20 km<sup>2</sup> of the comet's surface area were imaged by both missions, thereby providing important information about surface changes during 1 cometary year [158]. No other cometary nucleus has been as extensively imaged as comet 9P/Tempel.

Comparison of the Deep Impact and Stardust-NExT images revealed that in terms of its albedo, photometric properties, and morphology, most of the surface of comet 9P/Tempel remained unchanged during the cometary year between 2005 and 2011 [158]. According to Stardust-NExT measurements, the average geometric albedo of the 9P/Tempel surface is  $p = 0.059 \pm 0.009$ , which indicates a uniformly black surface [158]. The Stardust-NExT data images of 9P/Tempel's surface indicate that it is covered by rough and pitted terrain [158], similar to that on Wild 2 [15]. This pitted terrain contains – according to Veverka and coworkers – far more pits than can be accounted for by impacts; therefore most pits, which are typically 10–30 m in diameter, were suggested to originate due from “mini-outbursts,” which are considered to be sources of material ejected into the coma [158, 164].

The dust instruments onboard Stardust-NExT revealed that in 2011, the coma and jet activity of comet 9P/Tempel was less than in 2005 [158]. This difference is due to the encounter time of Stardust-NExT, which was 34 days after perihelion

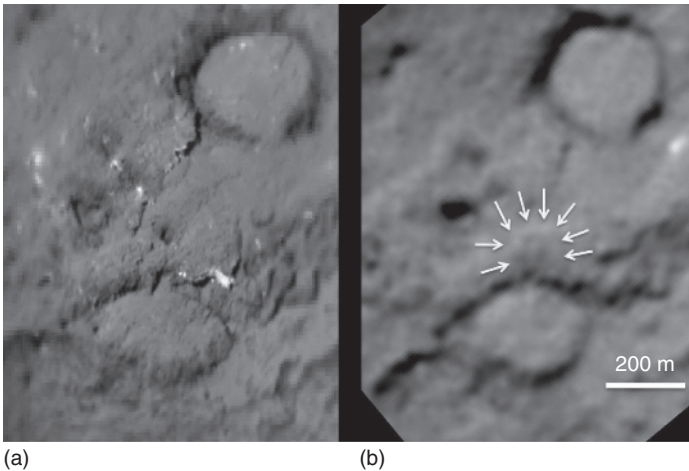


**Figure 1.35** Comparison of the surface of comet 9P/Tempel pre- and postimpact. The pre-impact image (a) was provided by NASA's Deep Impact impactor spacecraft prior to smashing into the comet's surface in July 2005. Its high resolution of the surface is due to its small distance of  $\sim 40$  km. The postimpact image (b) was recorded by the Stardust-NExT spacecraft in 2011 from a distance of  $>178$  km. The arrows indicate a possible rim of the crater that was caused by the impactor. The crater was estimated to be  $49 \pm 12$  m in diameter. It is surrounded by an area of slightly brightened material,

which marks a potential ejecta blanket that is 85–120 m in diameter [160], thereby implying surface properties that are similar to those of dry, loose snow [158], or lightly packed mountain snow [160]. The depth of the crater was too difficult to estimate [160]. The bright mound in the center of the created crater is most likely due to material that fell back into the crater. The crater may have originally been larger, but postimpact collapse or erosion and mass wasting might have modified its original size [161]. (Image credit: NASA/JPL-Caltech/University of Maryland/Cornell.)

passage, and it is most likely also due to a constant decline in cometary activity. Furthermore, the dust instruments detected bursts through which larger aggregates of material emitted from the nucleus subsequently fragmented into smaller particles within the coma [158].

Interestingly, and as also observed by Deep Impact [146, 147], most of the jets could be traced back to an apparently eroding terraced scarp [158] that surrounds the smoothed terrain. This activity indicates that the scarp is actively eroding. Remember that the 1986 missions to comet 1P/Halley did not allow active and inactive surfaces to be distinguished on the cometary nucleus [1, 4]. The height of one terraced scarp was determined to be 50 m, and it was found that the scarp morphology at the boundaries varies across the surface [158]. Some scarp edges were found to be sharp, some were concave, some were terraced, and others were scalloped [158]. Comparison of images taken by Deep Impact with images from Stardust-NExT revealed significant changes in the morphology along one scarp of a smooth terrain: in at least two places, this scarp receded by up to 50 m during the cometary year between 2005 and 2011 [158], which accounts for  $\sim 2\%$  of the total mass loss of comet 9P/Tempel per perihelion passage [163]. The smoothed

terrain itself was found to compose approximately one-third of the surface of comet 9P/Tempel [158]; a detailed discussion of the smooth terrain is provided by Thomas *et al.* [163]. Knowledge about the surface properties of comet 9P/Tempel, including its smooth terrain, led Veverka and colleagues [158] to propose it as an ideal candidate for a future cometary sample return mission.

The CIDA onboard Stardust and Stardust-NExT operated during the comet 9P/Tempel flyby. As it approached 9P/Tempel, CIDA captured dust particles at a velocity of  $10.9 \text{ km s}^{-1}$  ( $6.1 \text{ km s}^{-1}$  in the case of Wild 2 particles) [113], which were ionized when they impacted CIDA's silver target. CIDA recorded 46 mass spectra of comet 9P/Tempel dust particles in the negative-ion mode and 34 in the positive-ion mode [158]. The recorded mass spectra exhibited prominent signals at  $m/z = 1$  for  $\text{H}^-$  and at  $m/z = 26$  for cyanide ions (see Section 1.7). Many spectra were reported to exhibit long tails at high mass numbers, which were interpreted as indicative of the presence of complex molecules [158].

The spacecraft that completed the original Stardust and Stardust-NExT missions is in a 1.5-year solar orbit and was shut down on 24 March 2011 [158].

#### 1.8.4

##### **The Encounter of the Deep Impact Spacecraft with Comet 103P/Hartley**

Because of its successful observation and performance of a unique impact experiment on comet 9P/Tempel in 2005, NASA's Deep Impact mission was not terminated: rather, in 2010, the Deep Impact mother spacecraft, which was not destroyed during the impact and observation of comet 9P/Tempel in 2005 and which contains highly sophisticated payload for cometary flyby and observation, was redirected toward another comet. The Deep Impact extended mission was called *EPOXI (Extrasolar Planet Observation and Deep Impact Extended Investigation)*, and Michael F. A'Hearn from the University of Maryland was appointed as its principal investigator. Initially, comet 85P/Boethin was selected as the comet target for the Deep Impact extended mission, but 85P – which had been observed in 1975 and 1986 but not in 1997 – was declared lost in 2007, presumably because it had disintegrated into fragments [165]. Comet 103P/Hartley was selected as the new target comet for NASA's EPOXI Discovery mission. Comet 103P/Hartley was of particular interest because it has a smaller nucleus compared with the previously visited 1P/Halley, 19P/Borrelly, Wild 2, and 9P/Tempel comets [166]. The nucleus of comet Hartley 2 – the fifth nucleus imaged by spacecraft – is  $\sim 2 \text{ km}$  long and  $\sim 400 \text{ m}$  wide at the “neck,” its most narrow portion. Comet 103P/Hartley was known for its high activity.

The Deep Impact mother spacecraft approached comet 103P/Hartley in November 2010 at a distance of 694 km, when the comet was 1.06 AU from the Sun and 1 week after its perihelion passage [167]. The flyby speed of the EPOXI spacecraft was  $12.3 \text{ km s}^{-1}$  [167]; for comparison, the Stardust spacecraft approached comet Wild 2 at a much shorter distance of 236 km and at lower velocity of  $6.1 \text{ km s}^{-1}$  [128] during the approach of Wild 2 to the Sun at a 1.86 AU distance [113].

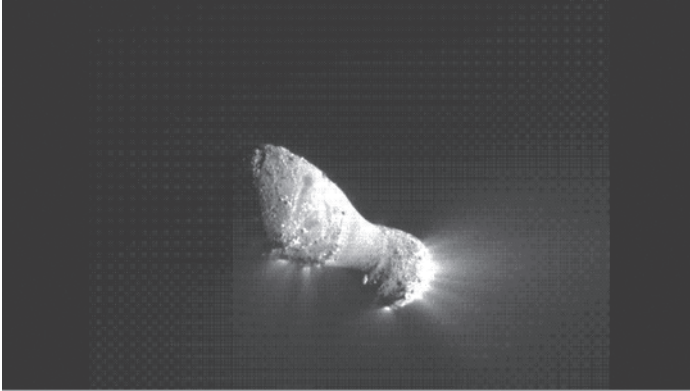


**Figure 1.36** Image of Comet Hartley 2 captured by NASA's EPOXI mission in November 2010 during the spacecraft's flyby at a distance of  $\sim 700$  km. It was captured using the medium-resolution instrument (MRI) onboard the EPOXI spacecraft, which provided a resolution of 8.5 m/pixel. The Sun is to the right [167]. (Image credit: NASA/JPL-Caltech/UMD.)

During the 3 months of EPOXI's 103P/Hartley investigations, more than 100 000 images and spectra were taken [167]. The shape of the nucleus of comet 103P/Hartley was found to be bilobed, elongated, and nearly axially symmetric [168] (Figure 1.36) and similar in form to the nucleus of comet 19P/Borrelly; its maximum length was determined to be 2.33 km [167], which should be compared with a value of  $\sim 8$  km for 19P/Borrelly. The nucleus of comet 103P/Hartley was observed by an international campaign that accompanied the EPOXI mission. This campaign used ground- and space-based telescopes in a coordinated fashion and determined a rapidly changing rotation period of comet 103P/Hartley ranging from  $\sim 16.4$  h prior to the onset of its activity to near 19 h in December 2010 [169].

Comet 103P/Hartley was found to be bilobed [168]. The central "waist" region of comet 103P/Hartley was observed to be of smooth shape, and its surface is mottled on horizontal scales of 10–30 m and exhibits isolated cases of local height relief  $>10$  m [167]. A smoothed region was also identified in part of the larger lobe. The nucleus of comet 103P/Hartley is composed of two lobes, and the smaller lobe points toward the Sun in the image presented in Figure 1.36. The main parts of both lobes exhibit rough and knobby terrain that is characterized by rounded-to-angular elevated forms that are as much as 50 m high and 80 m wide [167]. Many of these elevated forms exhibit two to three times greater geometric albedo than the average value of  $p = 0.04$ , which is a much greater albedo range than was observed for comet 9P/Tempel [167]. Systematic albedo maps were created for the parts of the nucleus of comet Hartley 2 that were visible from the EPOXI spacecraft [170]. The larger lobe contains several dark spots that are  $<80$  m diameter [167]. The combination of two types of terrain, the central smooth surface and the knobby terrain at the lobes of comet 103P/Hartley, is very different from 9P/Tempel or Wild 2, in which both exhibit a population of depressions [167].

Most importantly, jets can be observed to stream out of the nucleus of comet 103P/Hartley. These jets occur in all terrains but are clustered in the rough topography of the smaller lobe that points toward the Sun and in parts of the larger lobe, as shown in Figure 1.36 [167]. However, the resolution of 10–12 m was considered insufficient to clearly resolve the morphology of the sources of the jets [167]. First attempts to connect individual jets with morphological surface features using visible light images of Hartley 2 were reported to indicate correlations between specific surface structures and both narrow-angled and fan-shaped dust jets; associations included pits, depressions, scarps, and rimless depressions [171].

A'Hearn and coworkers reported an 8-day increase and decrease in the CN radical emission without a corresponding maximum in the cometary dust production, which is considered atypical of cometary outbursts [167]. An extended source, other than the well-established HCN photodissociation, that might involve the presence of HCN polymers in the nucleus of comet was proposed by the authors (extended sources for cometary volatiles will be presented in Section 2.5.6). As expected, the nucleus of comet 103P/Hartley was found to be very active. Surprisingly, the jets exhibited substantial differences in the relative abundance of volatiles such as H<sub>2</sub>O and CO<sub>2</sub> at several of the parts of the comet [167]. The waist of the nucleus exhibited water-vapor-rich emissions with relatively little CO<sub>2</sub> and water ice, whereas the small lobe that pointed toward the Sun exhibited ejecta that primarily contained CO<sub>2</sub>, organics, and water ice [167]. This phenomenon is still under investigation, and a sound explanation for it is still missing. Comet 103P/Hartley was observed by the HST to be among the most CO-depleted comets [172]. Figure 1.37 shows the near-nucleus environment in the form of clouds of particles and large chunks of particles emitted from the nucleus of comet 103P/Hartley [167].

Summarizing the obtained data, A'Hearn and colleagues conclude that comet 103P/Hartley is different from 9P/Tempel in many aspects, including its bilobed shape. Moreover, comet 103P/Hartley is hyperactive, like 46P/Wirtanen and 21P/Giacobini-Zinner, and it exhibits a CN-radical ejection anomaly, high H<sub>2</sub>O production rates from the waist region, and CO<sub>2</sub>/H<sub>2</sub>O variations of a factor of 2 from one lobe to the other [167].

The diversity of Jupiter-family comets is well, but not exclusively, represented by the differences in cometary surface morphologies: 103P/Hartley was found to be bilobed with smooth terrain at its waist and knobby terrain at the lobes. 81P/Wild 2 is dominated by steep-walled and flat-floored depressions, whereas 9P/Tempel 1 is relatively smooth and exhibits evidence of flows and layering [175]. In 2010, prior to EPOXI's 103P/Hartley observations, Belton [176] proposed a remarkable possible scenario for the long-term evolution of cometary surfaces near the Sun. This scenario suggested an evolutionary sequence by which Jupiter-family comets might evolve from a Wild 2-type morphology to a Tempel 1-type morphology and, finally, to a Hartley 2-type morphology [175]. Belton predicted that the surfaces of 103P/Hartley 2 (the EPOXI mission target observed in November 2010) and 67P/Churyumov-Gerasimenko (the Rosetta mission target that will be encountered in 2014) should exhibit multiple layers and collapse

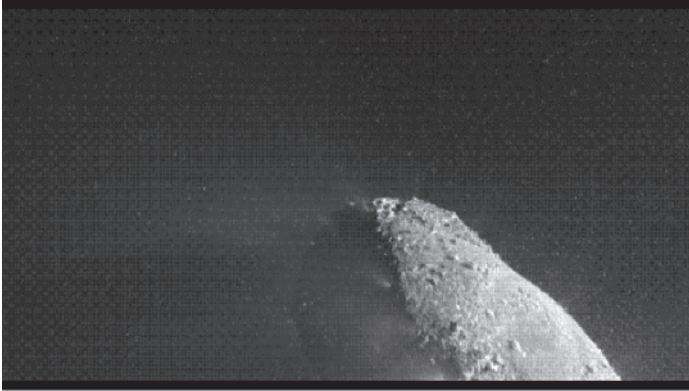


**Figure 1.37** Close-up image of a part of the nucleus of comet Hartley 2 taken by the high-resolution instrument (HRI) on NASA's EPOXI mission spacecraft in November 2010 during closest approach. The nucleus is illuminated by the Sun from the right. A distinct cloud of particles emitted by the cometary nucleus is visible. Individual large chunks of particles of size greater than a few centimeters – up to sizes of 20 cm – can be observed near the nucleus; these particles typically move with low velocities of  $<0.5 \text{ m s}^{-1}$  [167].

A detailed study of the detection, localization, and dynamics of large icy particles surrounding comet 103P/Hartley 2 was performed by Hermalyn and colleagues [173]. The particle size was estimated to be as large as 2 m [174]. The authors found that the emitted particles exhibit a temporally varying brightness, which suggests rotating, heterogeneous, and faceted geometries. Such a near-nucleus environment has not been observed in any other comet to date. (Image Credit: NASA/JPL-Caltech/UMD)

features that are more similar to those on 9P and 19P than to those on 81P [176]. The EPOXI encounter with Hartley 2 confirmed that the surface was unlike that of Wild 2, but it did not confirm or deny layering [175]. Considering the EPOXI data, Cheng and colleagues [175] argued instead that the diversity of cometary surface morphologies reflects geologic processing due to impact cratering, cometary activity, and eolian erosion; these processes provide diverse outcomes that are not necessarily the result of an evolutionary sequence of comets.

After the encounter with comet 103P/Hartley, the Deep Impact mother spacecraft, EPOXI, was directed toward a near-Earth asteroid, which will be reached in 2020. In August 2013, however, communication with the spacecraft failed and could not be reestablished as of September 2013, when NASA declared the mission lost.

## References

1. Huebner, W.F. and McKay, C.P. (1990) in *Physics and Chemistry of Comets* (ed. W.F. Huebner), Springer, Heidelberg, pp. 305–331.
2. Muñoz Caro, G.M., Meierhenrich, U.J., Schutte, W.A., Barbier, B., Arcones Segovia, A., Rosenbauer, H., Thiemann, W.H.-P., Brack, A., and Greenberg, J.M. (2002) Amino acids from ultraviolet irradiation of interstellar ice analogues. *Nature*, **416**, 403–406.
3. Weissman, P.R., Bottke, W.F. Jr., and Levison, H.F. (2002) in *Asteroids III*,

- (eds W.F. Bottke Jr., A. Cellino, P. Paolicchi, and R.P. Binzel), University of Arizona Press, Tucson, AZ, pp. 669–686.
4. Keller, H.U. (1990) in *Physics and Chemistry of Comets* (ed. W.F. Huebner), Springer, Heidelberg, pp. 13–68.
  5. Lamy, P.L., Toth, I., Weaver, H.A., Delahodde, C., Jorda, L., and A'Hearn, M.F. (2000) The nucleus of 13 short-period comets. Proceedings of the DPS Pasadena Meeting 2000, October 23–27, 2000. *Bull. Am. Astron. Soc.*, **32**, 36.04.
  6. Fernandez, Y.R. (2002) The nucleus of comet Hale-Bopp (C/1995 O1): size and activity. *Earth, Moon Planets*, **89**, 3–25.
  7. Reinhard, R. (1986) The Giotto encounter with comet Halley. *Nature*, **321**, 313–318.
  8. Rickman, H. and Huebner, W.F. (1990) in *Physics and Chemistry of Comets* (ed. W.F. Huebner), Springer, Heidelberg, pp. 245–304.
  9. Whipple, F.L. (1950) A comet model. I. The acceleration of comet Encke. *Astron. Astrophys. J.*, **111**, 375–394.
  10. Keller, H.U., Delamere, W.A., Huebner, W.F., Reitsema, H.J., Schmidt, H.U., Whipple, F.L., Wilhelm, K., Curdt, W., Kramm, R., Thomas, N., Arpigny, C., Barbieri, C., Bonnet, R.M., Cazes, S., Coradini, M., Cosmovici, C.B., Hughes, D.W., Jamar, C., Malaise, D., Schmidt, K., Schmidt, W.K.H., and Seige, P. (1987) Comet P/Halley's nucleus and its activity. *Astron. Astrophys.*, **187**, 807–823.
  11. Sagdeev, R.Z., Szabo, F., Avanesov, G.A., Cruvellier, P., Szabo, L., Szego, K., Abergel, A., Balazs, A., Barinov, I.V., Bertaux, J.-L., Blamont, J., Detaille, M., Demarelis, E., Dul'nev, G.N., Endröcyy, G., Gardos, M., Kanyo, M., Kostenko, V.I., Krasikov, V.A., Nguyen-Trong, T., Nyitrai, Z., Reny, I., Rusznyak, P., Shamis, V.A., Smith, B., Sukhanov, K.G., Szabo, F., Szalai, S., Tarnopolsky, V.I., Toth, I., Tsukanova, G., Valnicek, B.L., Varhalmi, L., Zaiko, Y.K., Zatsepin, S.I., Ziman, Y.L., Zsenei, M., and Zhukov, B.S. (1986) Television observations of comet Halley from Vega spacecraft. *Nature*, **321**, 262–266.
  12. Rosenberg, E.D. and Prialnik, D. (2010) The effect of internal inhomogeneity on the activity of comet nuclei – Application to comet 67P/Churyumov-Gerasimenko. *Icarus*, **209**, 753–765.
  13. A'Hearn, M.F. and Festou, M.C. (1990) in *Physics and Chemistry of Comets* (ed. W.F. Huebner), Springer, Heidelberg, pp. 69–112.
  14. Huebner, W.F. (1990) in *Physics and Chemistry of Comets* (ed. W.F. Huebner), Springer, Heidelberg, pp. 1–12.
  15. Brownlee, D.E., Horz, F., Newburn, R.L., Zolensky, M., Duxbury, T.C., Sandford, S., Sekanina, Z., Tsou, P., Hanner, M.S., Clark, B.C., Green, S.F., and Kissel, J. (2004) Surface of young Jupiter family comet 81 P/Wild 2: view from the Stardust Spacecraft. *Science*, **304**, 1764–1769.
  16. Prialnik, D. and Bar-Nun, A. (1992) Crystallization of amorphous ice as the cause of comet P/Halley's outburst at 14 AU. *Astron. Astrophys.*, **258**, L9–L12.
  17. Ip, W.-H. and Axford, W.I. (1990) in *Physics and Chemistry of Comets* (ed. W.F. Huebner), Springer, Heidelberg, pp. 177–234.
  18. Brandt, J.C. and Chapman, R.D. (2004) *Introduction to Comets*, 2nd edn, Cambridge University Press, Cambridge.
  19. Grün, E. and Jessberger, E.K. (1990) Dust, in *Physics and Chemistry of Comets* (ed. W.F. Huebner), Springer, Heidelberg, pp. 113–176.
  20. Boehnhardt, H. (2004) in *Comets II* (eds M.C. Festou, H.U. Keller, and H.A. Weaver), University of Arizona Press, Tucson, AZ, pp. 301–316.
  21. Altenhoff, W.J., Bertoldi, F., Menten, K.M., Sievers, A., Thum, C., and Kreysa, E. (2002) Radio continuum observations of Comet C/1999 S4 (LINEAR) before, during, and after break-up of its nucleus. *Astron. Astrophys.*, **391**, 353–360.
  22. Weaver, H.A., Sekanina, Z., Toth, I., Delahodde, C.E., Hainaut, O.R., Lamy, P.L., Bauer, J.M., A'Hearn, M.F.,

- Arpigny, C., Combi, M.R., Davies, J.K., Feldman, P.D., Festou, M.C., Hook, R., Jorda, L., Keesey, M.S.W., Lisse, C.M., Marsden, B.G., Meech, K.J., Tozzi, G.P., and West, R. (2001) HST and VLT investigations of the fragments of Comet C/1999 S4 (LINEAR). *Science*, **292**, 1329–1333.
23. Sekanina, Z. (1982) in *Comets* (ed. L.L. Wilkening), University of Arizona Press, Tucson, AZ, pp. 251–287.
24. Artemieva, N. (2013) Russian skyfall. *Nature*, **503**, 202–203.
25. Brown, P.G., Assink, J.D., Astiz, L., Blaauw, R., Boslough, M.B., Borovička, J., Brachet, N., Brown, D., Campbell-Brown, M., Ceranna, L., Cooke, W., de Groot-Hedlin, C., Drob, D.P., Edwards, W., Evers, L.G., Garces, M., Gill, J., Hedlin, M., Kingery, A., Laske, G., Le Pichon, A., Mialle, P., Moser, D.E., Saffer, A., Silber, E., Smets, P., Spalding, R.E., Spurný, P., Tagliaferri, E., Uren, D., Weryk, R.J., Whitaker, R., and Krzeminski, Z. (2013) A 500-kiloton airburst over Chelyabinsk and an enhanced hazard from small impactors. *Nature*, **503**, 238–241.
26. Borovička, J., Spurný, P., Brown, P., Wiegert, P., Kalenda, P., Clark, D., and Shrubbený, L. (2013) The trajectory, structure and origin of the Chelyabinsk asteroidal impactor. *Nature*, **503**, 235–237.
27. Moberley, M. (2010) *Hunting and Imaging Comets*, Springer, Heidelberg.
28. Bailey, M.E., Chambers, J.E., and Hahn, G. (1992) Origin of sungrazers: a frequent cometary end-state. *Astron. Astrophys.*, **257**, 315–322.
29. Whitman, K., Morbidelli, A., and Jedicke, R. (2006) The size-frequency distribution of dormant Jupiter family comets. *Icarus*, **183**, 101–114.
30. Meech, K.J. and Belton, M.J.S. (1990) The atmosphere of 2060 Chiron. *Astron. J.*, **100**, 1323–1338.
31. Prialnik, D., Brosch, N., and Ianovici, D. (1995) Modelling the activity of 2060 Chiron. *Mon. Not. R. Astron. Soc.*, **276**, 1148–1154.
32. Beust, H., Lagrange-Henri, A.M., Vidal-Madjar, A., and Ferlet, R. (1990) The  $\beta$  Pictoris circumstellar disk. *Astron. Astrophys.*, **236**, 202–216.
33. Zuckerman, B. and Song, I. (2012) A 40 Myr old gaseous circumstellar disk at 49 Ceti: massive CO-rich comet clouds at young A-type stars. *Astrophys. J.*, **758**, 77 (10 pp.).
34. Halleio, E. (1882) *Astronomiae cometicae synopsis*. *Philos. Trans. R. Soc. London*, **24**, 289–304.
35. Oort, J.H. (1990) in *Physics and Chemistry of Comets* (ed. W.F. Huebner), Springer, Heidelberg, pp. 235–244.
36. A'Hearn, M.F. (2006) Whence comets? *Science*, **314**, 1708–1709.
37. Oort, J.H. (1950) The structure of the cloud of comets surrounding the Solar System and a hypothesis concerning its origin. *Bull. Astron. Inst. Neth.*, **11**, 91–110.
38. Levison, H.F., Dones, L., and Duncan, M.J. (2001) The origin of Halley-type comets: probing the inner Oort cloud. *Astron. J.*, **121**, 2253–2267.
39. Weissman, P.R. (1991) in *Comets in the Post-Halley Era* (eds R.L. Newburn Jr., M. Neugebauer, and J. Rahe), Kluwer Academic Publishers, Dordrecht, pp. 463–486.
40. Edgeworth, K.E. (1949) The origin and evolution of the solar system. *Mon. Not. R. Astron. Soc.*, **192**, 600–609.
41. Kuiper, G.P. (1951) in *Astrophysics* (ed. J.A. Hynek), McGraw Hill Book Co., New York, pp. 357–424.
42. Jewitt, D. and Luu, J. (1993) Discovery of the candidate Kuiper belt object 1992 QB1. *Nature*, **362**, 730–732.
43. Harker, D.E., Woodward, C.E., and Wooden, D.H. (2005) The dust grains from 9P/Tempel 1 before and after encounter with Deep Impact. *Science*, **310**, 278–280.
44. Carusi, A. and Valsecchi, G. (1987) in *Interplanetary Matter* (eds Z. Ceplecha and P. Pecina), Czech. Acad. Sci., Ondrejov, pp. 21–28.
45. Horner, J., Evans, N.W., Bailey, M.E., and Asher, D.J. (2003) The populations of comet-like bodies in the Solar System. *Mon. Not. R. Astron. Soc.*, **343**, 1057–1066.
46. Levison, H.F. and Duncan, M.J. (1994) The long-term dynamical behavior

- of short-period comets. *Icarus*, **108**, 18–36.
47. Morbidelli, A., Levison, H.F., Tsiganis, K., and Gomes, R. (2005) Chaotic capture of Jupiter's Trojan asteroids in the early Solar System. *Nature*, **435**, 462–465.
  48. Mumma, M.J. and Charnley, S.B. (2011) The chemical composition of comets – emerging taxonomies and natal heritage. *Annu. Rev. Astron. Astrophys.*, **49**, 471–524.
  49. Levison, H.F., Duncan, M.J., Brassier, R., and Kaufmann, D.E. (2010) Capture of the Sun's Oort Cloud from stars in its birth cluster. *Science*, **326**, 187–190.
  50. Maddox, J. (1986) First journey to a comet. *Nature*, **321**, 366.
  51. Hirao, K. and Itoh, T. (1986) The Planet-A Halley encounters. *Nature*, **321**, 294–297.
  52. Kremnev, R.S., Linkin, V.M., Lipatov, A.N., Pichkadze, K.M., Shurupov, A.A., Terterashvili, A.V., Bakitko, R.V., Blamont, J.E., Malique, C., Ragent, B., Preston, R.A., Elson, L.S., and Crisp, D. (1986) Vega balloon system and instrumentation. *Science*, **231**, 1408–1411.
  53. Sagdeev, R.Z., Blamont, J., Galeev, A.A., Moroz, V.I., Shapiro, V.D., Shevchenko, V.I., and Szegő, K. (1986) Vega spacecraft encounters with comet Halley. *Nature*, **321**, 259–262.
  54. Grün, E., Pailer, N., Fechtig, H., and Kissel, J. (1980) Orbital and physical characteristics of micrometeoroids in the inner Solar System as observed by Helios 1. *Planet. Space Sci.*, **28**, 333–349.
  55. Kissel, J., Sagdeev, R.Z., Bertaux, J.L., Angarov, V.N., Audouze, J., Blamont, J.E., Büchler, K., Evlanov, E.N., Fechtig, H., Fomenkova, M.N., von Hoerner, H., Inogamov, N.A., Khromov, V.N., Knabe, W., Krueger, F.R., Langevin, Y., Leonas, V.B., Levasseur-Regourd, A.C., Managadze, G.G., Podkolzin, S.N., Shapiro, V.D., Tabaldyev, S.R., and Zubkov, B.V. (1986) Composition of comet Halley dust particles from Vega observations. *Nature*, **321**, 280–282.
  56. Krueger, F.R. and Kissel, J. (1987) The chemical composition of the dust of comet P/Halley as measured by “PUMA” on board Vega-1. *Naturwissenschaften*, **74**, 312–316.
  57. Kissel, J. and Krueger, F.R. (1987) The organic component in dust from comet Halley as measured by the PUMA mass spectrometer on board Vega 1. *Nature*, **326**, 755–760.
  58. Jessberger, E.K., Christoforidis, A., and Kissel, J. (1988) Aspects of the major element composition of Halley's dust. *Nature*, **332**, 691–695.
  59. Meierhenrich, U.J., Muñoz Caro, G.M., Schutte, W.A., Thiemann, W.H.-P., Barbier, B., and Brack, A. (2005) Precursors of biological cofactors from ultraviolet irradiation of circumstellar/interstellar ice analogues. *Chem. Eur. J.*, **11**, 4895–4900.
  60. Combes, M., Moroz, V.I., Crifo, J.F., Lamarre, J.M., Charra, J., Sanko, N.F., Soufflot, A., Bibring, J.P., Cazes, S., Coron, N., Crovisier, J., Emerich, C., Encrenaz, T., Gispert, R., Grigoryev, A.V., Guyot, G., Krasnopolsky, V.A., Nikolsky, Y.V., and Rocard, F. (1986) Infrared sounding of comet Halley from Vega 1. *Nature*, **321**, 266–268.
  61. Combes, M., Moroz, V.I., Crovisier, J., Encrenaz, T., Bibring, J.-P., Grigoriev, A.V., Sanko, N.F., Coron, N., Crifo, J.F., Gispert, R., Bockelée-Morvan, D., Nikolsky, Y.V., Krasnopolsky, V.A., Owen, T., Emerich, C., Lamarre, J.M., and Rocard, F. (1988) The 2.5–12  $\mu\text{m}$  spectrum of comet Halley from the IKS-VEGA experiment. *Icarus*, **76**, 404–436.
  62. Krasnopolsky, V.A., Gogoshev, M., Moreels, G., Moroz, V.I., Krysko, A.A., Gogosheva, T., Palazov, K., Sargoichev, S., Clairemidi, J., Vincent, M., Bertaux, J.L., Blamont, J.E., Troshin, V.S., and Valníček, B. (1986) Spectroscopic study of comet Halley by the Vega 2 three-channel spectrometer. *Nature*, **321**, 269–271.
  63. Moreels, G., Gogoshev, M., Krasnopolsky, V.A., Clairemidi, J., Vincent, M., Parisot, J.P., Bertaux, J.L., Blamont, J.E., Festou, M.C., Gogosheva, T., Sargoichev, S., Palasov, K., Moroz, V.I., Krysko, A.A., and Vanyšek, V. (1986) Near-ultraviolet and visible

- spectrophotometry of comet Halley from Vega 2. *Nature*, **321**, 271–273.
64. Moreels, G., Clairemidi, J., Hermine, P., Brechignac, P., and Rousselot, P. (1994) Detection of a polycyclic aromatic molecule in comet P/Halley. *Astron. Astrophys.*, **282**, 634–656.
  65. Crovisier, J. and Bockelée-Morvan, D. (1999) Remote observations of the composition of cometary volatiles. *Space Sci. Rev.*, **90**, 19–32.
  66. Crovisier, J., Leech, K., Bockelée-Morvan, D., Brooke, T.Y., Hanner, M.S., Altieri, B., Keller, H.U., and Lellouch, E. (1997) The spectrum of comet Hale-Bopp (C/1995 O1) observed with the Infrared Space Observatory at 2.9 astronomical units from the sun. *Science*, **275**, 1904–1907.
  67. Clairemidi, J., Moreels, G., Mousis, O., and Bréchignac, P. (2008) Identification of anthracene in comet 1P/Halley. *Astron. Astrophys.*, **492**, 245–250.
  68. Clairemidi, J., Bréchignac, P., Moreels, G., and Pautet, D. (2004) Tentative identification of pyrene as a polycyclic aromatic molecule in UV spectra of comet P/Halley: an emission from 368 to 384 nm. *Planet. Space Sci.*, **52**, 761–772.
  69. Vaisberg, O.L., Smirnov, V.N., Gorn, L.S., Iovlev, M.V., Balikhin, M.A., Klimov, S.I., Savin, S.P., Shapiro, V.D., and Shevchenko, V.I. (1986) Dust coma structure of comet Halley from SP-1 detector measurements. *Nature*, **321**, 274–276.
  70. Mazets, E.P., Aptekar, R.L., Golenetskii, S.V., Guryan, Y.A., Dyachkov, A.V., Ilyinskii, V.N., Panov, V.N., Petrov, G.G., Savvin, A.V., Sagdeev, R.Z., Sokolov, I.A., Khavenson, N.G., Shapiro, V.D., and Shevchenko, V.I. (1986) Comet Halley dust environment from SP-2 detector measurements. *Nature*, **321**, 276–278.
  71. Simpson, J.A., Sagdeev, R.Z., Tuzzolino, A.J., Perkins, M.A., Ksanfomality, L.V., Rabinowitz, D., Lentz, G.A., Afonin, V.V., Erö, J., Keppler, E., Kosorokov, J., Petrova, E., Szabó, L., and Umlauf, G. (1986) Dust counter and mass analyser (DUCMA) measurements of comet Halley's coma from Vega spacecraft. *Nature*, **321**, 278–280.
  72. Keppler, E., Afonin, V.V., Curtis, C.C., Dyachkov, A.V., Erö, J., Fan, C.Y., Hsieh, K.C., Hunten, D.M., Ip, W.-H., Richter, A.K., Somogyi, A.J., and Umlauf, G. (1986) Neutral gas measurements of comet Halley from Vega 1. *Nature*, **321**, 273–274.
  73. Gringauz, K.I., Gombosi, T.I., Remizov, A.P., Apáthy, I., Szemerey, I., Verigin, M.I., Denchikova, L.I., Dyachkov, A.V., Keppler, E., Klimenko, I.N., Richter, A.K., Somogyi, A.J., Szegő, K., Szendrő, S., Tátrallyay, M., Varga, A., and Vladimirova, G.A. (1986) First in situ plasma and neutral gas measurements at comet Halley. *Nature*, **321**, 282–285.
  74. Klimov, S., Savin, S., Aleksevich, Y., Avanesova, G., Balebanov, V., Balikhin, M., Galeev, A., Gribov, B., Nozdrachev, M., Smirnov, V., Sokolov, A., Vaisberg, O., Oberc, P., Krawczyk, Z., Grzedzielski, S., Juchniewicz, J., Nowak, K., Orłowski, D., Parfianovich, B., Woźniak, D., Zbyszynski, Z., Voita, Y., and Triska, P. (1986) Extremely-low-frequency plasma waves in the environment of comet Halley. *Nature*, **321**, 292–293.
  75. Somogyi, A.J., Gringauz, K.I., Szegő, K., Szabó, L., Kozma, G., Remizov, A.P., Erö, J., Klimenko, I.N., Szücs, I.T., Verigin, M.I., Windberg, J., Cravens, T.E., Dyachkov, A., Erdős, G., Faragó, M., Gombosi, T.I., Kecskeméty, K., Keppler, E., Kovács, T., Kondor, A., Logachev, Y.I., Lohonyai, L., Marsden, R., Redl, R., Richter, A.K., Stolpovskii, V.G., Szabó, J., Szentpétery, I., Szepesváry, A., Tátrallyay, M., Varga, A., Vladimirova, G.A., Wenzel, K.P., and Zarándy, A. (1986) First observations of energetic particles near comet Halley. *Nature*, **321**, 285–288.
  76. Gard, R., Pedersen, A., Trotignon, J.-G., Beghin, C., Mogilevsky, M., Mikhailov, Y., Molchanov, O., and Formisano, V. (1986) Observations of waves and plasma in the environment of comet Halley. *Nature*, **321**, 290–291.
  77. Riedler, W., Schwingenschuh, K., Yeroshenko, Y.G., Styashkin, V.A., and

- Russell, C.T. (1986) Magnetic field observations in comet Halley's coma. *Nature*, **321**, 288–289.
78. Bobrovnikoff, N.T. (1942) Physical theory of comets in the light of spectroscopic data. *Rev. Mod. Phys.*, **14**, 164–178.
  79. Mendis, D.A. and Horányi, M. (2013) Dusty plasma effects in comets: expectations for Rosetta. *Rev. Geophys.*, **51**, 53–75.
  80. Biermann, L. (1951) Kometenschweife und solare Korpuskularstrahlung. *Z. Astrophys.*, **29**, 274–286.
  81. Niedner, M.B. Jr., Rothe, E.D., and Brandt, J.C. (1978) Interplanetary gas. XXII. Interaction of comet Kohoutek's ion tail with the compression region of a solar-wind corotating system. *Astrophys. J.*, **221**, 1014–1025.
  82. Axford, W.I. (1964) The interaction of solar wind with comets. *Planet. Space Sci.*, **12**, 719–720.
  83. Hansen, K.C., Bagdonat, T., Motschmann, U., Alexander, C., Combi, M.R., Cravens, T.E., Gombosi, T.I., Jia, Y.-D., and Robertson, I.P. (2009) in *Rosetta – ESA's Mission to the Origin of the Solar System* (eds R. Schulz, C. Alexander, H. Boehnhardt, and K.-H. Glassmeier), Springer, Heidelberg, pp. 69–98.
  84. Gortsas, N., Motschmann, U., Kührt, E., Glassmeier, K.-H., Hansen, K.C., Müller, J., and Schmidt, A. (2010) Global plasma-parameter simulation of Comet 67P/Churyumov-Gerasimenko approaching the Sun. *Astron. Astrophys.*, **520**, A92.
  85. Ip, W.-H. (1989) On charge exchange effect in the vicinity of the cometopause of Comet Halley. *Astrophys. J.*, **343**, 946–952.
  86. McComas, D.J., Elliott, H.A., Gosling, J.T., Reisenfeld, D.B., Skoug, R.M., Goldstein, B.E., Neugebauer, M., and Balogh, A. (2002) Ulysses' second fast-latitude scan: Complexity near solar maximum and the reformation of polar coronal holes. *Geophys. Res. Lett.*, **29** (9), 4-1–4-4.
  87. Barnard, E.E. (1903) Photographic observations of Borrelly's comet and explanation of the phenomenon of the tail on July 24. *Astrophys. J.*, **18**, 210–217.
  88. Niedner, M.B. Jr., and Brandt, J.C. (1978) Interplanetary gas. XXIII. Plasma tail disconnection events in comets: evidence for magnetic field reconnection at interplanetary sector boundaries. *Astrophys. J.*, **223**, 655–670.
  89. Brandt, J.C., Caputo, F.M., Hoeksema, J.T., Niedner, M.B. Jr., Yi, Y., and Snow, M. (1999) Disconnection events (DEs) in Halley's comet 1985–1986: the correlation with crossings of the heliospheric current sheet (HCS). *Icarus*, **137**, 69–83.
  90. Saito, T., Yumoto, K., Hirao, K., Nakagawa, T., and Saito, K. (1986) Interaction between comet Halley and the interplanetary magnetic field observed by Sakigake. *Nature*, **321**, 303–306.
  91. Münch, R.E., Sagdeev, R.Z., and Jordan, J.F. (1986) Pathfinder: accuracy improvement of comet Halley trajectory for Giotto navigation. *Nature*, **321**, 318–320.
  92. Biermann, L. (1968) On the Emission of Atomic Hydrogen in Comets. Joint Institute for Laboratory Astrophysics (JILA) Report No. 93, University of Colorado, Boulder, CO.
  93. Kaneda, E., Ashihara, O., Shimizu, M., Takagi, M., and Hirao, K. (1986) Observation of comet Halley by the ultraviolet imager of Suisei. *Nature*, **321**, 297–299.
  94. Mukai, T., Miyake, W., Terasawa, T., Kitayama, M., and Hirao, K. (1986) Plasma observation by Suisei of solar-wind interaction with comet Halley. *Nature*, **321**, 299–303.
  95. Oyama, K.I., Hirao, K., Hirano, T., Yumoto, K., and Saito, T. (1986) Was the solar wind decelerated by comet Halley? *Nature*, **321**, 310–313.
  96. Oya, H., Morioka, A., Miyake, W., Smith, E.J., and Tsurutani, B.T. (1986) Discovery of cometary kilometric radiations and plasma waves at comet Halley. *Nature*, **321**, 307–310.

97. West, R.M., Pedersen, H., Monderen, P., Vio, R., and Grosbøl, P. (1986) Post-perihelion imaging of comet Halley at ESO. *Nature*, **321**, 363–365.
98. Keller, H.U., Arpigny, C., Barbieri, C., Bonnet, R.M., Cazes, S., Coradini, M., Cosmovici, C.B., Delamere, W.A., Huebner, W.F., Hughes, D.W., Jamar, C., Malaise, D., Reitsema, H.J., Schmidt, H.U., Schmidt, W.K.H., Seige, P., Whipple, F.L., and Wilhelm, K. (1986) First Halley multicolour camera imaging results from Giotto. *Nature*, **321**, 320–326.
99. Weaver, H.A. (2004) Not a rubble pile? *Science*, **304**, 1760–1762.
100. Belton, M.J.S., Julian, W.H., Anderson, A.J., and Mueller, B.E.A. (1991) The spin state and homogeneity of comet Halley's nucleus. *Icarus*, **93**, 183–193.
101. Samarasinha, N.H. and A'Hearn, M.F. (1991) Observational and dynamical constraints on the rotation of Comet P/Halley. *Icarus*, **93**, 194–225.
102. Soderblom, L.A., Becker, T.L., Bennett, G., Boice, D.C., Britt, D.T., Brown, R.H., Buratti, B.J., Isbell, C., Giese, B., Hare, T., Hicks, M.D., Howington-Kraus, E., Kirk, R.L., Lee, M., Nelson, R.M., Oberst, J., Owen, T.C., Rayman, M.D., Sandel, B.R., Stern, S.A., Thomas, N., and Yelle, R.V. (2002) Observations of comet 19P/Borrelly by the miniature integrated camera and spectrometer aboard Deep Space 1. *Science*, **296**, 1087–1091.
103. Sekanina, Z. and Larson, S.M. (1986) Dust jets in comet Halley observed by Giotto and from the ground. *Nature*, **321**, 357–361.
104. McDonnell, J.A.M., Alexander, W.M., Burton, W.M., Bussolletti, E., Clark, D.H., Grard, R.J.L., Grün, E., Hanner, M.S., Hughes, D.W., Igenbergs, E., Kuczera, H., Lindblad, B.A., Mandeville, J.-C., Minafra, A., Schwehm, G.H., Sekanina, Z., Wallis, M.K., Zarnecki, J.C., Chakaveh, S.C., Evans, G.C., Evans, S.T., Firth, J.G., Littler, A.N., Massonne, L., Olearczyk, R.E., Pankiewicz, G.S., Stevenson, T.J., and Turner, R.F. (1986) Dust density and mass distribution near comet Halley from Giotto observations. *Nature*, **321**, 338–341.
105. Grün, E., Graser, U., Kohoutek, L., Thiele, U., Massonne, L., and Schwehm, G. (1986) Structures in the coma of comet Halley. *Nature*, **321**, 144–147.
106. Festou, M.C., Feldman, P.D., A'Hearn, M.F., Arpigny, C., Cosmovici, C.B., Danks, A.C., McFadden, L.A., Gilmozzi, R., Patriarchi, P., Tozzi, G.P., Wallis, M.K., and Weaver, H.A. (1986) IUE observations of comet Halley during the Vega and Giotto encounters. *Nature*, **321**, 361–363.
107. Krankowsky, D., Lämmerzahl, P., Herrwerth, I., Woweries, J., Eberhardt, P., Dolder, U., Herrmann, U., Schulte, W., Berthelier, J.J., Illiano, J.M., Hodges, R.R., and Hoffman, J.H. (1986) *In situ* gas and ion measurements at comet Halley. *Nature*, **321**, 326–329.
108. Eberhardt, P. (1999) Comet Halley's gas composition and extended sources: results from the neutral mass spectrometer on Giotto. *Space Sci. Rev.*, **90**, 45–52.
109. Balsiger, H., Altwegg, K., Bühler, F., Geiss, J., Ghielmetti, A.G., Goldstein, B.E., Goldstein, R., Huntress, W.T., Ip, W.-H., Lazarus, A.J., Meier, A., Neugebauer, M., Rettenmund, U., Rosenbauer, H., Schwenn, R., Sharp, R.D., Shelley, E.G., Ungstrup, E., and Young, D.T. (1986) Ion composition and dynamics at comet Halley. *Nature*, **321**, 330–334.
110. Korth, A., Richter, A.K., Loidl, A., Anderson, K.A., Carlson, C.W., Curtis, D.W., Lin, R.P., Rème, H., Sauvaud, J.A., d'Uston, C., Cotin, F., Cros, A., and Mendis, D.A. (1986) Mass spectra of heavy ions near comet Halley. *Nature*, **321**, 335–336.
111. Levasseur-Regourd, A.C., Bertaux, J.L., Dumont, R., Festou, M., Giese, R.H., Giovane, E., Lamy, P., Le Blanc, J.M., Llebaria, A., and Weinberg, J.L. (1986) Optical probing of comet Halley from the Giotto spacecraft. *Nature*, **321**, 341–344.
112. Kissel, J., Brownlee, D.E., Büchler, K., Clark, B.C., Fechtig, H., Grün, E., Hornung, K., Igenbergs, E.B., Jessberger, E.K., Krueger, F.R., Kuczera, H., McDonnell, J.A.M., Morfill, G.M., Rahe, J., Schwehm, G.H., Sekanina,

- Z., Utterback, N.G., Völk, H.J., and Zook, H.A. (1986) Composition of comet Halley dust particles from Giotto observations. *Nature*, **321**, 336–337.
113. Kissel, J., Krueger, F.R., Silén, J., and Clark, B.C. (2004) The cometary and interstellar dust analyzer at comet 81P/Wild 2. *Science*, **304**, 1774–1776.
114. Eberhardt, P., Reber, M., Krankowsky, D., and Hodges, R.R. (1995) The D/H and  $^{18}\text{O}/^{16}\text{O}$  ratios in water from comet P/Halley. *Astron. Astrophys.*, **302**, 301–316.
115. Edenhofer, P., Bird, M.K., Brenkle, J.P., Buschert, H., Esposito, P.B., Porsche, H., and Volland, H. (1986) First results from the Giotto Radio-Science Experiment. *Nature*, **321**, 355–357.
116. McKenna-Lawlor, S., Kirsch, E., O’Sullivan, D., Thompson, A., and Wenzel, K.-P. (1986) Energetic ions in the environment of comet Halley. *Nature*, **321**, 347–349.
117. Johnstone, A., Coates, A., Kellock, S., Wilken, B., Jockers, K., Rosenbauer, H., Studemann, W., Weiss, W., Formisano, V., Amata, E., Cerulli-Irelli, R., Dobrowolny, M., Terenzi, R., Egidi, A., Borg, H., Hultquist, B., Winningham, J., Gurgiolo, C., Bryant, D., Edwards, T., Feldman, W., Thomsen, M., Wallis, M.K., Biermann, L., Schmidt, H., Lust, R., Haerendel, G., and Paschmann, G. (1986) Ion flow at comet Halley. *Nature*, **321**, 344–347.
118. Rème, H., Sauvaud, J.A., d’Uston, C., Cotin, F., Cros, A., Anderson, K.A., Carlson, C.W., Curtis, D.W., Lin, R.P., Mendis, D.A., Korth, A., and Richter, A.K. (1986) Comet Halley–solar wind interaction from electron measurements aboard Giotto. *Nature*, **321**, 349–352.
119. Neubauer, F.M., Glassmeier, K.H., Pohl, M., Raeder, J., Acuna, M.H., Burlaga, L.F., Ness, N.F., Musmann, G., Mariani, F., Wallis, M.K., Ungstrup, E., and Schmidt, H.U. (1986) First results from the Giotto magnetometer experiment at comet Halley. *Nature*, **321**, 352–355.
120. McDonnell, J.A.M., McBride, N., Beard, R., Bussoletti, E., Colangeli, L., Eberhardt, P., Firth, J.G., Grard, R., Green, S.F., Greenberg, J.M., Grün, E., Hughes, D.W., Keller, H.U., Kissel, J., Lindblad, B.A., Mandeville, J.-C., Perry, C.H., Rembor, K., Rickman, H., Schwehm, G.H., Turner, R.F., Wallis, M.K., and Zarnecki, J.C. (1993) Dust particle impacts during the Giotto encounter with comet Grigg–Skjellerup. *Nature*, **362**, 732–734.
121. McBride, N., Green, S.F., Levasseur-Regourd, A.-C., Goidet-Devel, B., and Renard, J.-B. (1997) The inner dust coma of comet 26P/Grigg-Skjellerup: multiple jets and nucleus fragments. *Mon. Not. R. Astron. Soc.*, **289**, 535–553.
122. Neubauer, F.M., Marschall, H., Pohl, M., Glassmeier, K.-H., Musmann, G., Mariani, F., Acuna, M.H., Burlaga, L.F., Ness, N.F., Wallis, M.K., Schmidt, H.U., and Ungstrup, E. (1993) First results from the Giotto magnetometer experiment during the P/Grigg-Skjellerup encounter. *Astron. Astrophys.*, **268**, L5–L8.
123. Rayman, M.D. (2003) The successful conclusion of the Deep Space 1 Mission: important results without a flashy title. *Space Technol.*, **23**, 185.
124. Rayman, M.D., Varghese, P., Lehman, D.H., and Livesay, L.L. (2000) Results from the Deep Space 1 technology validation mission. *Acta Astronaut.*, **47**, 475–487.
125. Kerr, R.A. (2001) Close look at the heart of Borrelly. *Science*, **294**, 27–28.
126. Lamy, P.L., Toth, I., and Weaver, H.A. (1999) Hubble Space Telescope observations of the nucleus and inner coma of comet 19P/1904 Y2 (Borrelly). *Astron. Astrophys.*, **337**, 945–954.
127. Lamy, P.L., Toth, I., Davidsson, B.J.R., Groussin, O., Gutiérrez, P., Jorda, L., Kaasalainen, M., and Lowry, S.C. (2009) in *Rosetta – ESA’s Mission to the Origin of the Solar System* (eds R. Schulz, C. Alexander, H. Boehnhardt, and K.-H. Glassmeier), Springer, Heidelberg, pp. 21–54.
128. Rowan, L. (2004) Sweet dreams are made of these. *Science*, **304**, 1760.
129. Baker, J. (2006) Look into the seeds of time. *Science*, **314**, 1707.

130. Burnett, D.S. (2006) NASA returns rocks from a comet. *Science*, **314**, 1709–1710.
131. Elsila, J.E., Glavin, D.P., and Dworkin, J.P. (2009) Cometary glycine detected in samples returned by Stardust. *Meteorit. Planet. Sci.*, **44**, 1323–1330.
132. Brownlee, D., Tsou, P., Aléon, J., Alexander, C.M.O'D., Araki, T., Bajt, S., Baratta, G.A., Bastien, R., Bland, P., Bleuét, P., Borg, J., Bradley, J.P., Brearley, A., Brenker, F., Brennan, S., Bridges, J.C., Browning, N.D., Brucato, J.R., Bullock, E., Burchell, M.J., Busemann, H., Butterworth, A., Chaussidon, M., Cheuvront, A., Chi, M., Cintala, M.J., Clark, B.C., Clemett, S.J., Cody, G., Colangeli, L., Cooper, G., Cordier, P., Daghljan, C., Dai, Z., d'Hendecourt, L., Djouadi, Z., Dominguez, G., Duxbury, T., Dworkin, J.P., Ebel, D.S., Economou, T.E., Fakra, S., Fairey, S.A.J., Fallon, S., Ferrini, G., Ferroir, T., Fleckenstein, H., Floss, C., Flynn, G., Franchi, I.A., Fries, M., Gainsforth, Z., Gallien, J.-P., Genge, M., Gilles, M.K., Gillet, P., Gilmour, J., Glavin, D.P., Gounelle, M., Grady, M.M., Graham, G.A., Grant, P.G., Green, S.F., Grossemy, E., Grossman, L., Grossman, J.N., Guan, Y., Hagiya, K., Harvey, R., Heck, P., Herzog, G.F., Hoppe, P., Hörz, F., Huth, J., Hutcheon, I.D., Ignatyev, K., Ishii, H., Ito, M., Jacob, D., Jacobsen, C., Jacobsen, S., Jones, S., Joswiak, D., Jurewicz, A., Kearsley, A.T., Keller, L.P., Khodja, H., Kilcoyne, A.L.D., Kissel, J., Krot, A., Langenhorst, F., Lanzirotti, A., Le, L., Leshin, L.A., Leitner, J., Lemelle, L., Leroux, H., Liu, M.-C., Luening, K., Lyon, I., MacPherson, G., Marcus, M.A., Marhas, K., Marty, B., Matrajt, G., McKeegan, K., Meibom, A., Mennella, V., Messenger, K., Messenger, S., Mikouchi, T., Mostefaoui, S., Nakamura, T., Nakano, T., Newville, M., Nittler, L.R., Ohnishi, I., Ohsumi, K., Okudaira, K., Papanastassiou, D.A., Palma, R., Palumbo, M.E., Pepin, R.O., Perkins, D., Perronnet, M., Pianetta, P., Rao, W., Rietmeijer, F.J.M., Robert, F., Rotundi, A., Ryan, R., Sandford, S.A., Schwandt, C.S., See, T.H., Schlutter, D., Sheffield-Parker, J., Simionovici, A., Simon, S., Sittitsky, I., Snead, C.J., Spencer, M.K., Stadermann, F.J., Steele, A., Stephan, T., Stroud, R., Susini, J., Sutton, S.R., Suzuki, Y., Taheri, M., Taylor, S., Teslich, N., Tomeoka, K., Tomioka, N., Toppiani, A., Trigo-Rodríguez, J.M., Troadec, D., Tsuchiyama, A., Tuzzolino, A.J., Tyliczszak, T., Uesugi, K., Velbel, M., Vellenga, J., Vicenzi, E., Vincze, L., Warren, J., Weber, I., Weisberg, M., Westphal, A.J., Wirick, S., Wooden, D., Wopenka, B., Wozniakiewicz, P., Wright, I., Yabuta, H., Yano, H., Young, E.D., Zare, R.N., Zega, T., Ziegler, K., Zimmerman, L., Zinner, E., and Zolensky, M. (2006) Comet 81P/Wild 2 under a microscope. *Science*, **314**, 1711–1715.
133. Hörz, F., Bastien, R., Borg, J., Bradley, J.P., Bridges, J.C., Brownlee, D.E., Burchell, M.J., Chi, M., Cintala, M.J., Dai, Z.R., Djouadi, Z., Dominguez, G., Economou, T.E., Fairey, S.A.J., Floss, C., Franchi, I.A., Graham, G.A., Green, S.F., Heck, P., Hoppe, P., Huth, J., Ishii, H., Kearsley, A.T., Kissel, J., Leitner, J., Leroux, H., Marhas, K., Messenger, K., Schwandt, C.S., See, T.H., Snead, C., Stadermann, F.J., Stephan, T., Stroud, R., Teslich, N., Trigo-Rodríguez, J.M., Tuzzolino, A.J., Troadec, D., Tsou, P., Warren, J., Westphal, A., Wozniakiewicz, P., Wright, I., and Zinner, E. (2006) Impact features on Stardust: implications for comet 81P/Wild 2 dust. *Science*, **314**, 1716–1719.
134. Flynn, G.J., Bleuét, P., Borg, J., Bradley, J.P., Brenker, F.E., Brennan, S., Bridges, J., Brownlee, D.E., Bullock, E.S., Burghammer, M., Clark, B.C., Dai, Z.R., Daghljan, C.P., Djouadi, Z., Fakra, S., Ferroir, T., Floss, C., Franchi, I.A., Gainsforth, Z., Gallien, J.-P., Gillet, P., Grant, P.G., Graham, G.A., Green, S.F., Grossemy, E., Heck, P.R., Herzog, G.F., Hoppe, P., Hörz, F., Huth, J., Ignatyev, K., Ishii, H.A., Janssens, K., Joswiak, D., Kearsley, A.T., Khodja, H., Lanzirotti, A., Leitner, J., Lemelle, L., Leroux, H., Luening,

- K., MacPherson, G.J., Marhas, K.K., Marcus, M.A., Matrajt, G., Nakamura, T., Nakamura-Messenger, K., Nakano, T., Newville, M., Papanastassiou, D.A., Pianetta, P., Rao, W., Riekel, C., Rietmeijer, F.J.M., Rost, D., Schwandt, C.S., See, T.H., Sheffield-Parker, J., Simionovici, A., Sitnitsky, I., Snead, C.J., Stadermann, F.J., Stephan, T., Stroud, R.M., Susini, J., Suzuki, Y., Sutton, S.R., Taylor, S., Teslich, N., Troadec, D., Tsou, P., Tsuchiyama, A., Uesugi, K., Vekemans, B., Vicenzi, E.P., Vincze, L., Westphal, A.J., Wozniakiewicz, P., Zinner, E., and Zolensky, M.E. (2006) Elemental compositions of comet 81P/Wild 2 samples collected by Stardust. *Science*, **314**, 1731–1735.
135. Kerr, R.A. (2004) A surprisingly ancient cometary visage. *Science*, **303**, 151.
136. Tuzzolino, A.J., Economou, T.E., Clark, B.C., Tsou, P., Brownlee, D.E., Green, S.F., McDonnell, J.A.M., McBride, N., and Colwell, M.T.S.H. (2004) Dust measurements in the coma of comet 81P/Wild 2 by the Dust Flux Monitor Instrument. *Science*, **304**, 1776–1780.
137. Zolensky, M.E., Zega, T.J., Yano, H., Wirick, S., Westphal, A.J., Weisberg, M.K., Weber, I., Warren, J.L., Velbel, M.A., Tsuchiyama, A., Tsou, P., Toppani, A., Tomioka, N., Tomeoka, K., Teslich, N., Taheri, M., Susini, J., Stroud, R., Stephan, T., Stadermann, F.J., Snead, C.J., Simon, S.B., Simionovici, A., See, T.H., Robert, F., Rietmeijer, F.J.M., Rao, W., Perronnet, M.C., Papanastassiou, D.A., Okudaira, K., Ohsumi, K., Ohnishi, I., Nakamura-Messenger, K., Nakamura, T., Mostefaoui, S., Mikouchi, T., Meibom, A., Matrajt, G., Marcus, M.A., Leroux, H., Lemelle, L., Le, L., Lanzirotti, A., Langenhorst, F., Krot, A.N., Keller, L.P., Kearsley, A.T., Joswiak, D., Jacob, D., Ishii, H., Harvey, R., Hagiya, K., Grossman, L., Grossman, J.N., Graham, G.A., Gounelle, M., Gillet, P., Genge, M.J., Flynn, G., Ferroir, T., Fallon, S., Ebel, D.S., Dai, Z.R., Cordier, P., Clark, B., Chi, M., Butterworth, A.L., Brownlee, D.E., Bridges, J.C., Brennan, S., Brearley, A., Bradley, J.P., Bleuet, P., Bland, P.A., and Bastien, R. (2006) Mineralogy and petrology of comet 81P/Wild 2 nucleus samples. *Science*, **314**, 1735–1739.
138. McKeegan, K.D., Aléon, J., Bradley, J., Brownlee, D., Busemann, H., Butterworth, A., Chaussidour, M., Fallon, S., Floss, C., Gilmour, J., Gounelle, M., Graham, G., Guan, Y., Heck, P.R., Hoppe, P., Hutcheon, I.D., Huth, J., Ishii, H., Ito, M., Jacobsen, S.B., Kearsley, A., Leshin, L.A., Liu, M.-C., Lyon, I., Marhas, K., Marty, B., Matrajt, G., Meibom, A., Messenger, S., Mostefaoui, S., Mukhopadhyay, S., Nakamura-Messenger, K., Nittler, L., Palma, R., Pepin, R.O., Papanastassiou, D.A., Robert, F., Schlutter, D., Snead, C.J., Stadermann, F.J., Stroud, R., Tsou, P., Westphal, A., Young, E.D., Ziegler, K., Zimmermann, L., and Zinner, E. (2006) Isotopic compositions of cometary matter returned by Stardust. *Science*, **314**, 1724–1728.
139. Marty, B., Robert, P., and Zimmermann, L. (2005) Nitrogen and noble gases in micrometeorites. *Meteorit. Planet. Sci.*, **40**, 881–894.
140. Keller, L.P., Bajt, S., Baratta, G.A., Borg, J., Bradley, J.P., Brownlee, D.E., Busemann, H., Brucato, J.R., Burchell, M., Colangeli, L., d'Hendecourt, L., Djouadi, Z., Ferrini, G., Flynn, G., Franchi, I.A., Fries, M., Grady, M.M., Graham, G.A., Grossemy, F., Kearsley, A., Matrajt, G., Nakamura-Messenger, K., Mennella, V., Nittler, L., Palumbo, M.E., Stadermann, F.J., Tsou, P., Rotundi, A., Sandford, S.A., Snead, C., Steele, A., Wooden, D., and Zolensky, M. (2006) Infrared spectroscopy of comet 81P/Wild 2 samples returned by Stardust. *Science*, **314**, 1728–1731.
141. Meierhenrich, U.J. (2008) *Amino Acids and the Asymmetry of Life – Caught in the Act of Formation*, Springer, Heidelberg.
142. Sandford, S.A., Aléon, J., Alexander, C.M.O.D., Araki, T., Bajt, S., Baratta, G.A., Borg, J., Bradley, J.P., Brownlee, D.E., Brucato, J.R., Burchell, M.J., Busemann, H., Butterworth, A., Clemett, S.J., Cody, G., Colangeli,

- L., Cooper, G., d'Hendecourt, L., Djouadi, Z., Dworkin, J.P., Ferrini, G., Fleckenstein, H., Flynn, G.J., Franchi, I.A., Fries, M., Gilles, M.K., Glavin, D.P., Gounelle, M., Grossemy, F., Jacobsen, C., Keller, L.P., Kilcoyne, A.L.D., Leitner, J., Matrajt, G., Meibom, A., Mennella, V., Mostefaoui, S., Nittler, L.R., Palumbo, M.E., Papanastassiou, D.A., Robert, F., Rotundi, A., Snead, C.J., Spencer, M.K., Stadermann, F.J., Steele, A., Stephan, T., Tsou, P., Tylliszczak, T., Westphal, A.J., Wirick, S., Wopenka, B., Yabuta, H., Zare, R.N., and Zolensky, M.E. (2006) Organics captured from comet 81P/Wild 2 by the Stardust spacecraft. *Science*, **314**, 1720–1724.
143. Glavin, D.P., Dworkin, J.P., and Sandford, S.A. (2008) Detection of cometary amines in samples returned by Stardust. *Meteorit. Planet. Sci.*, **43**, 399–413.
144. Sekanina, Z., Brownlee, D.E., Economou, T.E., Tuzzolino, A.J., and Green, S.F. (2004) Modeling the nucleus and jets of comet 81P/Wild 2 based on the Stardust encounter data. *Science*, **304**, 1769–1774.
145. Levasseur-Regourd, A.-C. (2004) Cometary dust unveiled. *Science*, **304**, 1762–1763.
146. Kerr, R.A. (2005) Deep Impact finds a flying snowbank of a comet. *Science*, **309**, 1667.
147. A'Hearn, M.F., Belton, M.J.S., Delamere, W.A., Kissel, J., Klaasen, K.P., McFadden, L.A., Meech, K.J., Melosh, H.J., Schultz, P.H., Sunshine, J.M., Thomas, P.C., Veverka, J., Yeomans, D.K., Baca, M.W., Busko, I., Crockett, C.J., Collins, S.M., Desnoyer, M., Eberhardy, C.A., Ernst, C.M., Farnham, T.L., Feaga, L., Groussin, O., Hampton, D., Ipatov, S.I., Li, J.-Y., Lindler, D., Lisse, C.M., Mastrodemos, N., Owen, W.M. Jr., Richardson, J.E., Wellnitz, D.D., and White, R.L. (2005) Deep Impact: excavating comet Tempel 1. *Science*, **310**, 258–264.
148. Küppers, M., Bertini, I., Fornasier, S., Gutierrez, P.J., Hviid, S.F., Jorda, L., Keller, H.U., Knollenberg, J., Koschny, D., Kramm, R., Lara, L.-M., Sierks, H., Thomas, N., Barbieri, C., Lamy, P., Rickman, H., Rodrigo, R., and The OSIRIS Team (2005) A large dust/ice ratio in the nucleus of comet 9P/Tempel 1. *Nature*, **437**, 987–990.
149. Lamy, P.L., Toth, I., A'Hearn, M.F., Weaver, H.A., and Weissman, P.R. (2001) Hubble Space Telescope observations of the nucleus of Comet 9P/Tempel 1. *Icarus*, **154**, 337–344.
150. Lamy, P.L., Toth, I., A'Hearn, M.F., Weaver, H.A., and Jorda, L. (2007) Rotational state of the nucleus of Comet 9P/Tempel 1: results from Hubble Space Telescope observations in 2004. *Icarus*, **187**, 132–143.
151. Meech, K.J., Ageorges, N., A'Hearn, M.F., Arpigny, C., Ates, A., Aycock, J., Bagnulo, S., Bailey, J., Barber, R., Barrera, L., Barrera, R., Bauer, J.M., Belton, M.J.S., Bensch, F., Bhattacharya, B., Biver, N., Blake, G., Bockelée-Morvan, D., Boehnhardt, H., Bonev, B.P., Bonev, T., Buie, M.W., Burton, M.G., Butner, H.M., Cabanac, R., Campbell, R., Campins, H., Capria, M.T., Carroll, T., Chaffee, F., Charney, S.B., Cleis, R., Coates, A., Cochran, A., Colom, P., Conrad, A., Coulson, I.M., Crovisier, J., deBuizer, J., Dekany, R., de León, J., Dello Russo, N., Delsanti, A., DiSanti, M., Drummond, J., Dundon, L., Etzel, P.B., Farnham, T.L., Feldman, P., Fernández, Y.R., Filipovic, M.D., Fisher, S., Fitzsimmons, A., Fong, D., Fugate, R., Fujiwara, H., Fujiyoshi, T., Furusho, R., Fuse, T., Gibb, E., Groussin, O., Gulkis, S., Gurwell, M., Hadamcik, E., Hainaut, O., Harker, D., Harrington, D., Harwit, M., Hasegawa, S., Hergenrother, C.W., Hirst, P., Hodapp, K., Honda, M., Howell, E.S., Hutsemékers, D., Iono, D., Ip, W.-H., Jackson, W., Jehin, E., Jiang, Z.J., Jones, G.H., Jones, P.A., Kadono, T., Kamath, U.W., Käufel, H.U., Kasuga, T., Kawakita, H., Kelley, M.S., Kerber, F., Kidger, M., Kinoshita, D., Knight, M., Lara, L., Larson, S.M., Lederer, S., Lee, C.-F., Levasseur-Regourd, A.C., Li, J.Y., Li, Q.-S., Licandro, J., Lin, Z.-Y., Lisse, C.M., LoCurto, G., Lovell, A.J., Lowry, S.C., Lyke, J., Lynch, D., Ma, J., Magee-Sauer, K., Maheswar, G., Manfroid, J., Marco,

- O., Martin, P., Melnick, G., Miller, S., Miyata, T., Moriarty-Schieven, G.H., Moskovitz, N., Mueller, B.E.A., Mumma, M.J., Muneer, S., Neufeld, D.A., Ootsubo, T., Osip, D., Pande, S.K., Pantin, E., Paterno-Mahler, R., Patten, B., Penprase, B.E., Peck, A., Petitas, G., Pinilla-Alonso, N., Pittichova, J., Pompei, E., Prabhu, T.P., Qi, C., Rao, R., Rauer, H., Reitsema, H., Rodgers, S.D., Rodriguez, P., Ruane, R., Ruch, G., Rujopakarn, W., Sahu, D.K., Sako, S., Sakon, I., Samarasinha, N., Sarkissian, J.M., Saviane, I., Schirmer, M., Schultz, P., Schulz, R., Seitzer, P., Sekiguchi, T., Selman, F., Serra-Ricart, M., Sharp, R., Snell, R.L., Snodgrass, C., Stallard, T., Stecklein, G., Sterken, C., Stüwe, J.A., Sugita, S., Sumner, M., Suntzeff, N., Swaters, R., Takakuwa, S., Takato, N., Thomas-Osip, J., Thompson, E., Tokunaga, A.T., Tozzi, G.P., Tran, H., Troy, M., Trujillo, C., Van Cleve, J., Vasundhara, R., Vazquez, R., Vilas, F., Villanueva, G., von Braun, K., Vora, P., Wainscoat, R.J., Walsh, K., Watanabe, J., Weaver, H.A., Weaver, W., Weiler, M., Weissman, P.R., Welsh, W.F., Wilner, D., Wolk, S., Womack, M., Wooden, D., Woodney, L.M., Woodward, C., Wu, Z.-Y., Wu, J.-H., Yamashita, T., Yang, B., Yang, Y.-B., Yokogawa, S., Zook, A.C., Zauderer, A., Zhao, X., Zhou, X., and Zucconi, J.-M. (2005) Deep Impact: observations from a worldwide Earth-based campaign. *Science*, **310**, 265–269.
152. Richardson, J.E., Melosh, H.J., Lisse, C.M., and Carcich, B. (2007) A ballistics analysis of the Deep Impact ejecta plume: determining comet Tempel 1's gravity, mass, and density. *Icarus*, **190**, 357–390.
153. Lisse, C.M., VanCleve, J., Adams, A.C., A'Hearn, M.F., Fernández, Y.R., Farnham, T.L., Armus, L., Grillmair, C.J., Ingalls, J., Belton, M.J.S., Groussin, O., McFadden, L.A., Meech, K.J., Schultz, P.H., Clark, B.C., Feaga, L.M., and Sunshine, J.M. (2006) Spitzer spectral observations of the Deep Impact ejecta. *Science*, **313**, 635–640.
154. Mumma, M.J., DiSanti, M.A., Magee-Sauer, K., Bonev, B.P., Villanueva, G.L., Kawakita, H., Dello Russo, N., Gibb, E.L., Blake, G.A., Lyke, J.E., Campbell, R.D., Aycock, J., Conrad, A., and Hill, G.M. (2005) Parent volatiles in comet 9P/Tempel 1: before and after impact. *Science*, **310**, 270–274.
155. Keller, H.U., Jorda, L., Küppers, M., Gutierrez, P.J., Hviid, S.F., Knollenberg, J., Lara, L.-M., Sierks, H., Barbieri, C., Lamy, P., Rickman, H., and Rodrigo, R. (2005) Deep Impact observations by OSIRIS onboard the Rosetta spacecraft. *Science*, **310**, 281–283.
156. Sugita, S., Ootsubo, T., Kadono, T., Honda, M., Sako, S., Miyata, T., Sakon, I., Yamashita, T., Kawakita, H., Fujiwara, H., Fujiyoshi, T., Takato, N., Fuse, T., Watanabe, J., Furusho, R., Hasegawa, S., Kasuga, T., Sekiguchi, T., Kinoshita, D., Meech, K.J., Wooden, D.H., Ip, W.H., and A'Hearn, M.F. (2005) Subaru Telescope observations of Deep Impact. *Science*, **310**, 274–278.
157. Hanson, B. (2005) Inside out; outside in. *Science*, **310**, 257.
158. Veverka, J., Klaasen, K., A'Hearn, M., Belton, M., Brownlee, D., Chesley, S., Clark, B., Economou, T., Farquhar, R., Green, S.F., Groussin, O., Harris, A., Kissel, J., Li, J.-Y., Meech, K., Melosh, J., Richardson, J., Schultz, P., Silen, J., Sunshine, J., Thomas, P., Bhaskaran, S., Bodewits, D., Carcich, B., Chevront, A., Farnham, T., Sackett, S., Wellnitz, D., and Wolf, A. (2013) Return to comet Tempel 1: overview of Stardust-NExT results. *Icarus*, **222**, 424–435.
159. Wellnitz, D.D., Collins, S.M., A'Hearn, M.F., and The Deep Impact Mission Team, and the Stardust-NExT Mission Team (2013) The location of the impact point of the Deep Impact Impactor on Comet 9P/Tempel 1. *Icarus*, **222**, 487–491.
160. Richardson, J.E. and Melosh, H.J. (2013) An examination of the Deep Impact collision site on Comet Tempel 1 via Stardust-NExT: Placing further constraints on cometary surface properties. *Icarus*, **222**, 492–501.
161. Schultz, P.H., Hermaly, B., and Veverka, J. (2013) The Deep Impact

- crater on 9P/Tempel-1 from Stardust-NExT. *Icarus*, **222**, 502–515.
162. Klaasen, K.P., Brown, D., Carcich, B., Farnham, T., Owen, W., and Thomas, P. (2013) Stardust–NExT NAVCAM calibration and performance. *Icarus*, **222**, 436–452.
163. Thomas, P., A’Hearn, M., Belton, M.J.S., Brownlee, D., Carcich, B., Hermalyn, B., Klaasen, K., Sackett, S., Schultz, P.H., Veverka, J., Bhaskaran, S., Bodewits, D., Chesley, S., Clark, B., Farnham, T., Groussin, O., Harris, A., Kissel, J., Li, J.-Y., Meech, K., Melosh, J., Quick, A., Richardson, J., Sunshine, J., and Wellnitz, D. (2013) The nucleus of Comet 9P/Tempel 1: shape and geology from two flybys. *Icarus*, **222**, 453–466.
164. Belton, M.J.S., Thomas, P., Carcich, B., Quick, A., Veverka, J., Melosh, H.J., A’Hearn, M.F., Li, J.-Y., Brownlee, D., Schultz, P., Klaasen, K., and Sarid, G. (2013) The origin of pits on 9P/Tempel 1 and the geologic signature of outbursts in Stardust-NExT images. *Icarus*, **222**, 477–486.
165. Meech, K.J., Kleyna, J., Hainaut, O.R., Lowry, S.C., Fuse, T., A’Hearn, M.F., Chesley, S., Yeomans, D.K., Fernández, Y., Lisse, C., Reach, W., Bauer, J.M., Mainzer, A.K., Pittichová, J., Christensen, E., Osip, D., Brink, T., Mateo, M., Motta, V., Challis, P., Holman, M., and Ferrín, I. (2013) The demise of Comet 85P/Boethin, the first EPOXI mission target. *Icarus*, **222**, 662–678.
166. Mann, A. (2010) Glimpsing a comet’s heart. *Nature*, **467**, 1013–1014.
167. A’Hearn, M.F., Belton, M.J.S., Delamere, W.A., Feaga, L.M., Hampton, D., Kissel, J., Klaasen, K.P., McFadden, L.A., Meech, K.J., Melosh, H.J., Schultz, P.H., Sunshine, J.M., Thomas, P.C., Veverka, J., Wellnitz, D.D., Yeomans, D.K., Besse, S., Bodewits, D., Bowling, T.J., Carcich, B.T., Collins, S.M., Farnham, T.L., Groussin, O., Hermalyn, B., Kelley, M.S., Li, J.-Y., Lindler, D.J., Lisse, C.M., McLaughlin, S.A., Merlin, F., Protopapa, S., Richardson, J.E., and Williams, J.L. (2011) EPOXI at Comet Hartley 2. *Science*, **332**, 1396–1400.
168. Thomas, P.C., A’Hearn, M.F., Veverka, J., Belton, M.J.S., Kissel, J., Klaasen, K.P., McFadden, L.A., Melosh, H.J., Schultz, P.H., Besse, S., Carcich, B.T., Farnham, T.L., Groussin, O., Hermalyn, B., Li, J.-Y., Lindler, D.J., Lisse, C.M., Meech, K., and Richardson, J.E. (2013) Shape, density, and geology of the nucleus of Comet 103P/Hartley 2. *Icarus*, **222**, 550–558.
169. Meech, K.J., A’Hearn, M.F., Adams, J.A., Bacci, P., Bai, J., Barrera, L., Battelino, M., Bauer, J.M., Becklin, E., Bhatt, B., Biver, N., Bockelée-Morvan, D., Bodewits, D., Bönhardt, H., Boissier, J., Bonev, B.P., Borghini, W., Brucato, J.R., Bryssinck, E., Buie, M.W., Canovas, H., Castellano, D., Charnley, S.B., Chen, W.P., Chiang, P., Choi, Y.-J., Christian, D.J., Chuang, Y.-L., Cochran, A.L., Colom, P., Combi, M.R., Coulson, I.M., Crovisier, J., Dello Russo, N., Dennerl, K., DeWahl, K., DiSanti, M.A., Facchini, M., Farnham, T.L., Fernandez, Y., Florén, H.G., Frisk, U., Fujiyoshi, T., Furusho, R., Fuse, T., Galli, G., Garcia-Hernandez, D.A., Gersch, A., Getu, Z., Gibb, E.L., Gillon, M., Guido, E., Guillermo, R.A., Hadamcik, E., Hainaut, O., Hammel, H.B., Harker, D.E., Harmon, J.K., Harris, W.M., Hartogh, P., Hashimoto, M., Häusler, B., Herter, T., Hjalmarsen, A., Holland, S.T., Honda, M., Hosseini, S., Howell, E.S., Howes, N., Hsieh, H.H., Hsiao, H.-Y., Hutsemékers, D., Immler, S.M., Jackson, W.M., Jeffers, S.V., Jehin, E., Jones, T.J., de Juan Ovelar, M., Kaluna, H.M., Karlsson, T., Kawakita, H., Keane, J.V., Keller, L.D., Kelley, M.S., Kinoshita, D., Kiselev, N.N., Kleyna, J., Knight, M.M., Kobayashi, H., Kobulnicky, H.A., Kolokolova, L., Kreiny, M., Kuan, Y.-J., Küppers, M., Lacruz, J.M., Landsman, W.B., Lara, L.M., Lecacheux, A., Lévassieur-Regourd, A.C., Li, B., Licandro, J., Ligustri, R., Lin, Z.-Y., Lippi, M., Lis, D.C., Lisse, C.M., Lovell, A.J., Lowry, S.C., Lu, H., Lundin, S., Magee-Sauer, K., Magain, P., Manfroid, J., Mazzotta Epifani, E., McKay, A., Melita, M.D., Mikuz, H., Milam, S.N., Milani, G., Min, M., Moreno, R., Mueller, B.E.A., Mumma, M.J.,

- Nicolini, M., Nolan, M.C., Nordh, H.L., Nowajewski, P.B., Team, O., Ootsubo, T., Paganini, L., Perrella, C., Pittichova, J., Prosperi, E., Radeva, Y.L., Reach, W.T., Remijan, A.J., Rengel, M., Riesen, T.E., Rodenhuis, M., Rodriguez, D.P., Russell, R.W., Sahu, D.K., Samarasinha, N.H., Sanchez Caso, A., Sandqvist, A., Sarid, G., Sato, M., Schleicher, D.G., Schwieterman, E.W., Sen, A.K., Shenoy, D., Shi, J.-C., Shinnaka, Y., Skvarc, J., Snodgrass, C., Sitko, M.L., Sonnett, S., Sosseini, S., Sostero, G., Sugita, S., Swinyard, B.M., Szutowicz, S., Takato, N., Tanga, P., Taylor, P.A., Tozzi, G.-P., Trabatti, R., Trigo-Rodriguez, J.M., Tubiana, C., de Val-Borro, M., Vacca, W., Vandenbussche, B., Vaubaillon, J., Velichko, E.P., Velichko, S.F., Vervack, R.J. Jr., Vidal-Nunez, M.J., Villanueva, G.L., Vinante, C., Vincent, J.-B., Wang, M., Wasserman, L.H., Watanabe, J., Weaver, H.A., Weissman, P.R., Wolk, S., Wooden, D.H., Woodward, C.E., Yamaguchi, M., Yamashita, T., Yanamandra-Fischer, P.A., Yang, B., Yao, J.-S., Yeomans, D.K., Zenn, T., Zhao, H., and Ziffer, J.E. (2011) EPOXI: comet 103P/Hartley 2 observations from a worldwide campaign. *Astrophys. J. Lett.*, **734**, L1 (9 pp).
170. Li, J.-Y., Besse, S., A'Hearn, M.F., Belton, M.J.S., Bodewits, D., Farnham, T.L., Klaasen, K.P., Lisse, C.M., Meech, K.J., Sunshine, J.M., and Thomas, P.C. (2013) Photometric properties of the nucleus of Comet 103P/Hartley 2. *Icarus*, **222**, 559–570.
171. Bruck Syal, M., Schultz, P.H., Sunshine, J.M., A'Hearn, M.F., Farnham, T.L., and Dearborn, D.S.P. (2013) Geologic control of jet formation on Comet 103P/Hartley 2. *Icarus*, **222**, 610–624.
172. Weaver, H.A., Feldmann, P.D., A'Hearn, M.F., Dello Russo, N., and Stern, S.A. (2011) The carbon monoxide abundance in comet 103P/Hartley 2 during the EPOXI flyby. *Astrophys. J. Lett.*, **734**, L5 (5 pp).
173. Hermalyn, B., Farnham, T.L., Collins, S.M., Kelley, M.S., A'Hearn, M.F., Bodewits, D., Carcich, B., Lindler, D.J., Lisse, C., Meech, K., Schultz, P.H., and Thomas, P.C. (2013) The detection, localization, and dynamics of large icy particles surrounding Comet 103P/Hartley 2. *Icarus*, **222**, 625–633.
174. Kelley, M.S., Lindler, D.J., Bodewits, D., A'Hearn, M.F., Lisse, C.M., Kolokolova, L., Kissel, J., and Hermalyn, B. (2013) A distribution of large particles in the coma of Comet 103P/Hartley 2. *Icarus*, **222**, 634–652.
175. Cheng, A.F., Lisse, C.M., and A'Hearn, M. (2013) Surface geomorphology of Jupiter Family Comets: a geologic process perspective. *Icarus*, **222**, 808–817.
176. Belton, M.J.S. (2010) Cometary activity, active areas, and a mechanism for collimated outflows on 1P, 9P, 19P, and 81P. *Icarus*, **210**, 881–897.